The transport of PM_{10} over Cape Town during high pollution episodes

Koketso Michelle Molepo
(MLPKOK002)

Dissertation presented for the degree of

Master of Science in Environmental and Geographical Science

Faculty of Science
University of Cape Town

Supervisor: Associate Professor Babatunde J. Abiodun

February 2019

Table of contents

Table of contents i
Plagiarism declaration iii
Abstract iv
Acknowledgements vi
List of acronyms and abbreviations vii
List of figures ix
List of tables xii
Chapter 1 – Introduction 1
1.1. What is PM_{10}? 1
1.2. Sources and general characteristics of PM_{10} 2
1.3. Impacts of PM_{10} pollution 3
1.4. Air quality in Cape Town and the problem of PM_{10} pollution 5
1.5. Aims and objectives 8
Chapter 2 – Literature review 9
2.1. Factors inducing high PM_{10} levels 9
2.1.1. Meteorological conditions 9
2.1.2. Local pollution emissions 11
2.1.3. Long-range transport 12
2.2. Approaches for studying transport of PM_{10} 14
Chapter 3 – Methodology 17
3.1. Station observation data 17
3.2. Selection of PM_{10} episodes in Cape Town 18
3.3. WRF-Chem model and simulations 19
3.4. Air parcel trajectories 22
Chapter 4 – Results and discussion part I: Temporal variation of observed PM_{10} in Cape Town 24
4.1. Diurnal variation 24
4.2. Daily variation 27
4.3. Seasonal variation 29
Chapter 5 – Results and discussions part II: The simulated transport of PM_{10} over Cape Town during the episodes 32
5.1. Model evaluation 32

5.2. Trajectories of air parcels associated with the observed PM_{10} episodes 37
5.3. The transport and spatial distribution of PM_{10} during peak days 41
5.4. Impact of topography 47
Chapter 6 – Results and discussion part IV: Sensitivity of the simulated PM_{10} and atmospheric conditions to a change in chemistry parameterisation 50
6.1. Atmospheric conditions and PM_{10} concentrations over Cape Town..... 50
6.2. Air parcel trajectories 52
6.3. PM_{10} transport and spatial distribution during peak days 54
Chapter 7 – The influence of emissions from Khayelitsha on PM_{10} distribution over Cape Town..... 63
Chapter 8 – Conclusions..... 66
8.1. Summary..... 66
8.2. Recommendations for future research..... 68
8.3. Publication 69
References..... 70

Plagiarism declaration

1. I know that plagiarism is a serious form of academic dishonesty.
2. I have read the document about avoiding plagiarism, I am familiar with its contents and I have avoided all forms of plagiarism mentioned there.
3. Where I have used the words of others, I have indicated this by the use of quotation marks.
4. I have referenced all quotations and other ideas borrowed from others.
5. I have not and shall not allow others to plagiarise my work.

Koketso Michelle Molepo (student number: MLPKOK002)

February 2019

Abstract

PM_{10} is a notorious air pollutant that often degrades the air quality in Cape Town. Previous studies have attributed high concentrations of PM_{10} over Cape Town to local sources, neglecting the influence of remote sources. The present study investigates the influence of remote and local pollution sources to PM_{10} episodes over the city. The study analysed observations from Cape Town's air quality monitoring stations and simulations from the Weather Research and Forecasting model with Chemistry (WRF-Chem). The observation data were used to identify PM_{10} episodes over the city between 2008 and 2014 and WRF-Chem was applied to simulate the atmospheric conditions and PM_{10} transport over southern Africa a few days before, during, and after each episode. To examine the sensitivity of the simulations to chemistry parameterisation, two chemistry parameterisation schemes were used in the study. The two schemes are RADM2 chemistry scheme coupled with the MADE/SORGAM aerosol module (RMS) and RADM2 coupled with the GOCART aerosol module (RGC). While RMS accounts for aerosol feedbacks, RGC does not. The capability of the model (with each scheme) to reproduce the PM_{10} concentration and wind over Cape Town was quantified by comparing the simulations with the station observation data. To identify the paths of air parcels that arrived in Cape Town during each episode, the study employed back trajectory simulations from the Hybrid Single-Particle Lagrangian Integrated Trajectory (HYSPLIT) model and from the WRF-Chem output. A third WRF-Chem simulation (KAYE) was performed in order to investigate the influence of idealized local emissions from Khayelitsha (one of the largest local sources of the pollutant in Cape Town) on the spatial distribution of PM_{10} concentration over the city.

The results show that all the WRF-Chem simulations reproduce well the observed wind speed and direction over Cape Town during the episodes but struggle to reproduce the observed PM_{10}. The simulations under-estimate the observed PM_{10} concentration over the city and, in most cases, reproduce peaks in PM_{10} concentration days earlier or later than the observations. However, the simulations agree with the HYSPLIT back-trajectory simulations that most of the air parcels over Cape Town during the episodes came from central southern Africa or the Namibian coast and

travelled over the Kalahari, Namib, or both deserts **before** reaching Cape Town. The RMS simulations link the peaks in PM_{10} concentration over Cape Town with the transport of the pollutant from the north-west coast of southern Africa, featuring a coastal trough and a plume of PM_{10} along the coast. The study reveals that north-westerly flows provides a conducive condition for the long-range transport of PM_{10} to Cape Town, while south-easterly winds favour the transport of PM_{10} from Khayelitsha emissions to the city.

Acknowledgements

First and foremost, I would like to thank my supervisor, Associate Professor Babatunde Abiodun, for his guidance and expertise throughout this degree. I am also grateful for his constant motivation, encouragement, and his faith in me when I had none in myself. I would have not made it this far without his support.

To Phillip Mukwena, who selflessly provided technical assistance whenever I asked, I am thankful. I would have not been able to configure WRF-Chem without him.

For financial support, I wish to thank the Applied Centre for Climate & Earth Systems Science (ACCESS), the City of Cape, and Associate Professor Babatunde Abiodun.

My gratitude also goes to the Scientific Services, Water and Sanitation Department at the City of Cape Town, Airports Company South Africa (ACSA, Cape Town), and the Western Cape Government: Department of Environmental Affairs and Development Planning for providing the station observations, and to the Centre for High Performance Computing (CHPC, South Africa) for providing the computations facility I needed to conduct the WRF-Chem simulations.

To Doctor Rembu Magoba at the Scientific Services, Water and Sanitation Department, thank you for your encouragement and for facilitating my engagements with the City of Cape Town.

To my fellow students, Mariam, Michelle, Myra, Roland, Sabina, Sawadogo, Stefaan, and Naomi, I am grateful for the ideas shared during our weekly writing sessions.

Finally, to my parents, I am thankful for your patience and support through this journey and for always encouraging me to follow my dreams.

List of acronyms and abbreviations

ARL	Air Resources Laboratory
CBD	Central Business District
CAMx	Comprehensive Air Quality Model with Extensions
CCN	Cloud Condensation Nuclei
CFSR	Climate Forecast System Reanalysis
EDGAR	Emission Database for Global Atmospheric Research
GDAS1	Global Data Assimilation System with a horizontal resolution of 1^{o} x 1^{o}, 23 vertical layers, and a 3-hour temporal resolution
GOCART	Goddard Chemistry Aerosol Radiation and Transport model
H_2S	Hydrogen sulphide
H_2SO_4	Sulphuric acid
HNO_3	Nitric acid
HYSPLIT	Hybrid Single-Particle Lagrangian Integrated Trajectory
KAYE	WRF-Chem using the RADM2 chemistry scheme combined with the GOCART aerosol module and an idealised continuous area emission (of 10 mol km^{-2} h^{-1}) introduced over the Khayelitsha area
LSM	Land Surface Model
MADE	Modal Aerosol Dynamics Model for Europe
Mt	Million tons
NCEP	National Centres for Environmental Prediction
NH_3	Ammonia
NO_2	Nitrogen dioxide
NOAA	National Oceanic and Atmospheric Administration
NOAH	NCEP, Oregon State University, Air Force, and Hydrological Research Lab

NO_x	Nitrogen oxides
O_3	Ozone
PM	Particulate matter
$PM_{2.5}$	Particulate matter with a diameter less than or equal to 2.5 μm
$PM_{2.5-10}$	Particulate matter with a diameter between 2.5 and 10 μm
PM_{10}	Particulate matter with a diameter less than or equal to 10 μm
RADM2	Regional Acid Deposition Model version 2
READY	Real-time Environmental Applications and Display sYstem
RETRO	REanalysis of the TROpospheric chemical composition over the the past 40 years
RGC	WRF-Chem using the RADM2 chemistry scheme combined with the GOCART aerosol module
RMS	WRF-Chem using the RADM2 chemistry scheme combined with the MADE/SORGAM aerosol module
RRTMG	Rapid Radiative Transfer Model for GCMs
SeaWiFS	Sea-viewing Wide Field-of-view Sensor
SO_2	Sulphur dioxide
SORGAM	Secondary Organic Aerosol Model
TOMS	Total Ozone Mapping Spectrometer
UTC	Universal Time Coordinated
WRF-Chem	Weather Research and Forecasting model with Chemistry

List of figures

Figure 1.1: The relative sizes of PM_{10} and $PM_{2.5}$ particles (source: https://www.arb.ca.gov/research/aaqs/common-pollutants/pm/pm.htm). 1

Figure 1.2: Potential biological mechanisms of cardiopulmonary disease and mortality linked to PM exposure (Source: Pope and Dockery, 2006). 5

Figure 1.3: Layer of brown haze pollution over the Cape Flats in Cape Town (Source: City Health Department, 2005). 6

Figure 1.4: Brown haze pollution over the southern suburbs of Cape Town (Source: http://footage.framepool.com/en/shot/900287203-table-mountain-cape-town-haze-landmark-sights). 6

Figure 3.1: (a) The WRF-Chem simulation area showing the three nesting domains (d01, d02, and d03) used in this study. The brown contour lines show the topography, while the small black box indicates the location of Cape Town. The bottom panel (b) shows locations of the air quality monitoring stations in Cape Town used in the present study. 18

Figure 3.2: Anthropogenic emissions rates of PM_{10} over the study domain. 22

Figure 4.1: The diurnal variation of observed (a) PM_{10} concentration, (b) surface wind speed, and (c) temperature at various monitoring stations in Cape Town between 2008 and 2014. 26

Figure 4.2: Time series of the observed daily mean PM_{10} concentration at Cape Town monitoring stations between 2008 and 2014. The thin and thick red horizontal lines show the World Health Organization (WHO) and the South African 24-hourly mean PM_{10} standards (50 μg m^{-3} and 75 μg m^{-3}, respectively). 28

Figure 4.3: Seasonal variation of (a) PM_{10} concentration anomalies (in μg m^{-3}), (b) surface wind speed, and (c) temperature as observed at various monitoring stations in Cape Town over the study period. The PM_{10} anomalies are with respect to the annual mean over each station. The annual mean values for the stations are shown inside the brackets (in μg m^{-3}). Stations with less than 11 months' data have been excluded. 31

Figure 5.1: Observed, RMS-simulated, and RGC-simulated daily PM_{10} concentration (in μg m^{-3}) over Cape Town during the 11 – 12 days window of the episodes identified in this study. The dashed vertical lines indicate the episode day(s). For each episode window and each dataset, the PM_{10} concentration has been standardised with the mean and standard deviation. The observed, RMS-simulated, and RGC-simulated PM_{10} mean values ($\bar{x}_O$, $\bar{x}_{RMS}$, and $\bar{x}_{RGC}$, respectively; in μg m^{-3}) are shown for each episode window. 34

Figure 5.2: Observed, RMS-simulated, and RGC-simulated daily surface wind speed and direction over Cape Town during the 11 – 12 days window of the episodes identified in the study. The dashed vertical lines indicate the episode day(s) and the arrows show the wind direction. Wind observations are not available for 2008..... 35

Figure 5.3: Pollution rose plots of the observations, RMS simulations and RGC simulations over Cape Town during the 11 – 12 days window of the episodes. The plots show the simulated and observed PM_{10} concentration for wind coming from the indicated directions. For comparison purposes, the simulated PM_{10} for RMS has been multiplied by 10. Wind observations are not available for 2008..... 36

Figure 5.4: 4-day back trajectories of air parcels in Cape Town at different heights (10, 100, and 1000 m) during the identified PM_{10} episodes, computed with HYSPLIT. 38

Figure 5.5: Similar to Figure 5.4, but computed with a separate trajectory model using RMS simulations as input. 40

Figure 5.6: The spatial distribution of RMS-simulated PM_{10} concentration and associated sea-level pressure for the sequence of days linked to the RMS peaks in Cape Town. Each row shows the two days before the peak (Day -2; Day -1) and the day of the peak..... 42

Figure 5.7: Synoptic sea level pressure over the sequence of days linked to RMS peaks 2011a (top row), 2011b (middle row), and 2012 (bottom row). Each row shows the two days before the peak (Day -2; Day -1) and the day of the peak. The observed synoptic charts are only available from 2011 (adapted from South African Weather Service, http://www.weathersa.co.za/climate/publications)..... 44

Figure 5.8: Vertical cross-section of the RMS-simulated PM_{10} concentration and wind vector profile (the arrow scale is indicated below the bottom left panel; unit: m s^{-1}) at latitude 24^{o} S (i.e., across the Namibian coast) on Day -2 of each RMS peak. The light grey shading represents topography. 45

Figure 5.9: Spatial distribution of the RMS-simulated PM_{10} concentration and the associated 10 m wind field (the arrow scale is indicated below the bottom left panel; unit: m s^{-1}) over the Western Cape region, overlain with topography (black contour lines; unit: m), for the sequence of days linked to the RMS PM_{10} peaks in Cape Town. Each row shows the two days before the peak (Day -2; Day -1) as well as the day of peak..... 46

Figure 5.10: Similar to Figure 5.6, but overlain with topography (black contour lines; unit: m). 48

Figure 6.1: Similar to Figure 5.5, but using RGC simulations as input. 54

Figure 6.2: Similar to Figure 5.6, but for the RGC simulations and RGC peaks. 56

Figure 6.3: Similar to Figure 5.8, but on for the RGC simulations and on Day -2 of the RGC peaks. 58

Figure 6.4: Similar to Figure 5.9, but for the RGC simulations and RGC peaks. 59

Figure 6.5: Similar to Figure 5.10, but for the RGC simulations and RGC peaks. 61

Figure 7.1: The spatial distribution of PM_{10} concentrations in Cape Town resulting solely from emissions in Khayelitsha. The figure shows the spatial distribution of the pollutant for each RGC peak and is overlain with topography (black contours; unit: m) and 10 m wind (the arrow scale is indicated below the lower left panel). The cyan triangles show the locations of the air quality monitoring stations over Cape Town. 65

List of tables

Table 3.1: The durations and dates of the PM_{10} episodes identified in Cape Town between 2008 and 2014. 19

Table 6.1: Summary of the comparison between RMS and RGC in simulating PM_{10} and 10 m wind speed over Cape Town during the 11 – 12-day windows of the PM_{10} episodes. The table shows mean PM_{10} concentration over the episode windows, correlation of the daily mean PM_{10} concentration with observations, day of the peak PM_{10} concentration (relative to the observations), and correlation of the daily mean wind speed with the observations for each parameterisation scheme..... 53

Chapter 1 – Introduction

1.1. What is PM_{10}?

Particulate matter (PM), also known as aerosols, is a mixture of tiny solid and/or liquid particles that are suspended in the atmosphere (WHO, 2006; Perrino, 2010). It is a complex air pollutant which comprises a wide variety of particles such as acids, dust, sea salt, volcanic ash, pollen, and soot. The particles vary in size, or aerodynamic diameter, from a few nanometers to about 100 µm (WHO, 2006; Perrino, 2010). PM_{10} refers to the particles with an aerodynamic diameter less than or equal to 10 µm (Figure 1.1). Moreover, PM_{10}, as opposed to other PM sizes, is adopted by many regulatory bodies as the main health standard or indicator for particulate pollution (Wicking-Baird et al., 1997; Triantafyllou, 2001; WHO, 2005). This standard is chosen as PM_{10} represents the particle size range responsible for most of the adverse health effects from particulate pollution (Wicking-Baird et al., 1997; Triantafyllou, 2001; WHO, 2005).

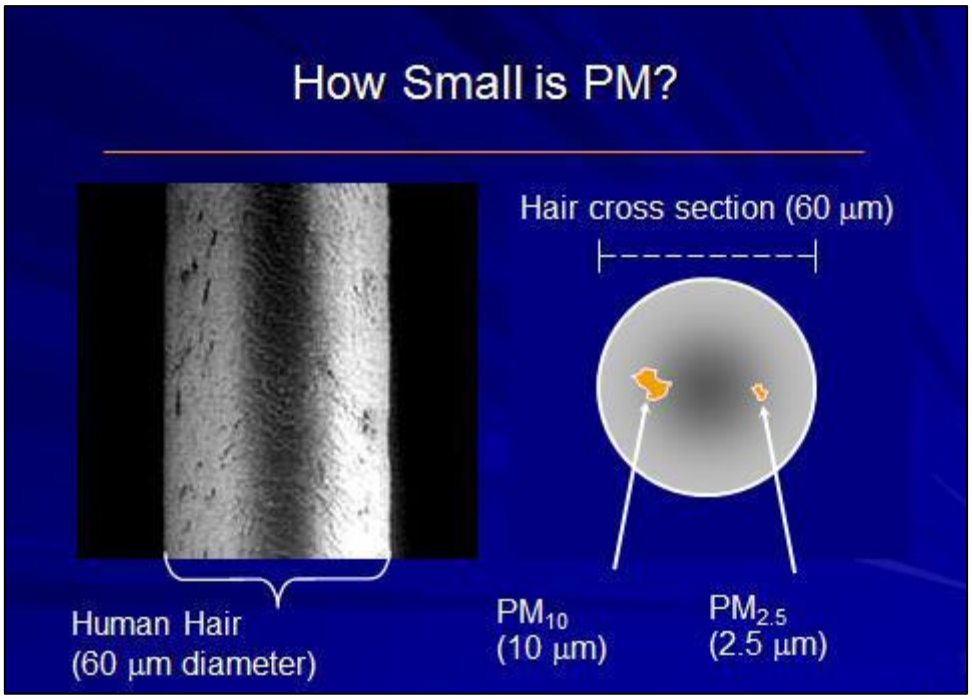

Figure 1.1: The relative sizes of PM_{10} and $PM_{2.5}$ particles (source: https://www.arb.ca.gov/research/aaqs/common-pollutants/pm/pm.htm).

Based on simultaneous measurement of number and size of particles present in the atmosphere, PM_{10} is usually classified into three size categories (or modes), namely: nucleation, accumulation and coarse modes (Wicking-Baird et al., 1997; Pope and Dockery, 2006; WHO, 2006; Perrino, 2010). These PM_{10} number-size distribution categories are frequently associated with certain types of source mechanisms and transformation processes of atmospheric particulates. Nucleation mode particles (also known as ultrafine or Aitken mode particles), which have an aerodynamic diameter less than 0.1 μm, are produced by condensation of gases as well as combustion processes (Wicking-Baird et al., 1997; Pope and Dockery, 2006; WHO, 2006; Perrino, 2010). Accumulation mode particles, which are between 0.1 and 1 μm in aerodynamic diameter, are generated by coagulation of particles in the nucleation mode and by condensation of gases (Wicking-Baird et al., 1997; Pope and Dockery, 2006; WHO, 2006; Perrino, 2010). Coarse mode particles, with an aerodynamic diameter between 1 and 10 μm, are formed by mechanical processes (Wicking-Baird et al., 1997; Pope and Dockery, 2006; WHO, 2006; Perrino, 2010). Nevertheless, the three categories are usually simplified into two principal groups, namely, fine particles (or the fine fraction) and coarse particles (or the coarse fraction) (Wicking-Baird et al., 1997; WHO, 2006; Pope and Dockery, 2006; Perrino, 2010). The boundary between the two fractions is typically between 1 and 2.5 μm (WHO, 2006), however, for measuring purposes, the limit is fixed at an aerodynamic diameter of 2.5 μm (WHO, 2006). As such, the coarse fraction (often referred to as $PM_{2.5-10}$) encompasses the particles with an aerodynamic diameter between 2.5 and 10 μm, and the fine fraction (referred to as $PM_{2.5}$) comprises those that are smaller than 2.5 μm in diameter.

1.2. Sources and general characteristics of PM_{10}

PM_{10} can be generated by a wide variety of natural as well as anthropogenic sources. Natural sources of the pollutant include sea spray, wind-blown dust, volcanic eruptions, and wildfires. Anthropogenic particles can be produced by combustion of fossil-fuels (for example, coal, oil, and gas in industrial processes, vehicles, and power plants), biomass burning, and construction activities. A distinction is also made between primary and secondary particles. Primary particles are released directly from their sources into the atmosphere, while secondary particles form in the atmosphere from chemical reactions (mostly oxidation) of gaseous precursors such as sulphur

dioxide (SO_2), ammonia (NH_3), nitrogen oxides (NOx), and heavy organic gases (Perrino, 2010; Edgerton et al., 1999; Kumar et al., 2016).

The sources from which the PM_{10} derives influence the characteristics (such as size and chemical composition) of the particles present in the atmosphere (Perrino, 2010). For example, wind-blown dust tends to comprise of mineral oxides (Perrino, 2010), fossil fuel and biomass combustion emit mainly carbonaceous particles (Lenschow et al., 2001; Perrino, 2010), while oxidation of precursor gases such as NO_x and SO_2 produces inorganic acids such as nitric acid (HNO_3) and sulphuric acid (H_2SO_4), respectively (Perrino, 2010). Similarly, mechanical processes such as wind and road-dust resuspension mainly generate coarse particles, while combustion activities mainly generate fine particles (WHO, 2005).

The characteristics of the particles, especially their size, in turn determine how long they remain suspended in the atmosphere (i.e., their residence time) (WHO, 2006; Perrino, 2010). For example, fine particles, due to their smaller size, have longer residence times than coarse particles as they are not easily removed from the atmosphere via dry deposition (WHO, 2006; Perrino, 2010). Residence time, in turn, determines how far the particles can be transported from where they are formed; particles with longer residence times tend to travel furthest from their source. Travel distances typically range between 500 and 1000 km for coarse particles and between 2000 and 4000 km for fine particles (WHO, 2006).

1.3. Impacts of PM_{10} pollution

Accumulation of PM_{10} in the atmosphere has a wide-range of consequences for climate, visibility, and human health. Based on their chemical compositions, the particles can affect climate by absorbing or scattering incoming solar radiation (the so-called ‘direct aerosol effect’) (Charlson et al., 1992; Tie and Cao, 2009; Perrino, 2010; Forkel et al., 2012). Absorption of solar radiation can lead to regional heating of the atmosphere, while scattering of solar radiation can cause cooling (Forkel et al., 2012). PM_{10} can also affect climate indirectly, through its influence on the optical properties of clouds (Tie and Cao, 2009; Forkel et al., 2012). Particles which serve as cloud condensation nuclei (CCN) can affect properties such as precipitation efficiency,

lifetime of clouds, and cloud cover (Tie and Cao, 2009; Forkel et al., 2012), thereby leading to indirect forcing through the changes in these properties (Tie and Cao, 2009; Forkel et al., 2012).

Absorption and scattering of solar radiation by PM_{10} can also reduce visible light (Wicking-Baird et al., 1997; Walton, 2005; Tie and Cao, 2009). Under high pollutant concentrations, the reduction of visible light can lead to impaired visibility (Knight et al., 1975; Wicking-Baird et al., 1997; Walton, 2005; Tie and Cao, 2009; Hidy et al., 1975), which can cause havoc on transportation, leading to difficulties in day to day life and economic development (Tie and Cao, 2009).

Due to their small size, PM_{10} can penetrate human lungs and cause a wide variety of cardiopulmonary diseases (Figure 1.2) (Folinsbee, 1992; Pope and Dockery, 2006; WHO, 2006). Exposure to the pollutant can decrease lung function (Pope et al., 1991), aggravate diseases such as asthma (Whittemore and Korn, 1980; Pope, 1991; Pope et al., 1991; Choudhury et al., 1997) and ischemia (Bell et al., 2008; Yitshak-Sade et al., 2015), and raise the likelihood of developing lung cancer (Pope et al., 2002; Parent et al, 2007; Tie et al., 2009). Studies have also linked maternal exposure to PM_{10} during pregnancy to adverse birth outcomes such as pre-term delivery (Ha et al., 2014), very pre-term delivery (Ha et al., 2014), and low birth weight (Chen et al., 2002; Dugandzic et al., 2006; Bell et al., 2007; Seo et al., 2010; Ha et al., 2014). Children born with these outcomes have a higher risk of respiratory failure shortly after birth (Escobar et al., 2006), childhood asthma (Sonnenschein-van der Voort et al., 2014), and developing disorders such as type 2 diabetes and insulin resistance later in life (Hofman et al., 2006).

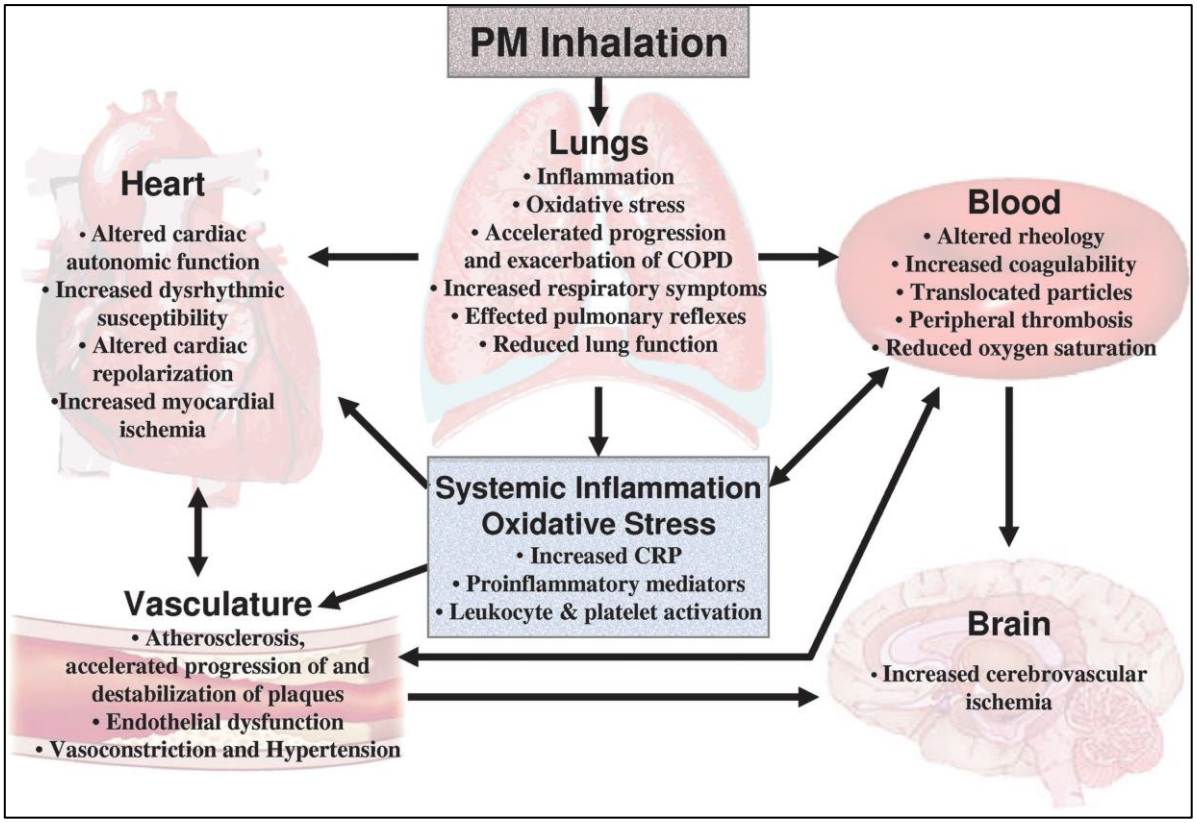

Figure 1.2: Potential biological mechanisms of cardiopulmonary disease and mortality linked to PM exposure (Source: Pope and Dockery, 2006).

1.4. Air quality in Cape Town and the problem of PM_{10} pollution

Poor quality is a problem which has long been a major concern in Cape Town (Wicking-Baird et al., 1997). During the 1950s and 1960s, the city experienced thick smog which was attributed to the three power stations in the city, industrial incinerators, coal-burning locomotives and tugs, and heavy fuel burning appliances (Wicking-Baird et al., 1997; Walton, 2005). In 1968, measures were taken by city council to reduce the air pollution, which was achieved successfully by the late 1970s through closure of two of the power stations, termination of coal-burning locomotives and tugs, and enforcement of standards for fuel burning appliances (Wicking-Baird et al., 1997; Walton, 2005). Despite these efforts, brown-coloured smog, which came to be known as “brown haze” (Figures 1.3 and 1.4), began to emerge as a serious air pollution problem in the city (Wicking-Baird et al., 1997).

Figure 1.3: Layer of brown haze pollution over the Cape Flats in Cape Town (Source: City Health Department, 2005).

Figure 1.4: Brown haze pollution over the southern suburbs of Cape Town (Source: http://footage.framepool.com/en/shot/900287203-table-mountain-cape-town-haze-landmark-sights).

The brown haze, which is largely due to the accumulation of PM_{10} in the atmosphere (Wicking-Baird et al., 1997; Weber, 2004; City Health Department, 2005; Walton, 2005), is a recurrent occurrence over Cape Town. The phenomenon, often accompanied by reduced visibility, occurs mostly between April and September as climatic conditions during this period favour its formation (Wicking-Baird et al., 1997).

It extends over large parts of the Cape Town metropolitan area but shifts with the wind direction (Wicking-Baird et al., 1997). The pollution is most intense in the morning (Wicking-Baird et al., 1997), and particulate concentrations during haze events can reach levels comparable to heavily-polluted international cities (Wicking-Baird et al., 1997).

As part of the efforts to reduce health impacts of poor air quality in Cape Town, city council undertakes various measures to combat local pollution. To get a better understanding of the brown haze pollution, city council initiated two studies, the Cape Town Brown Haze Study I, directed by the Energy Research Institute, and the Cape Town Brown Haze Study II, directed by the Climatology Research Group (Wicking-Baird et al., 1997; Weber, 2004). The first study aimed to identify the major sources of the haze and their relative contributions (Wicking-Baird et al., 1997), while the second study aimed to characterise the nature and properties of the haze (Weber, 2004). The municipality (as well as the Western Cape Government: Department of Environmental Affairs and Development Planning and the Airports Company South Africa in Cape Town) also operates a number of air quality monitoring stations which continuously measure ambient concentrations of PM_{10} in the city (City Health Department, 2005). Furthermore, the municipality also works towards improving the air quality in informal areas and controls local vehicle emissions in the city (City Health Department, 2005).

The PM_{10} pollution in the city has largely been attributed to local vehicle emissions (Wicking-Baird et al., 1997; Weber, 2004). Other concerning sources include the glass producing factory and the oil refinery, both located in the northern suburbs of Cape Town, as well biomass burning in townships (Wicking-Baird et al., 1997; Walton, 2005). Particularly, the township of Khayelitsha has been implicated as a major source of particulate pollution over Cape Town (City Health Department, 2005; Walton, 2005). This has mainly been attributed to domestic biomass burning for cooking and heating, as many households in the township do not have electricity (City Health Department, 2005). However, given that sources of PM_{10} can be both local and remote, it is possible that PM_{10} from outside of Cape Town contributes to the pollution in the city. Therefore, in order to effectively manage the health impacts of PM_{10}, there is a need to study the atmospheric conditions that favour occurrence of widespread PM_{10} episodes over Cape Town and to understand transport of the pollutant from remote and local sources

over the city during the episodes. This information is crucial for development of a reliable early warning system on PM_{10} episodes over the city. The present study is an attempt to provide such information.

1.5. Aims and objectives

The aim of this study is to investigate the transport of PM_{10} over Cape Town during high pollution episodes in the city. The objectives are to:

i. understand the spatial and temporal variations of observed PM_{10} concentrations in Cape Town and the associated atmospheric conditions;
ii. study the spatial distribution of PM_{10} and atmospheric conditions during high pollution episodes in Cape Town and examine how well the WRF-Chem model captures them;
iii. study the sensitivity of the WRF-Chem simulations to different chemistry parameterisation schemes; and
iv. investigate the influence of idealised emissions from Khayelitsha on the spatial distribution of PM_{10} concentrations over Cape Town.

The dissertation is divided into eight chapters. After the introduction, Chapter 2 presents the literature review, while Chapter 3 describes the data and methods used in the study. The results are presented and discussed from Chapters 4 to 7. The concluding summary and suggestions for future research are presented in Chapter 8.

Chapter 2 – Literature review

Chapter 2 reviews the relevant literature pertaining to high PM_{10} episodes. It looks at the factors associated with heavy PM_{10} pollution, namely: meteorological conditions, local pollution emissions, and long-range PM_{10} transport. The chapter also looks at various methodologies which have been applied to study the transport of PM_{10} pollution.

2.1. Factors inducing high PM_{10} levels

2.1.1. Meteorological conditions

Various studies have discussed the meteorological conditions which are conducive to high PM_{10} concentrations in the atmosphere. For example, Bielawska and Wardencki (2014) found that winter-time heavy PM_{10} events in Gdańsk (Poland) are linked to anti-cyclonic circulation over the city. Under the circulation pattern, the city experiences low temperatures, low wind velocities, and stable atmospheric conditions, often with an inversion layer, leading to accumulation of PM_{10} (Bielawska and Wardencki, 2014). Across the Baltic Sea, Pohjola et al. (2004) examined a heavy air pollution episode which occurred in Helsinki (Finland), in which concentrations of PM_{10} (and other pollutants) in the city were considerably high over a period of three days. The study showed that the enhanced pollution was caused by high atmospheric pressure conditions which prevailed over southern Finland during the episode period, leading to weak surface winds and formation of a strong surface radiation inversion.

Triantafyllou (2001) investigated the major synoptic circulation patterns associated with high PM_{10} episodes in the Eordea mountain basin, north-west of Greece. The study found that the pollution events were mostly a result of anti-cyclonic circulation over the basin, which occurs when a high pressure system covers the Balkan Peninsula or an anticyclone over central and western Europe extends or strengthens over the Peninsular, weakening the pressure gradient over the area. Under such conditions, subsidence inversions and weak winds develop over Eordea, trapping PM_{10} pollution in the basin. Nevertheless, the study also found that some PM_{10}

episodes in the basin occur under strong wind conditions associated with south-eastward moving cold fronts over southern Europe. These episodes were attributed to resuspension of dust, as the strong winds entrain dust particles into the ambient air (Triantafyllou, 2001).

In Calexico/Mexicali (the border area between Mexico and the United States), Kelly et al. (2010) showed that local PM_{10} episodes in the region, which commonly occur over winter, are associated with weak wind speeds (<2 m s^{-1}) and a stable boundary layer height below 500 m. He et al. (2014), who investigated a severe haze episode in Beijing (China), where daily-averaged PM_{10} concentrations reached 450 µg kg^{-1}, also showed that wind speed as well boundary layer height are key variables controlling the particulate pollution. Additionally, He et al. (2014) demonstrated the interplay between the two variables during the haze formation. The study showed that during high wind conditions, particle concentrations were mainly influenced by horizontal transport, as the severe haze only formed when the wind speed decreased considerably (below 1 m s^{-1}). Under the low wind conditions, the horizontal transport became weak, and concentrations were influenced by vertical mixing (He et al., 2014). Under a shallow planetary boundary layer height, particles accumulated near the surface and generated the high concentrations over Beijing (He et al., 2014).

Jury et al. (1990) studied the meteorological conditions associated with winter-time air pollution episodes in Cape Town. The study reported that the episodes are initiated by the passage of anti-cyclonic systems over the south-west coast of southern Africa. Under the circulation pattern, Cape Town experiences extended periods of subsidence motion, which promotes accumulation of pollution in the city (Jury et al., 1990). In addition, the study found that dry, north-easterly ‘berg’ winds are a common feature over Cape Town during the high pollution episodes (Jury et al., 1990). The berg winds, which occur over the city ahead of an approaching cold front, result in strong overnight temperature inversions and contribute to the development of the pollution episodes (Jury et al., 1990). Tesfaye et al. (2015) investigated the spatio-seasonal distributions of aerosol dust loadings over southern Africa. Their study showed that during autumn and winter, anti-cyclonic circulation over the region generates PM_{10} dust particles over the Namib and Kalahari desert areas and transports the particles towards the western and southern parts of South Africa (including the Western Cape Province).

Nevertheless, Jury et al. (1990) only considered the conditions associated with SO_2 and NO_x episodes and did not include PM_{10}, and Tesfaye et al. (2015) did not examine the influence of the dust on local PM_{10} concentrations over Cape Town (or any specific location). The present study examines the atmospheric conditions that are associated with PM_{10} episodes over Cape Town.

2.1.2. Local pollution emissions

Besides the influence of meteorological conditions, localised PM_{10} episodes result from the emission of large amounts of pollution into the atmosphere. Moreover, some activities, either due to the large extent over which they are conducted or the large amounts that individual sources emit, can result in substantially high ambient PM_{10} concentrations. For example, Mira-Salama (2008) analysed the PM_{10} particles during a severe smog episode in Krakow (Poland) and concluded that the pollution was mainly due extensive residential coal burning in the city. In New Zealand, Krivacsy et al. (2005) examined the chemical composition of PM_{10} in the cities of Auckland and Christchurch during winter-time high-level pollution episodes. The study showed that during the events, the PM_{10} in both cities are dominated by carbonaceous material, which is attributed largely to biomass burning for domestic heating. Aarnio et al. (2008) investigated both the local pollution- and long-range transport-induced PM_{10} episodes in Helsinki (Finland) and reported that the locally-driven episodes are due to traffic-induced suspension of dust particles.

In some instances, uncharacteristically high PM_{10} levels can occur due to anomalous local pollutant emissions. Globally, annual firework and bonfire displays during festival celebrations have been shown to generate large smoke plumes which result in a sharp increase in local PM_{10} levels. In Naples (Italy), for instance, high PM_{10} concentration events are often observed on the 1st of January and the 17–18th of the same month (Fortelli et al., 2016). The former is due to PM_{10} emissions from fireworks for New Year's celebrations, while the latter results from bonfires generated during the Saint Antony Abbot festival (Fortelli et al., 2016). In India, peak PM_{10} concentrations are often observed during the annual Diwali celebrations in October/November. Ambade (2018) analysed the air pollution deriving from fireworks displays during the religious festivities in Jamshedpur (India) and found that during Diwali day, extremely high 12-

h PM_{10} concentrations, up to 500 µg m^{-3}, were recorded in the city. The study also estimated that pollution from the fireworks accounted for 21 – 27% of the ambient PM_{10} concentrations in the city. Barman et al. (2008) found that in Lucknow City, India, the daily-average PM_{10} concentration during Diwali day can reach over 700 µg m^{-3}, which is up to 5 times higher than normal-day concentrations. In the United Kingdom (UK), firework and bonfire-related PM_{10} peaks are often observed around 5 December, during Guy Fawkes (or Bonfire Night) celebrations. Pope et al. (2016) studied the influence of Guy Fawkes bonfire and firework displays on the levels of ambient pollution in the UK and observed a sharp increase in the PM_{10} concentrations at various monitoring sites across the country.

In Cape Town, Wicking-Baird et al. (1997) quantified the relative contributions of major sources of the brown haze. The study reported that local vehicle emissions are the main source of the pollution, contributing about 65%. Emissions from local industries were the next major source, contributing about 22%, followed by wood-burning, which contributes about 11% (Wicking-Baird et al., 1997). Weber (2004), in agreement with Wicking-Baird et al. (1997), reported that vehicle emissions are the main source of the haze. Furthermore, Walton (2005) indicated that two local industries, Consol Glass and Caltex Oil Refinery, are major point sources, while the Airport, the CBD, and the townships of Mitchell's Plain and Khayelitsha are major area sources contributing to the haze. The present study improves knowledge on the transport and spatial distribution of PM_{10} from Khayelitsha during PM_{10} episodes in Cape Town.

2.1.3. Long-range transport

While the prevailing atmospheric conditions and local pollution emissions in an area can largely explain the occurrence of high PM_{10} concentration events, studies have also shown that the transport of PM_{10} from remote sources can lead to enhanced pollution levels at receptor sites. For instance, Sun et al. (2000) and Wang et al. (2004) have shown that high PM_{10}-concentration events regularly experienced in the spring in Beijing (China) are linked to transport of dust from Kazakhstan, Mongolia, and Inner Mongolia. On the other hand, elevated PM_{10} concentrations in Seoul (South Korea) have been linked to transport of carbonaceous, fine, and coarse particles from heavily-industrialised areas in east and north-east China (Jeong et al., 2011). Between

October and November of 2012, Delhi (India) experienced a severe smog episode that enveloped the region for several consecutive days (Sati and Mohan, 2014), where daily-averaged PM_{10} concentrations of up to 989 μg m^{-3} were recorded over the city (Sati and Mohan, 2014). Sati and Mohan (2014) examined the air pollution during the episode and showed that the smog resulted from the transport of soot and smoke particles deriving from the agricultural waste burning in the Punjab area, north-west of Delhi.

The passage of deep low pressure systems and their associated cold fronts over Australia often generates strong winds that entrain large amounts of dust over the continent, resulting in massive dust storms (Knight et al., 1995; Leys et al., 2011). During one such event, which occurred in September of 2009 (Leys et al., 2011), particles were transported eastwards from central Australia and resulted in daily-average PM_{10} concentrations exceeding 1700 μg m^{-3} at various locations along the Australian east coast (Leys et al., 2011). Transport of dust particles during the storms can also surpass the continental boundary, crossing the Tasman Sea and into New Zealand (Knight et al., 1995). For instance, Knight et al. (1995) estimate that, of the ~1.9–3.4 Mt of dust lost from the Australian continent during a December 1987 dust storm, ~1.7–3.0 Mt were transported into New Zealand. Dust storms over Asia have also been shown to cause massive pollution episodes far beyond the continental boundary. For example, Husar et al. (2001) tracked an intense dust storm that formed over the Gobi Desert (Mongolia and north central China) in April of 1998 and demonstrated that over a few days, the dust crossed the Pacific Ocean and reached the North American west coast. The dust cloud covered most of the west coast, from California to British Columbia, increasing PM_{10} concentrations up to 100 μg m^{-3} over British Columbia (Husar et al., 2001). Furthermore, Zhao et al. (2008) investigated the influence of Asian dust transported across the Pacific on PM_{10} concentrations in North America and showed a strong correlation between inter-annual variability of Asian dust storms and PM_{10} levels the western United States.

Countless studies have also shown that dust from the Sahara Desert (in North Africa) is a major source of PM_{10} episodes well beyond the African continent. For instance, peak PM_{10} concentration events over the Canary Islands (Viana et al., 2002; Menendez et al., 2009) and across the Mediterranean region, including the Iberian

Peninsula (Rodriguez, et al., 2001; Escudero et al., 2006), central Italy (Nava et al., 2012), Greece (Matthaios et al., 2017), the Anatolian Peninsula (Kabatas et al., 2018), and Cyprus (Achilleos et al., 2014), have been associated with the intrusion of dust-rich air masses originating from the Sahara Desert. In south Germany, Flentje et al. (2015) estimated that almost all high-PM_{10} events between 1997 and 2013 resulted from transport of dust from the Sahara. In the UK, Ryall et al. (2002) examined a heavy PM_{10} episode which occurred over England and Wales in March of 2000 and showed that the pollution resulted from the long range transport of Saharan dust. Another study, Vieno et al. (2016), showed that dust from the Sahara Desert was one of the major contributors to the high PM_{10} event which occurred in the UK between March and April of 2014. The long-range transport of Saharan dust has also been linked to peak PM_{10} concentration events in Japan (Lee et al., 2003; Lee et al., 2010).

The findings of these studies show that there is a pressing need to monitor PM_{10} pollution on a regional scale over southern Africa. Some recent studies (i.e., Jenner & Abiodun, 2013, Abiodun et al., 2014, and Nzotungicimpaye et al., 2014) have investigated the influence of regional pollution transport in Cape Town. Abiodun et al. (2014) investigated the transport of nitrogen oxides (NOx) and nitric acid (HNO_3), Jenner and Abiodun (2013) studied the transport of atmospheric sulphur, and Nzotungicimpaye et al. (2014) the transport of tropospheric ozone (O_3). These studies linked episodes of NO_x, SO_2, and O_3 pollution, respectively, in Cape Town to regional transport of pollution from the coal field emissions on the Mpumalanga Highveld. However, none of the studies focused on remote sources of PM_{10} in Cape Town. Hence, the present study will improve knowledge on transport of PM_{10} into Cape Town.

2.2. Approaches for studying transport of PM_{10}

Previous studies have used adopted approaches or methods for studying transport of PM_{10} over an area. For example, Sati and Mohan (2014) used a combination of HYSPLIT and remote sensing data to study formation of the air pollution during the November 2012 smog episode over Delhi. The remote sensing data consisted of MODIS fire maps and ultra violet aerosol index (UVAI) data (Sati and Mohan, 2014). The fire maps were used to observe the occurrence and locations of agricultural waste fires over the Punjab area (north-west of Delhi) during the episode period, while

HYSPLIT forward trajectories were used to track the transport of air parcels from the fire locations into Delhi (Sati and Mohan, 2014). The study not only analysed the November 2012 smog event, but also looked the same period over the two previous two years, to observe the unique conditions which lead to the episode. The maps showed that fires over the Punjab were of the same extent in both 2010 and 2011, but the trajectories showed that the 2012 episode resulted from a larger number of air parcels from the fire area being advected towards Delhi (compared to the previous two years). Furthermore, the study used UVAI data to infer the increase in smoke and soot over Delhi during the 2012 episode, reflecting the biomass burning-origin of the particles over the city.

Cheng et al. (2013) used HYSPLIT, the MM5 meteorological model, and CAMx to investigate the regional transport pathways that result in high PM_{10} events Guangzhou (China) and their relative contributions to the pollution in the city. In the study, output from the MM5 was used as input for running HYSPLIT, which was applied to conduct back trajectories of air parcels into Guangzhou. CAMx was used to simulate PM_{10} concentrations over Guangzhou and its surrounding areas, as well as to calculate the source appointment from different pollution sources and regions over the area. After the major air pollution transport pathways to Guangzhou were identified from the trajectories, the contribution from the various transport pathways to the PM_{10} pollution in Guangzhou was then calculated from the CAMx source apportioning (Cheng et al., 2013).

Viana et al. (2002) combined HYSPLIT back trajectories, station observations, TOMS aerosol index maps, and SeaWiFS imagery to examine the impact of North African dust transport on high PM_{10} events in the Canary islands. The station observations were used to identify episodes, and HYSPLIT trajectories were used to track the sources of air parcels arriving over the Islands during the episodes. The trajectories showed that the heaviest episodes occurred when air parcels originated over North Africa, and then TOMS maps and SeaWIFs imagery were utilized to confirm dust plumes extending from North Africa into the islands during some of the heavy episodes.

Although WRF-Chem has not been as extensively used as HYSPLIT to investigate PM_{10} transport, some studies have shown that the model can be effectively applied for the purpose. For example, Gupta and Mohan (2013) used WRF-Chem to study the influence of long-range pollution transport during high PM_{10} levels in Delhi (India). For the investigation, the study examined the influence of different geographical areas by running the model with nested domains, each progressively smaller than the parent domain (viz., covering all of Asia, only India, only North India, and the inner most domain covering only the Delhi region). Then, the study assessed the influence of remote sources on the pollution by examining the correlation between PM_{10} observations and simulations (of varying geographical coverage) at various monitoring locations over the city. The results indicated that the model performed worst at reproducing the observed pollutant concentrations (especially the peaks) when the domain only covered the Delhi region, and improved progressively with increasing geographical domain coverage, which was used to infer the influence of regional and long-range transport pollution in the city. Kabatas et al. (2018) applied WRF-Chem to simulate and study the distribution of Saharan dust during an outbreak which contributed to enhanced daily PM_{10} concentrations over Turkey.

The studies reviewed show that both HYSPLIT and WRF-Chem are valuable tools which can be used to assess the influence of remote PM_{10} sources at receptor sites. Furthermore, the studies show how monitoring the transport of the pollutant is effectively achieved when multiple techniques are used together. Hence, this study combines HYSPLIT and WRF-Chem to study the transport of PM_{10} over Cape Town during high pollution episodes.

Chapter 3 – Methodology

Chapter 3 presents the data and methods used in the study. It describes the observations, the criteria applied to identify PM_{10} episodes in Cape Town, the WRF-Chem model set-up, and the series of simulations performed with the model. The datasets used for the WRF-Chem simulations and trajectory analyses are also described.

3.1. Station observation data

Various organisations operate air quality monitoring stations in Cape. The stations typically measure ambient concentrations of selected air pollutants (e.g., PM_{10}, NO_2, O_3, and SO_2) as well as relevant meteorological parameters (e.g., wind speed and direction, temperature, and rainfall) over Cape Town. This study used data from thirteen of the stations in the city (Figure 3.1b), obtained from the Scientific Services, Water and Sanitation Department of the City of Cape Town, the Department of Environmental Affairs and Development Planning (Western Cape), and Airports Company South Africa (ACSA, Cape Town). The data comprised hourly PM_{10} concentrations, temperature, wind speed, and wind direction for the period 2008 – 2014 (the study period). The data were used to study the temporal variations of PM_{10} in Cape Town and the associated atmospheric variables, to identify PM_{10} episodes in the city, and to evaluate the WRF-Chem model.

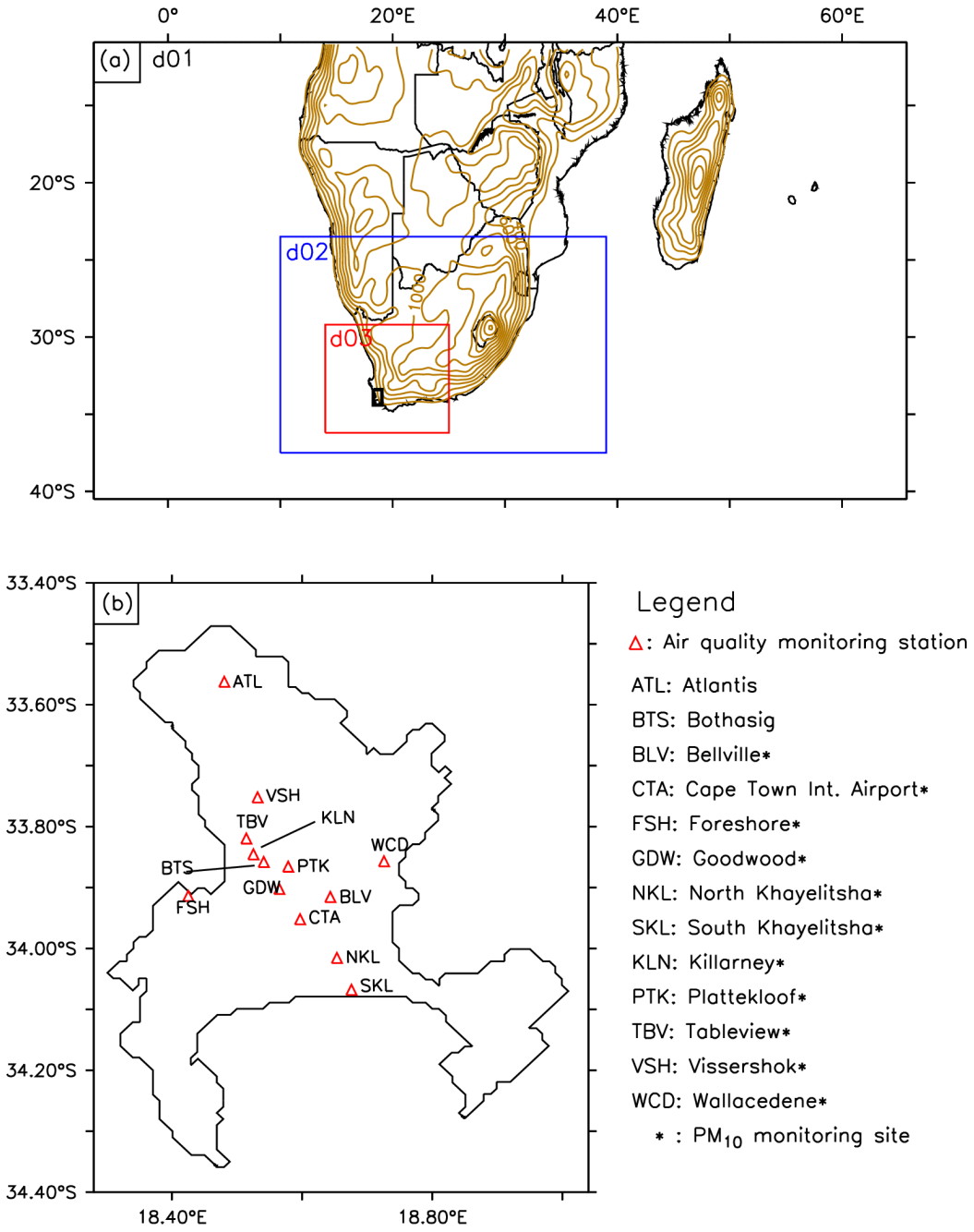

Figure 3.1: (a) The WRF-Chem simulation area showing the three nesting domains (d01, d02, and d03) used in this study. The brown contour lines show the topography, while the small black box indicates the location of Cape Town. The bottom panel (b) shows locations of the air quality monitoring stations in Cape Town used in the present study.

3.2. Selection of PM_{10} episodes in Cape Town

In this study, a PM_{10} episode was defined as a day where the daily average concentration of PM_{10} in Cape Town exceeded the South African daily (24-hour average) ambient air quality standard of 75 µg m^{-3} (Department of Environmental

Affairs, 2009) at two or more monitoring stations. Nine episodes were identified over the study period: one each in 2008 and 2012, two each in 2010 and 2011, and three in 2009. The episodes were named using the year in which they occurred. Where more than one episode was identified in a single year, alphabetical characters were used to represent the chronological order in which the episodes occurred. Table 3.1 provides a summary of the dates as well as the durations of the episodes.

Table 3.1: The durations and dates of the PM_{10} episodes identified in Cape Town between 2008 and 2014.

Episode	Duration (no. of days)	Date
2008	2	24 June 2008 − 25 June 2008
2009a	1	05-Mar-09
2009b	1	03-Apr-09
2009c	1	04-Jul-09
2010a	1	02-Jun-10
2010b	1	08-Jul-10
2011a	1	09-Jul-11
2011b	2	15 July 2011 − 16 July 2011
2012	1	25-Apr-12

3.3. WRF-Chem model and simulations

The Weather Research and Forecasting model with chemistry (WRF-Chem, version 3.6.1) (Grell et al., 2005; Fast et al., 2006) was used in the study. WRF-Chem is a fully-coupled online model which can simulate the transport, chemical transformation, and mixing of aerosols and trace gases simultaneously with meteorological fields (Grell et al., 2005). A detailed description of the model is provided in Grell et al. (2005). For this study, the model was configured with three two-way nested domains (Figure 3.1a), using the Lambert conformal projection. The largest domain (d01), which is centred at 29.57^{o} E and 27.00^{o} S, covers most of southern Africa with 384 x 200 (longitude x latitude) grid points at an 18 x 18 km horizontal resolution. The second largest domain (d02), which covers most of South Africa, has 502 x 295 (longitude x latitude) grid points at a 6 x 6 km horizontal resolution, while the smallest domain, covering most of the Western Cape Province, has 541 x 421 (longitude x latitude) grid points at a 2 x 2 km horizontal resolution. Vertically, the model spans 31 sigma levels.

The model was applied to perform three experiments. The first experiment (hereafter, RMS) was used to examine how well WRF-Chem reproduces the observed PM_{10} and wind over Cape Town during the nine episodes and to study the spatial and temporal distribution of wind and PM_{10} transport during the events. The RMS simulations used the RADM2 chemistry scheme (Stockwell et al., 1990) coupled with the MADE/SORGAM aerosol module (Ackermann et al., 1998; Schell et al., 2001) (i.e., chem_opt = 41), with the Lin microphysics scheme (Lin et al., 1983). The RMS simulations include aqueous phase chemistry and account for aerosol-radiation feedback and indirect aerosol effect (including wet-scavenging). RADM2 combined with the MADE/SORGAM aerosol module has been extensively applied in the literature (e.g., Forkel et al., 2012; Kumar et al., 2016) to study aerosols over different parts of the world, including in southern Africa (e.g., Kuik et al., 2015).

The second experiment (hereafter, RGC) was used to test the sensitivity of WRF-Chem simulations to a change in the chemistry parameterisation. The RGC set-up used the RADM2 chemistry scheme combined with the GOCART aerosol module (Chin et al., 2000) (i.e., chem_opt = 303), with the WSM5 microphysics scheme (Hong et al., 2004). RADM2 chemistry scheme combined with the GOCART aerosol module is a non-aqueous chemistry parameterisation scheme. Hence, while RMS simulations allowed for aerosol feedbacks, the RGC simulations did not.

The third experiment (KAYE) was used to study the influence of PM_{10} emissions from Khayelitsha, one of the major contributors to the PM_{10} load in Cape Town (e.g., Walton 2005). The set-up for KAYE is similar to that of RGC, except that an idealized continuous area emission (of 10 mol km^{-2} hr^{-1}) was introduced over the Khayelitsha area (18.61^{o} – 18.76^{o} E; 34.10^{o} – 33.98^{o} S). Since RGC and KAYE do not allow for aerosol feedbacks, their simulated atmospheric conditions will be the same and the difference between their simulated PM_{10} concentrations will be due to the influence of the idealised emissions from Khayelitsha.

For each experiment, nine simulations were performed, one for each episode identified in the study. Each simulation covers a period of either thirteen days (for episodes 2008 and 2011b) or twelve days (for the remaining seven episodes), which comprises the six days before, during, and the five days after the episode. The first day of each

simulation was regarded as model spin-up and not included in the analyses. For all the simulations, the Goddard short-wave radiation scheme (Chou and Suarez, 1994), the RRTMG long-wave radiation scheme (Mlawer et al., 1997), the YSU planetary boundary layer scheme (Hong et al., 2006), NOAH LSM scheme (Chen and Dudhia, 2001), the Fast-J photolysis scheme (Wild et al., 2000), and the Grell 3-D cumulus parameterisation scheme (Grell and Devenyi, 2002) were applied.

All the simulations were initialised and forced at the lateral boundaries using the NCEP CFSR data (Saha et al., 2010; Saha et al., 2011). The NCEP CFSR dataset, which has a 0.5^{o} x 0.5^{o} horizontal resolution and 6-h temporal resolution, was interpolated to the model grid using the WRF Pre-processing System (WPS). Due to the lack of comprehensive emission inventories for southern Africa, global emissions data obtained from the PREP-CHEM-SRC (version 1) emission pre-processor package (Freitas et al., 2011) were applied. The pre-processor utilised emissions from three inventories, viz., EDGAR version 4 (Olivier et al., 1996), GOCART (Chin et al., 2002), and RETRO (Schultz et al., 2007). Freitas et al. (2011) provide a detailed description of the pre-processor and the datasets. Although the resolution of emission datasets used in the simulations may be too low to account for local sources of PM_{10} (Figure 3.2), they were used to meet the aim of the study which is to investigate the influence of regional transport of PM_{10} (from the remote sources) on air quality over the city during PM_{10} episodes.

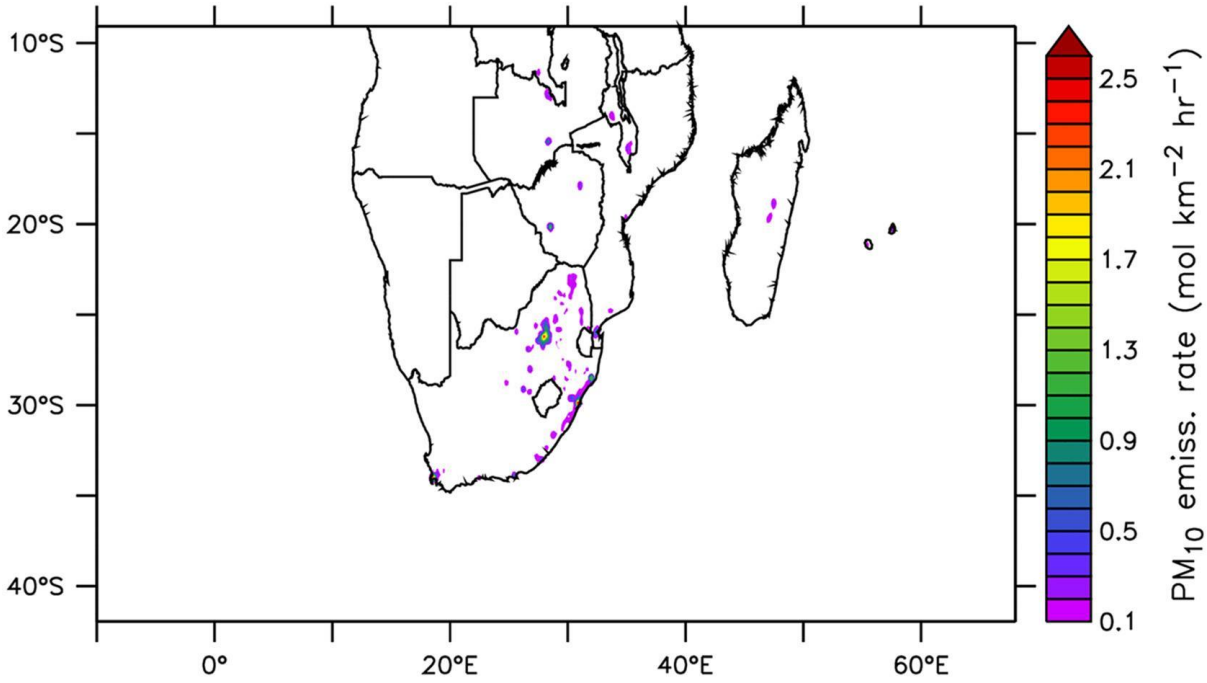

Figure 3.2: Emissions rates of PM_{10} over the study domain.

3.4. Air parcel trajectories

To identify the transport pathways of air parcels arriving in Cape Town during the identified PM_{10} episodes, the study analysed three sets of back-trajectory simulations: one from the HYSPLIT model (Draxler and Hess, 1998), one using the RMS simulations as input, and another using the RGC simulations as input. The HYSPLIT model is able to compute simple air parcel trajectories to complex chemical transformation, dispersion, and deposition simulations (Stein et al., 2015). A detailed description of the HYSPLIT model can be found in Draxler and Hess (1998). The model has been widely applied to compute back trajectory analyses to determine the origin of air masses (e.g., Escudero et al., 2006; Middleton et al., 2008; Lee et al., 2010; Jeong et al., 2011; He et al., 2014; Stein et al., 2015). A web-based version of HYSPLIT, provided through NOAA ARL's READY platform (Rolph et al., 2017), was used in this study. For each episode, the model was used to compute three back trajectories, one each at 10, 100, and 1000 m above ground level. The trajectories, with a starting location of 18.66° E, 33.92° S (roughly the centre of Cape Town), were calculated over a four-day (96-hour) period, starting at the end (0000 UTC) of each episode (or the end of the first day of the episode, in the cases of 2008 and 2011b). The Global Data Assimilation System with a horizontal resolution of 1° x 1°, 23 vertical

layers, and a 3-hour temporal resolution (GDAS1), available on READY, was used to drive HYSPLIT.

The other two sets of trajectories, one using the RMS simulations and the other using RGC simulations, were computed from a separate Lagrangian trajectory model. These trajectories were calculated with the same starting heights, location, and time as those of HYSPLIT.

Chapter 4 – Results and discussion part I: Temporal variation of observed PM_{10} in Cape Town

This chapter describes the temporal characteristics of the observed PM_{10} concentrations in Cape Town, with a focus on the diurnal, daily, and seasonal variations. It discusses how atmospheric conditions might have contributed to the variations and compares the pollutant characteristics in the study with those reported in previous studies.

4.1. Diurnal variation

The diurnal variation of PM_{10} concentrations over Cape Town (Figure 4.1a) shows two distinct peaks: a morning and an afternoon peak. The morning peak occurs between 07:00 and 09:00, while the afternoon one occurs between 16:00 (e.g., at Killarney) and 20:00 (e.g., at the Airport). The distinction between the two peaks is clear at all the stations except Foreshore and Plattekloof. While Foreshore features a morning peak only, Plattekloof features an afternoon peak only. The difference between the magnitudes of the morning and afternoon peaks varies across the stations; it is relatively large (over 11.00 μg m^{-3}) over North Khayelitsha and Vissershok (where the morning peak is noticeably higher than the evening peak), but small (less than 4.00 μg m^{-3}) for the remaining stations. The morning and afternoon peaks may be due to traffic emissions of PM_{10}, as many people commute to school and work in the morning and back home in the afternoon. Moreover, in the morning people generally commute to school and work around the same time, but tend to commute back home at different times. This could explain why the morning peak occurs over a shorter period than the afternoon peak. The traffic emissions could also explain why, for most of the stations, the difference in the magnitudes of the morning and afternoon peak is small. For those stations it could be that, overall, the volume of traffic that passes through and produces the peak in the morning is about the same as that in the afternoon.

Among the stations, North Khayelitsha features the highest PM_{10} concentration throughout the day (Figure 4.1a). This is likely due to additional emissions of PM_{10} from activities other than traffic. Many households in the township of Khayelitsha lack basic services such as electricity and resort to burning coal, wood, and paraffin for

cooking and heating (City of Cape Town, 2018). Although the cooking and heating may occur throughout the day (which might explain why the pollutant concentrations over North Khayelitsha are elevated all day), these activities are likely more prevalent in the afternoon/evening, as more people are in their homes around that time (having come from school and work), families cook dinner, and fires are generated for heating against cold night-time temperatures. This could explain why the afternoon peak is much higher than the morning peak in North Khayelitsha. Although the South Khayelitsha station is located in the same general area as the North Khayelitsha station, it experiences much lower PM_{10} concentrations. This may be because the South Khayelitsha station is located in a section of the township that has more formal housing, where biomass burning for cooking and heating is less prevalent. Nevertheless, the results agree with previous studies (e.g., Walton, 2005; Tessema, 2011), which observed that Khayelitsha has some of the highest PM_{10} concentrations in Cape Town.

Atmospheric conditions could also be contributing to the overall diurnal variation of PM_{10} concentrations in Cape Town. In the morning, weak surface wind speeds (Figure 4.1b) may inhibit pollution dispersion and increase concentrations of PM_{10}. In the afternoon, stronger winds may enhance dispersion, which lowers the pollutant concentrations. Moreover, in the morning, shallow temperature inversions, induced by low morning temperatures (Figure 4.1c), can inhibit vertical mixing, which increases PM_{10} concentrations. As the surface warms up In the afternoon, the increased temperature can erode the shallow inversion. This would in turn enhance vertical mixing and reduce PM_{10} concentrations. Most of the stations experience the lowest PM_{10} concentration between 12:00 and 14:00, when wind speeds and temperatures are the highest (Figure 4.1).

The characteristics of the diurnal variation of PM_{10} observed in the present study are similar to those reported by previous studies for SO_2 (Jenner and Abiodun, 2013), NO_x (Abiodun et al., 2014), and O_3 (Nzotungicimpaye et al., 2014) over Cape Town. For example, these studies also found two peaks in the diurnal cycles of SO_2, O_3, and NO_x over most of the stations. However, there are some differences in the timing of the peaks. While the morning peak in the diurnal variation of PM_{10} is comparable to that of SO_2 and NO_x (viz., at 08:00; Jenner and Abiodun, 2013; Abiodun et al., 2014), it is

different from those of O_3 (viz., between 01:00 and 05:00 and between 12:00 and 15:00; Nzotungicimpaye et al., 2014). This is expected as both SO_2 and NO_x are precursor gases for certain atmospheric particles (Perrino, 2010; Edgerton et al., 1999; Kumar et al., 2016), while O_3 is produced via photochemical processes (Nzotungicimpaye et al., 2014).

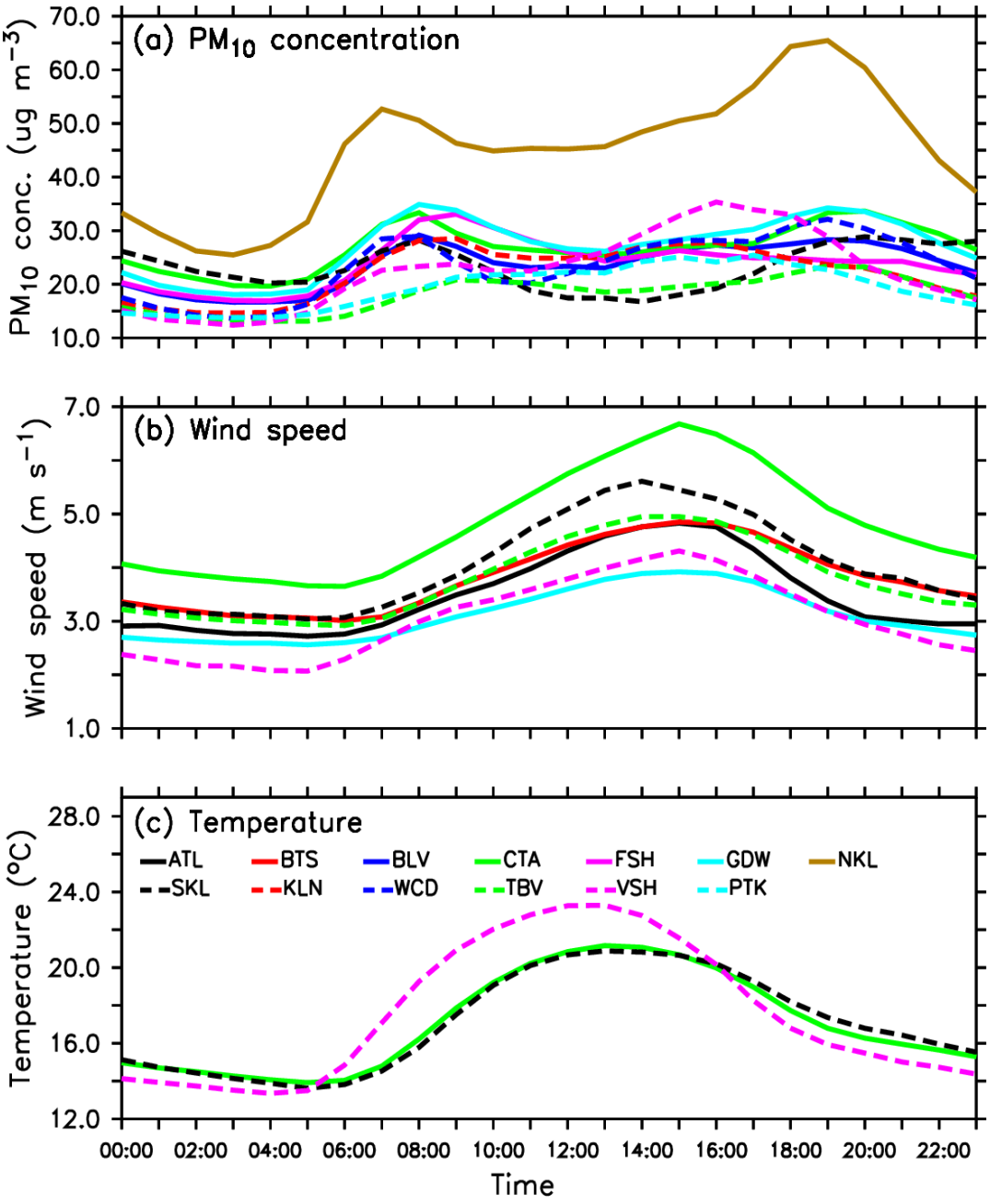

Figure 4.1: The diurnal variation of observed (a) PM_{10} concentration, (b) surface wind speed, and (c) temperature at various monitoring stations in Cape Town between 2008 and 2014.

4.2. Daily variation

The daily PM_{10} concentration at the stations is highly variable (Figure 4.2). The concentration can vary from 4.17 to 128.50 µg m^{-3} (at Wallacedene in 2008) or 6.17 to 192.80 µg m^{-3} (at North Khayelitsha in 2013) at a single station. Instances of daily concentrations of 0 µg m^{-3} are also observed (for example, Goodwood at the start of December 2008 or Goodwood in mid-July 2009), but these are likely due to mechanical failures at the monitoring stations. On numerous occasions, the concentration of the pollutant exceeded both the World Health Organization (WHO) and the South African 24-hourly mean standards for PM_{10} (50 µg m^{-3} and 75 µg m^{-3}, respectively) at one or more stations. Between 2008 and 2014, the daily concentration of PM_{10} in Cape Town exceeds the South African standard at one or more stations a total of 153 times (18, 36, 7, 11, 40, 22, and 19 days in 2008, 2009, 2010, 2011, 2012, 2013, and 2014, respectively). Days where the pollutant exceeds the national standard at a single station are spread out randomly and show no particular pattern. However, days of more widespread pollution, when the pollutant exceeds the standard at two or more stations (i.e., episodes) occur in the autumn to winter months (i.e. between March and July). Nonetheless, it is possible that more episodes occurred outside this period, but due to missing data, they could not be identified. For example, between September and mid-December 2010 (Figure 4.2c), or January to May 2011 (Figure 4.2d), PM_{10} data is available from only one station, so the criteria of an episode (as defined in this study) cannot be met.

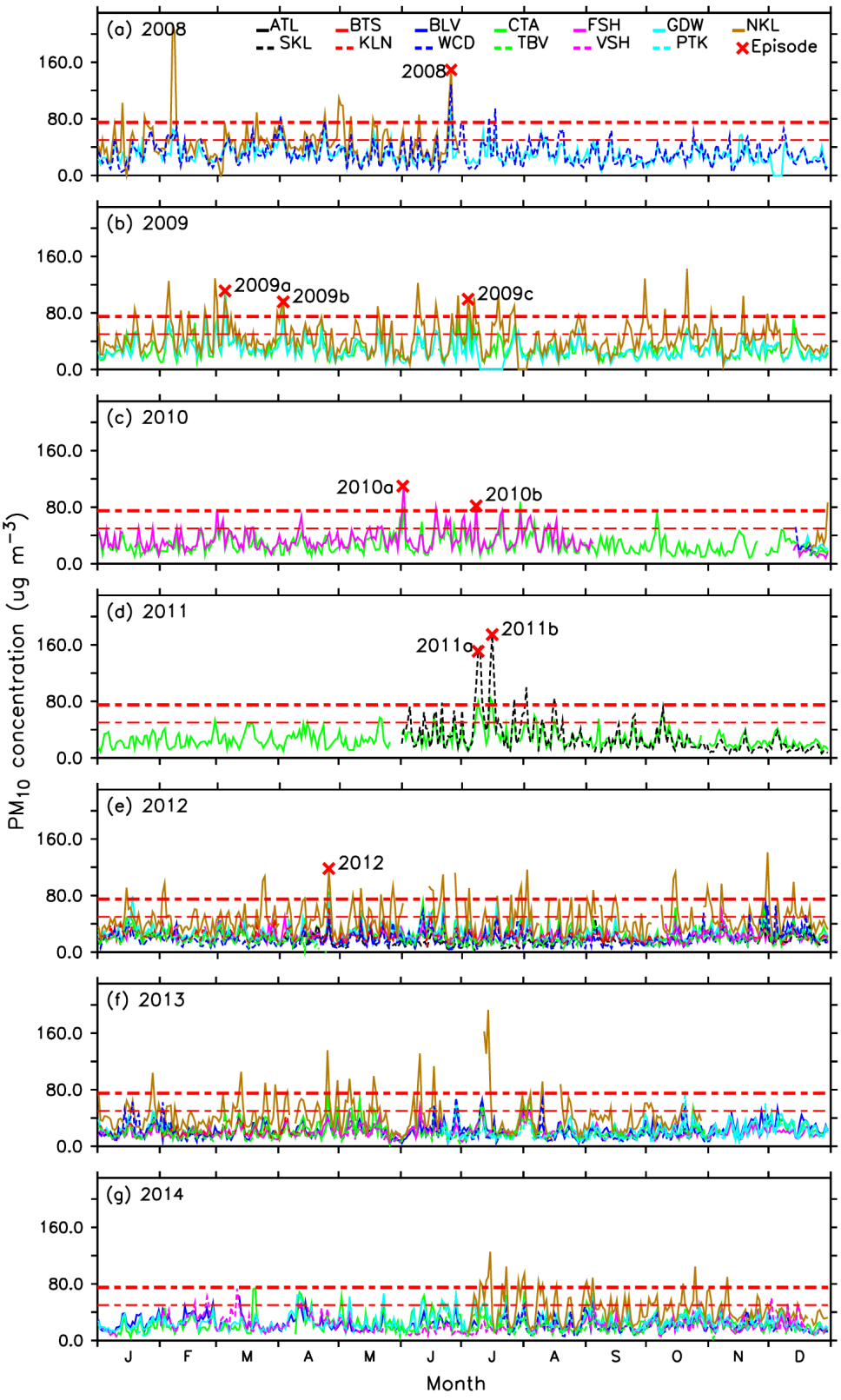

Figure 4.2: Time series of the observed daily mean PM_{10} concentration at Cape Town monitoring stations between 2008 and 2014. The thin and thick red horizontal lines show the World Health Organization (WHO) and the South African 24-hourly mean PM_{10} standards (50 µg m^{-3} and 75 µg m^{-3}, respectively).

4.3. Seasonal variation

The concentration of PM_{10} over the city also varies with seasons, and the pattern of the seasonal variation differs across the stations (Figure 4.3a). For instance, in autumn and winter (March to August), while four stations (Foreshore, the Airport, Killarney and North Khayelitsha) experience more than the annual mean PM_{10} concentration, Vissershok experiences less than the annual mean PM_{10} concentration. In late spring and early summer (October to December), two stations (Foreshore and the Airport) experience less than the annual mean PM_{10} concentration, while Bellville experiences more than the annual mean PM_{10} concentration. The seasonal amplitude of some stations (e.g., Tableview) is relatively weak.

The observed meteorological variables show that the seasonal variations in surface wind speed and temperature are similar across each set of stations (Figures 4.3b and 4.3c, respectively). This suggests that, generally, the whole area of Cape Town experiences weaker wind speeds and lower temperatures in winter (and the reverse in summer). The seasonal variation of the meteorological variables can thus be used to explain the seasonal PM_{10} variation over some of the stations. For instance, the weak surface wind speeds (Figure 4.3b) and low surface temperatures (Figure 4.3c) during autumn and winter are consistent with higher than annual PM_{10} concentrations observed at Foreshore, the Airport, Killarney, and North Khayelitsha during those seasons. Both meteorological conditions inhibit pollution dispersion and lead to high PM_{10} concentrations. Furthermore, the occurrence of elevated pollutant concentrations in the autumn and winter and the associated meteorological conditions are similar to those reported for other pollutants, such as SO_2 (Jenner and Abiodun, 2013) and NO_x (Abiodun et al., 2014), in Cape Town. However, the meteorological conditions do not explain the PM_{10} seasonal cycle over Vissershok or the weak seasonal variability of the pollutant at the other stations. Nevertheless, due to the lack of surface wind and temperature data at most of the PM_{10}-monitoring stations, the study cannot conduct an in-depth, station-by-station analysis of the influence of meteorology on the seasonal variation of the pollutant. A plausible explanation for the patterns at Vissershok and the other stations could be that missing PM_{10} data throw off the realistic seasonal cycle.

The seasonal variation in local emission sources may also contribute to the observed seasonal patterns of PM_{10} over the city. For example, in North Khayelitsha (a largely informal settlement), during autumn and winter it is likely that more fires are generated for heating against the cold(er) temperatures, contributing to the higher than normal PM_{10} concentrations observed in those seasons. Although the same reason may not be applicable to the non-informal settlement stations which also exhibit higher than normal PM_{10} concentrations in autumn and winter (i.e., Foreshore, the Airport, and Killarney), transport of the pollutant from North Khayelitsha could be responsible for the elevated pollution over the stations. This is consistent with the results of the thesis (see Chapter 7), which show that PM_{10} emitted in Khayelitsha can affect other parts of Cape Town.

In addition, seasonal variability in the load from regional transportation may also play a role. For instance, Tesfaye et al. (2015) showed that large areas of the Western Cape Province experience remote mineral dust from the Kalahari and Namib desert areas during the autumn to winter months. This is also consistent with the results of this thesis (see Chapter 6). However, while one might expect that regional transport should impose higher than normal PM_{10} concentrations over a wide area, the results of this thesis show how topography might influence the spatial distribution of the pollutant over Cape Town (see Chapter 6).

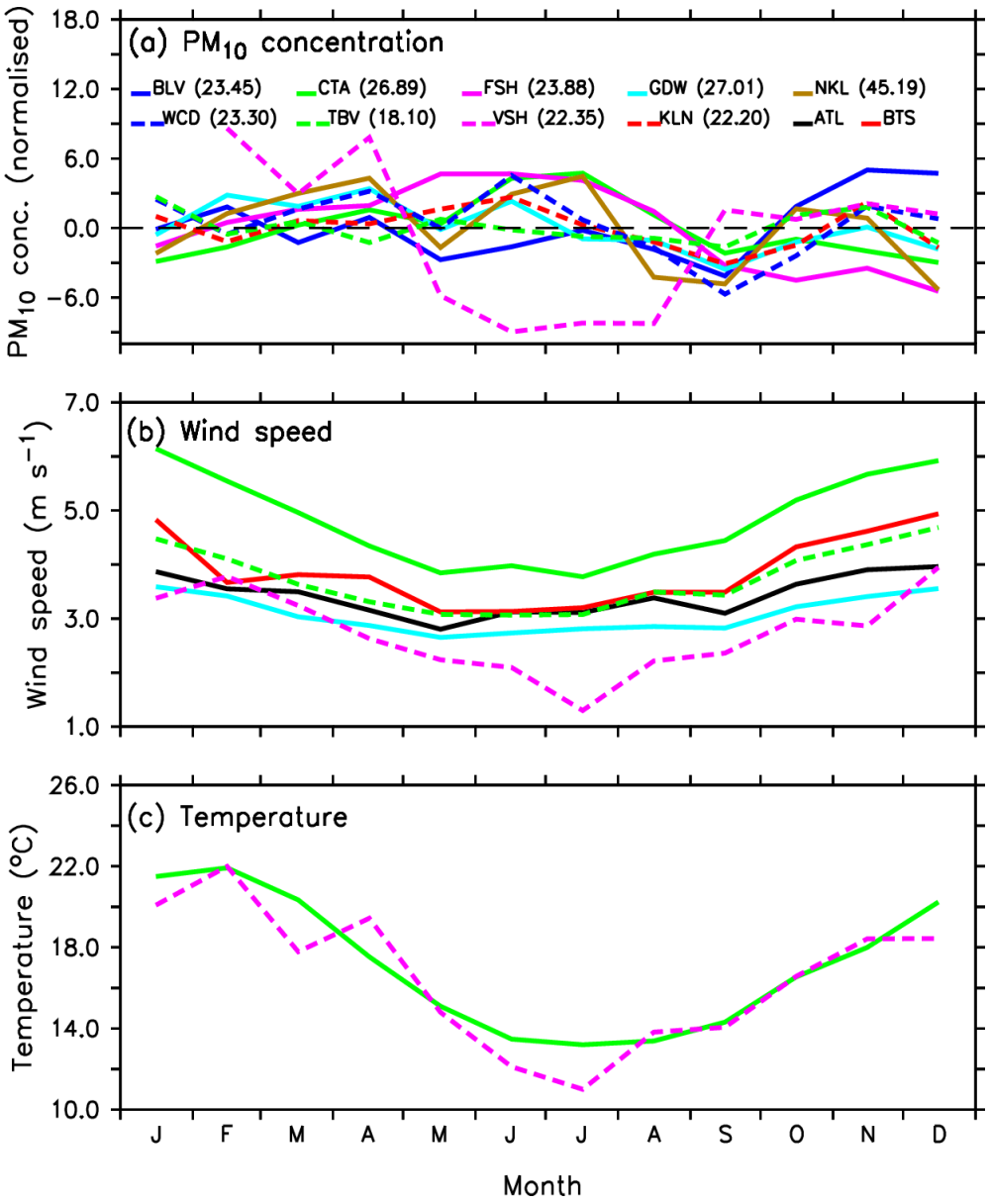

Figure 4.3: Seasonal variation of (a) PM_{10} concentration anomalies (in μg m^{-3}), (b) surface wind speed, and (c) temperature as observed at various monitoring stations in Cape Town over the study period. The PM_{10} anomalies are with respect to the annual mean over each station. The annual mean values for the stations are shown inside the brackets (in μg m^{-3}). Stations with less than 11 months' data have been excluded.

Chapter 5 – Results and discussions part II: The simulated transport of PM_{10} over Cape Town during the episodes

This chapter presents and discusses the results of the RMS simulations. The chapter starts by evaluating the capability of RMS in reproducing the observed PM_{10} and surface wind over Cape Town. The evaluation focuses on the capability of the model to simulate the daily PM_{10} concentration and surface wind speed and direction observed during the 11 to 12 days window of the episodes (i.e., the 5 days before, during, and 5 days after each episode). In the evaluation, measurements from the various monitoring stations over Cape Town have been averaged to represent the observations, while averages over the land area covering the city (18.40^o – 18.80^o E; 34.10^o – 33.50^o S) are used to represent the simulations. Additionally, for easy comparison, the observed and simulated PM_{10} concentrations are standardised (using the mean and standard deviation for each episode window in each dataset).

Following the evaluation is a discussion (and comparison) of the trajectory analyses (of air parcels in Cape Town during the PM_{10} episodes) from HYSPLIT and the RMS output. Next is a discussion of the synoptic conditions and PM_{10} transport associated with RMS-simulated peak days. RMS-simulated peak day refers to the day on which the parameterisation scheme simulates the highest PM_{10} concentration in Cape Town over the 11 to 12 day window of each observed episode (discussed in the evaluation). The discussion focuses on the spatial distribution of PM_{10} concentration and the associated meteorology (10 m wind as well mean sea level pressure) over the 2 days before and during each peak. Lastly, the chapter looks at the impact of topography on the spatial distribution of PM_{10} during the simulated peak days.

5.1. Model evaluation

The performance of RMS in capturing the daily variability of the observed PM_{10} concentration over Cape Town during the 11 to 12-day windows varies across the episodes (Figure 5.1). While the correlation between the observed and RMS-simulated PM_{10} concentrations over the windows is very high for episode 2008 (r = 0.86), it is poor for episodes 2010b and 2011a (r = 0.22 and 0.14, respectively) and very poor for 2009a, 2009b, 2009c, 2010a, 2011b, and 2012 (r = -0.38, -0.16, -0.15, -0.54, -0.02,

and -0.06, respectively). RMS generally underestimates the concentration of the observed PM_{10}, with the negative bias ranging from 7.31 µg m^{-3} (day +4 of episode 2012) to 122.10 µg m^{-3} (on the second day of episode 2011b). Nonetheless, the RMS simulations capture a local peak in PM_{10} concentration for all episode windows, although, in most cases the peak occurs earlier or later than in the observations. The local peak in the RMS-simulated PM_{10} occurs on the same day as in the observations for episode 2008, a day later for 2010a and 2012, two days earlier and two days later for episodes 2009b and 2011a, respectively, three days earlier for 2010b and 2011b, three days later for 2009a, and five days later for episode 2009c (Figure 5.1).

RMS's performance in simulating surface wind over Cape Town during the episode windows also varies (Figures 5.2 and 5.3). The model captures the wind speed very well for episodes 2009a, 2009b, 2009c, 2010a, 2010b, and 2012 (r = 0.86, 0.89, 0.82, 0.87, 0.84, and 0.87, respectively), and moderately well for episodes 2011a and 2011b (r = 0.50 and 0.46, respectively) (Figure 5.2). In general, the RMS-simulated wind speeds are comparable to the observed wind speeds, but the simulations underestimate the observations in some cases and overestimate them in others. The positive bias in the simulations ranges from 0.02 m s^{-1} (day -4 of episode 2010b) to 3.13 m s^{-1} (on the day of episode 2011a), while the negative bias ranges from 0.02 m s^{-1} (e.g., day +1 of 2010a) to 2.37 m s^{-1} (day +2 of 2009b). Regarding the wind direction, generally, RMS captures the south-easterly to south-westerly direction which is most frequently observed over the episode windows (Figures 5.2 and 5.3).

There is no direct relationship between RMS's performance in capturing the variability of the PM_{10} concentration and the variability of the wind over Cape Town. For instance, despite the good performance in reproducing the wind speed and wind direction for the 11-day window of episode 2009a, the model performs very poorly in reproducing the PM_{10} concentration for the same window. There may be several reasons for this. It could be due to the lack of exact PM_{10} emissions over the modelling domain. It could also be due to the shortcomings of the RMS set-up; the model may be struggling to simulate important processes (such vertical mixing or convection) which affect the modelled PM_{10}.

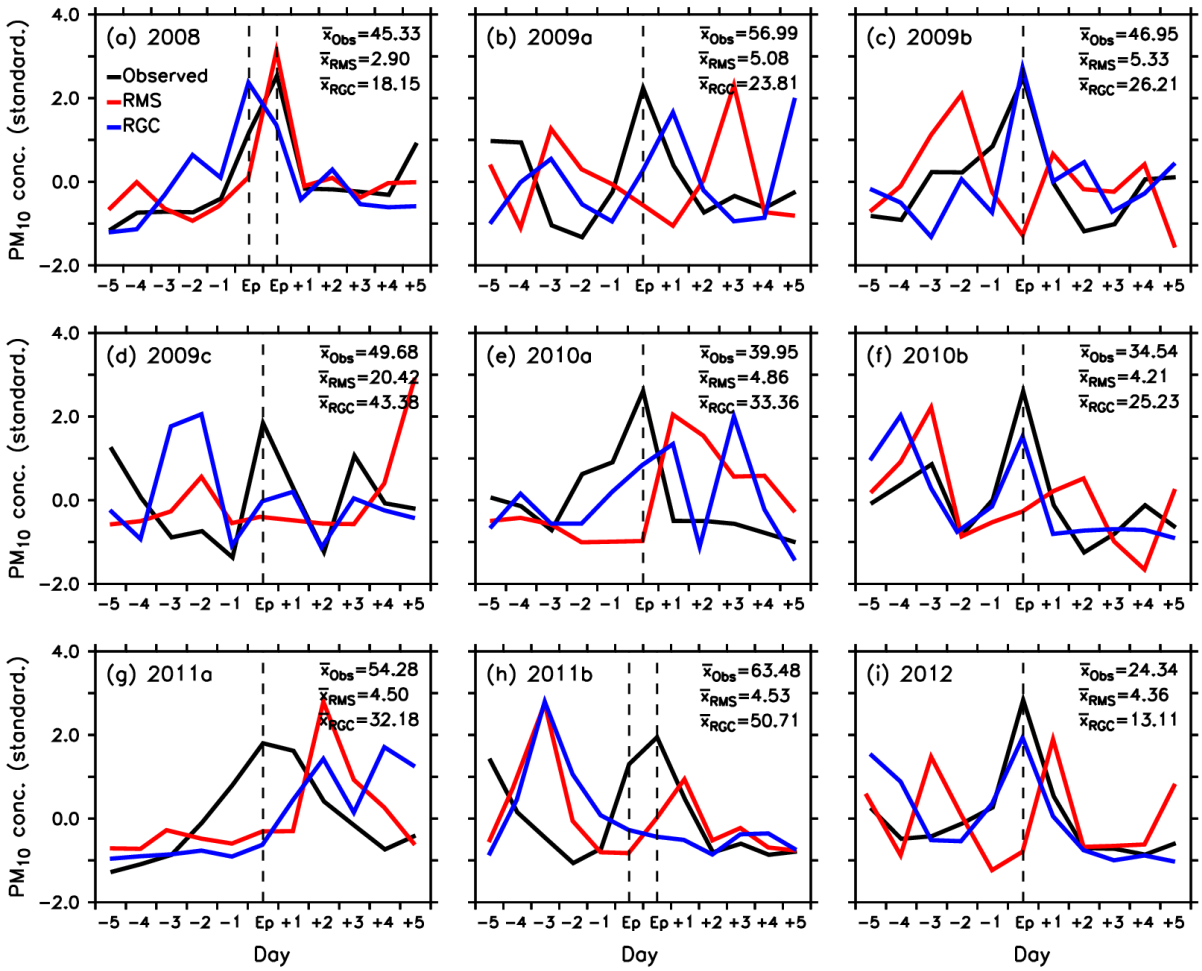

Figure 5.1: Observed, RMS-simulated, and RGC-simulated daily PM_{10} concentration (in μg m^{-3}) over Cape Town during the 11 – 12 days window of the episodes identified in this study. The dashed vertical lines indicate the episode day(s). For each episode window and each dataset, the PM_{10} concentration has been standardised with the mean and standard deviation. The observed, RMS-simulated, and RGC-simulated PM_{10} mean values ($\bar{x}_O$, $\bar{x}_{RMS}$, and $\bar{x}_{RGC}$, respectively; in μg m^{-3}) are shown for each episode window.

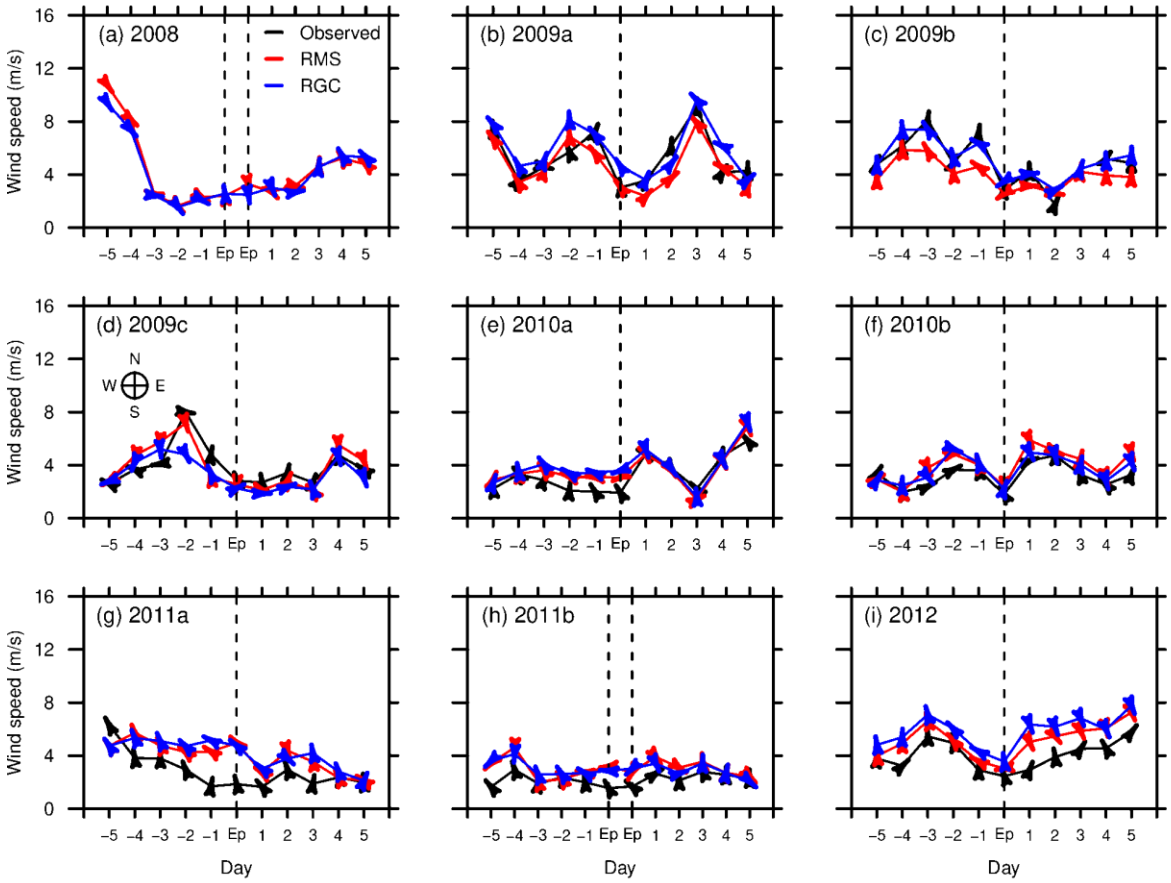

Figure 5.2: Observed, RMS-simulated, and RGC-simulated daily surface wind speed and direction over Cape Town during the 11 – 12 days window of the episodes identified in the study. The dashed vertical lines indicate the episode day(s) and the arrows show the wind direction. Wind observations are not available for 2008.

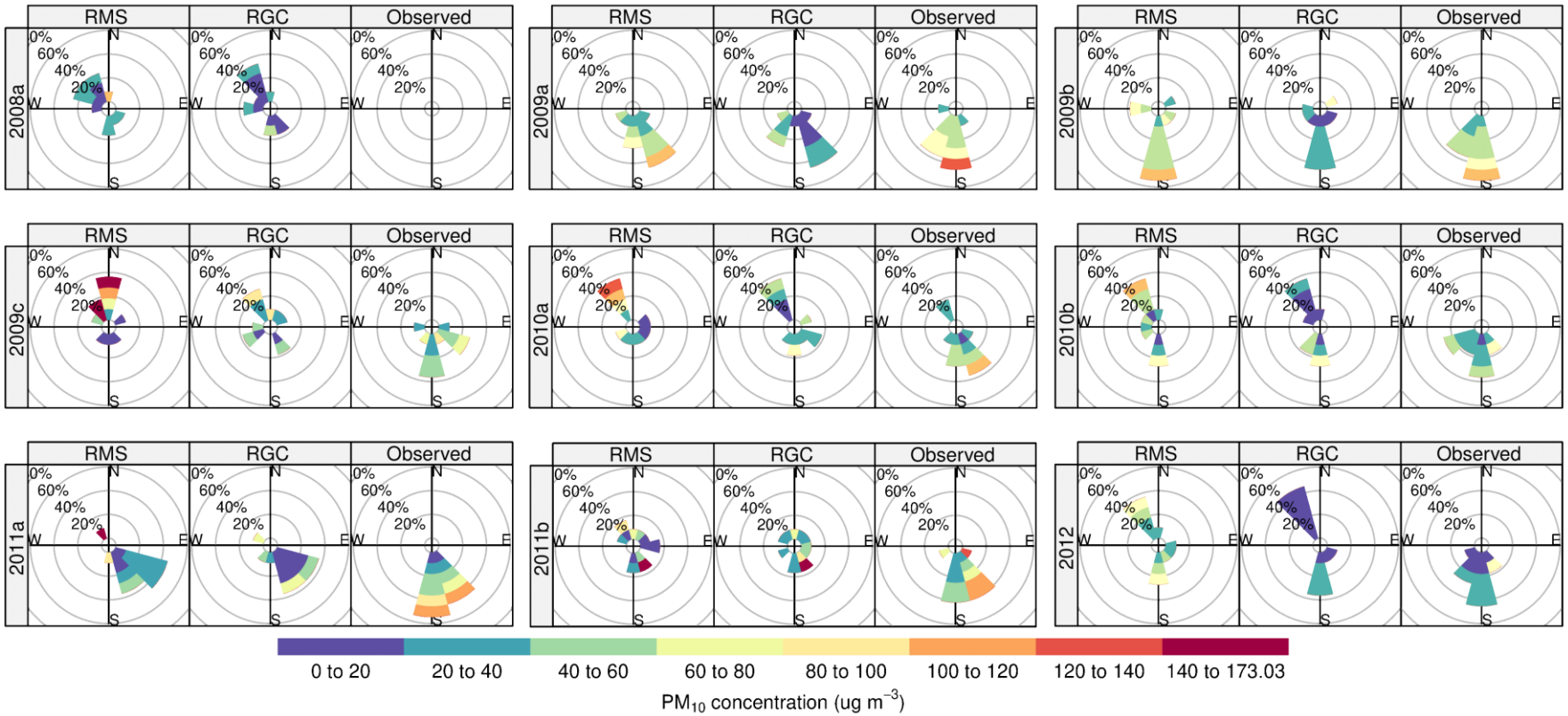

Figure 5.3: Pollution rose plots of the observations, RMS simulations and RGC simulations over Cape Town during the 11 – 12 days window of the episodes. The plots show the simulated and observed PM_{10} concentration for wind coming from the indicated directions. For comparison purposes, the simulated PM_{10} for RMS has been multiplied by 10. Wind observations are not available for 2008.

5.2. Trajectories of air parcels associated with the observed PM_{10} episodes

The HYSPLIT trajectories (Figure 5.4) show that most of the air parcels that arrived in Cape Town during the observed PM_{10} episodes were either from the southern African interior or the Namibian coast (or both). In some cases, all air parcels at the three heights (10, 100, and 1000 m) over the city were from the same area, while in others, they were from different areas. For example, all the air parcels were from the southern African interior during episodes 2009c, 2011b, and 2012 (Figures 5.4d, 5.4h, and 5.4i, respectively) and from the Namibian coast during episodes 2008 and 2011a (Figures 5.4a and 5.4g, respectively). In the remaining four episodes, 2009a, 2009b, 2010a, and 2010b, at least one of the air parcels was from either the southern African interior or the Namibian coast (Figures 5.4b, 5.4c, 5.4e, and 5.4f, respectively). There are only two episodes (2009a and 2009b; Figures 5.4b and 5.4c, respectively) in which the surface (i.e., 10 m) air parcel was from the ocean south of the continent. Nevertheless, the HYSPLIT trajectories indicate that the air parcels from the southern African interior undertook a north-easterly trajectory and travelled through the Kalahari Desert before reaching Cape Town. All the air parcels from the Namibian coast were either advected south along the Namib Desert and then the South African coast, or were transported towards the Kalahari and then deviated south towards Cape Town. The surface air parcel from the ocean travelled in a south-westerly or southerly direction, and then deviated easterly to reach Cape Town.

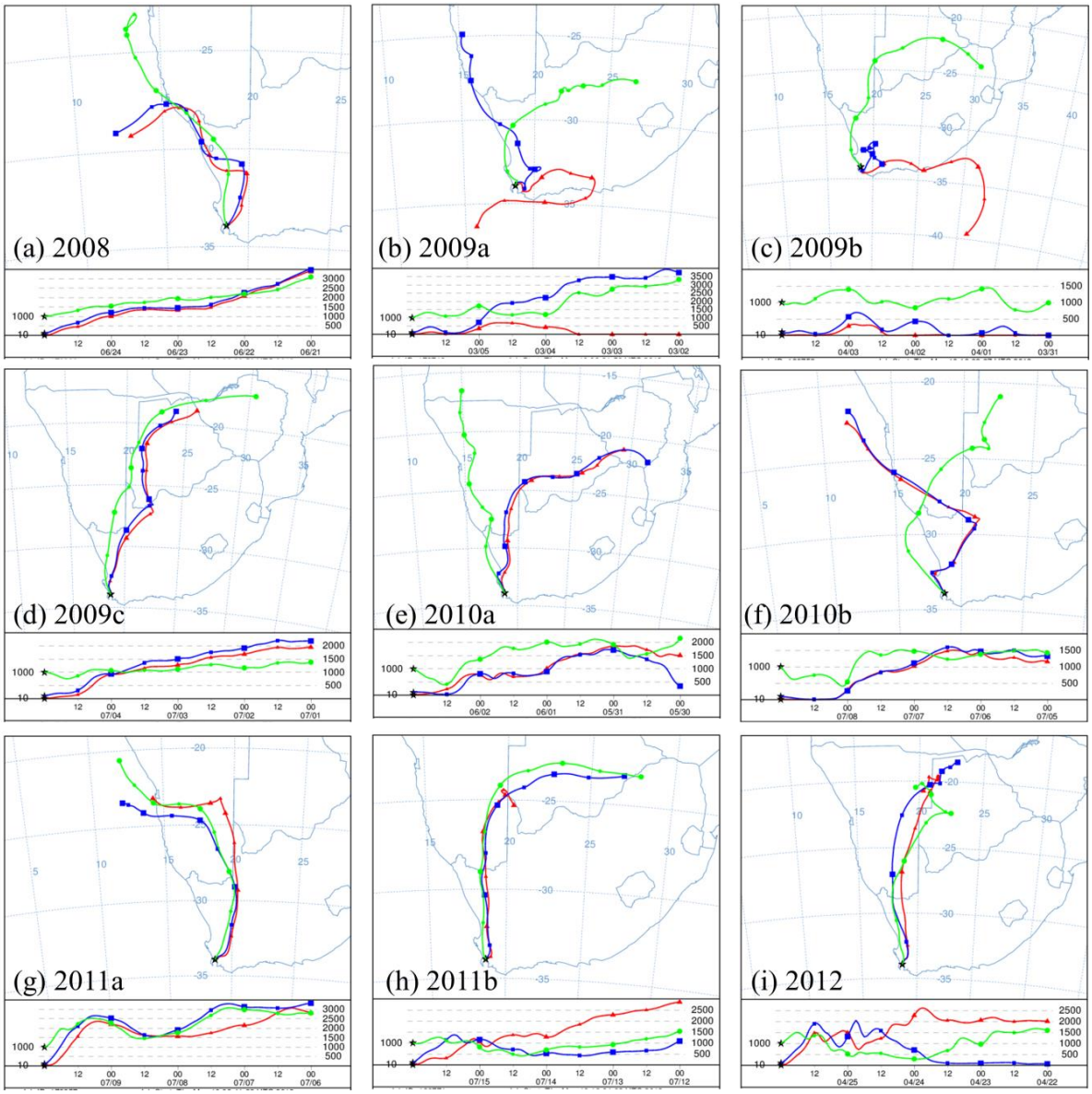

Figure 5.4: 4-day back trajectories of air parcels in Cape Town at different heights (10, 100, and 1000 m) during the identified PM_{10} episodes, computed with HYSPLIT.

The trajectories generated with the RMS output (Figure 5.5) are similar to those of HYSPLIT, showing that most of the air parcels in Cape Town were from central southern Africa or the Namibian coast. In particular, RMS agrees with HYSPLIT that all the air parcels over Cape Town during episode 2008 were from the Namibian coast. However, there is some disagreement between the RMS and HYSPLIT trajectories during some of the episodes. For instance, during episode 2012, HYSPLIT indicates that all the air parcels (at all three heights) were from central southern Africa, but RMS shows that they were from the west coast of Namibia and Angola (Figures 5.4i and 5.5i). In addition, with HYSPLIT, there is a better agreement between the trajectories of the air parcels at the three heights than with RMS. For example, during episodes

2009c, 2011a, and 2011b, HYSPLIT shows that the three parcels (at the different heights) were from the same area (Figures 5.4d, 5.4g, and 5.4h, respectively), but RMS indicates that they were from different areas (Figures 5.5d, 5.5g, and 5.5h, respectively). Although the RMS trajectories also show the ocean-originating 10 m air parcel during episode 2009a, the parcel originates further north-east than in the HYSPLIT results (Figures 5.4b and 5.5b). The discrepancies between the trajectories of the two Lagrangian models may be largely due to the differences in the meteorological datasets used to drive the models. Trajectory calculations are sensitive to properties such as vertical and horizontal resolutions of the input meteorological data (e.g., Su et al., 2015), both of which were different in the datasets used to drive the two models in the present study. Nevertheless, the back trajectories generated with both HYSPLIT and RMS driven trajectory model agree that the air parcels associated with the PM_{10} episodes in Cape Town travelled along (and possibly picked up dust from) one of the major dust sources on the sub-continent, viz., the Namib and Kalahari deserts.

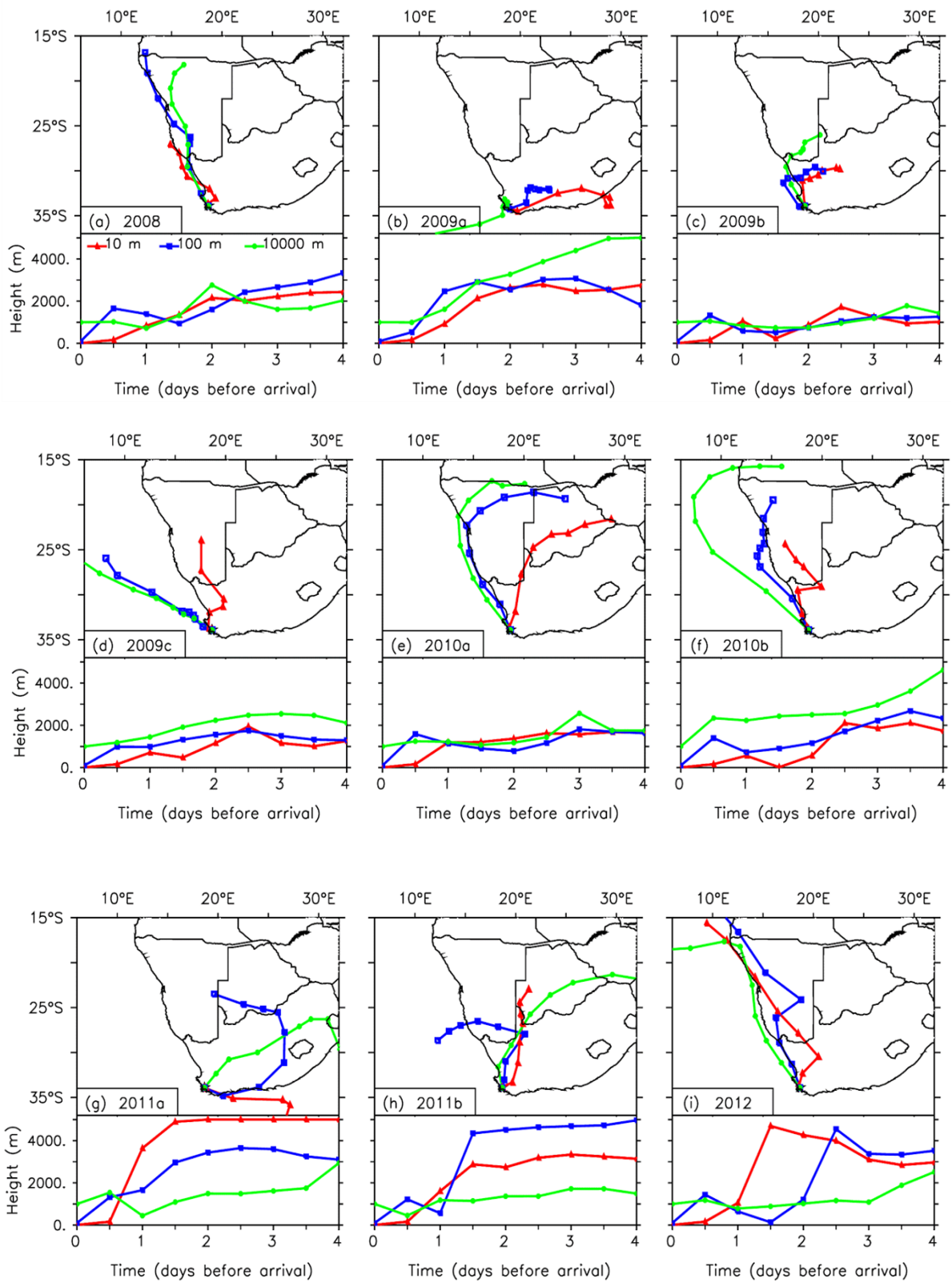

Figure 5.5: Similar to Figure 5.4, but computed with a separate trajectory model using RMS simulations as input.

5.3. The transport and spatial distribution of PM_{10} during peak days

In the RMS simulations, the peaks in PM_{10} concentration over Cape Town are linked to transport of the pollutant from the north-west coast of southern Africa (Figures 5.6 and 5.9). The sequence of days linked to the peaks feature a trough which produces a plume of PM_{10} along the west coast. The coastal trough, which is well-established on the days prior to the peaks, is associated with north-easterlies over the sub-continent and south-westerlies over the Atlantic Ocean. The north-westerlies transport PM_{10} over the Namib Desert into the trough, while the south-easterlies transport some of the PM_{10} towards the Atlantic Ocean; however, some of the PM_{10} accumulates and forms the pollution plume along the trough, with highest concentrations mostly along the edge of the continent (Figures 5.6 and 5.8). Through various mechanisms, PM_{10} from the plume is transported into Cape Town and induces the peaks. For most of the peaks (2008, 2009c, 2010a, 2010b, 2011a, and 2011b), the pollution is channelled into the city by northerly flows associated with the trough and a high-pressure system over the sub-continent (Figures 5.6 and 5.9). Furthermore, on some of the peak days, for example 2010a and 2011a (Figures 5.6o and 5.6u, respectively), a col[1] is present over Cape Town, producing weak wind and poor dispersion of the pollutant. Transport of the PM_{10} into Cape Town for peak 2012 is largely driven by a coastal low-pressure system as it moves towards the city (Figures 5.6y – 5.6a* and 5.9y – 5.9a*). For the remaining two peaks (2009a and 2009b), the PM_{10} is transported into Cape Town by south-westerly winds along the trough. The RMS-simulated synoptic patterns agree well with observations for peaks 2011a, 2011b, and 2012 (Figures 5.6 and 5.7)[2].

[1] Col refers to a neutral area of low pressure that lies between two high pressure systems, or the point of intersection between a ridge and a trough (Abiodun et al., 2014), and is associated with weak winds that produce stagnant air flow (Abiodun et al., 2014).

[2] Synoptic weather charts for previous years are not available.

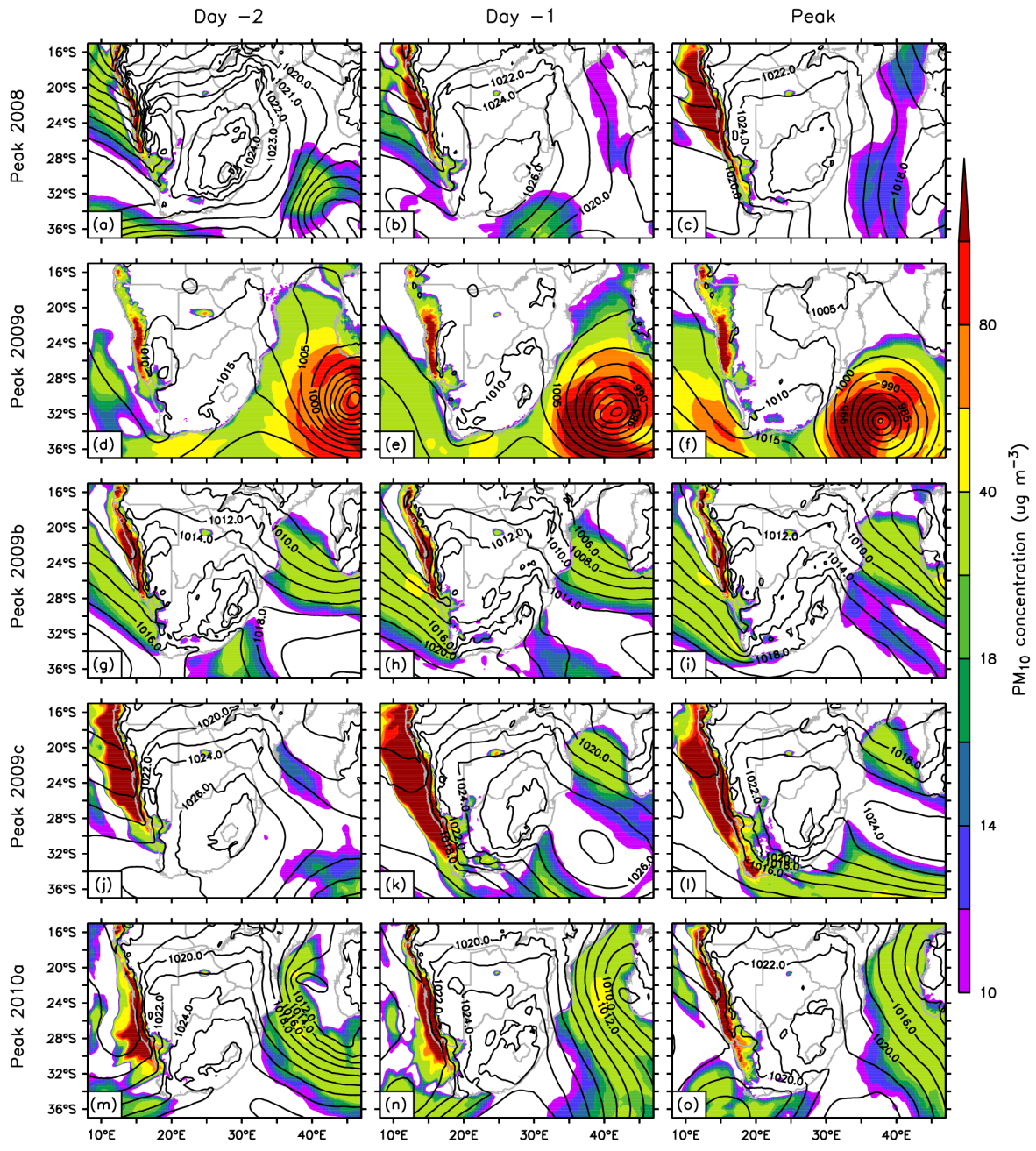

Figure 5.6: The spatial distribution of RMS-simulated PM_{10} concentration and associated sea-level pressure for the sequence of days linked to the RMS peaks in Cape Town. Each row shows the two days before the peak (Day -2; Day -1) and the day of the peak.

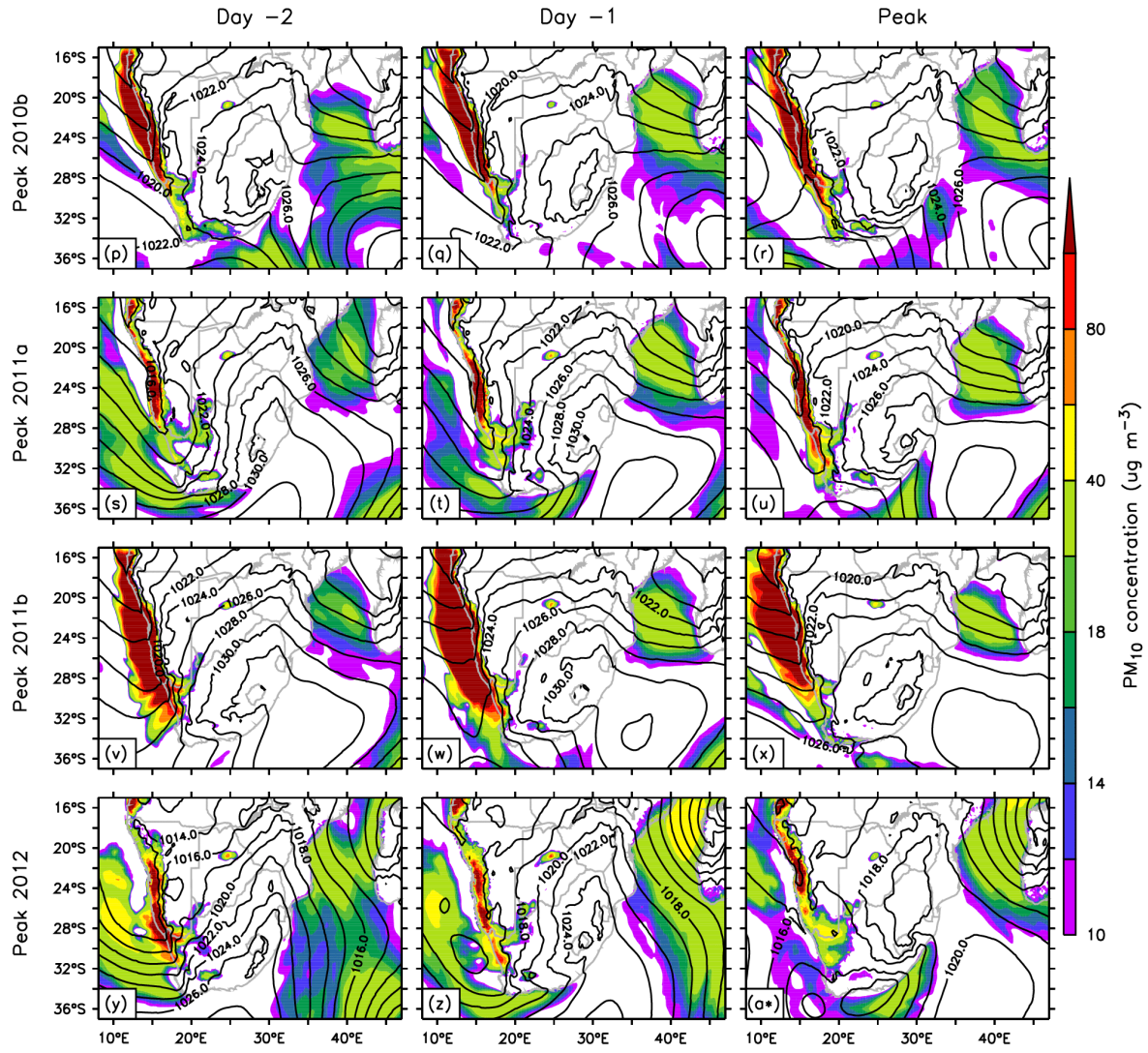

Figure 5.6: (continued).

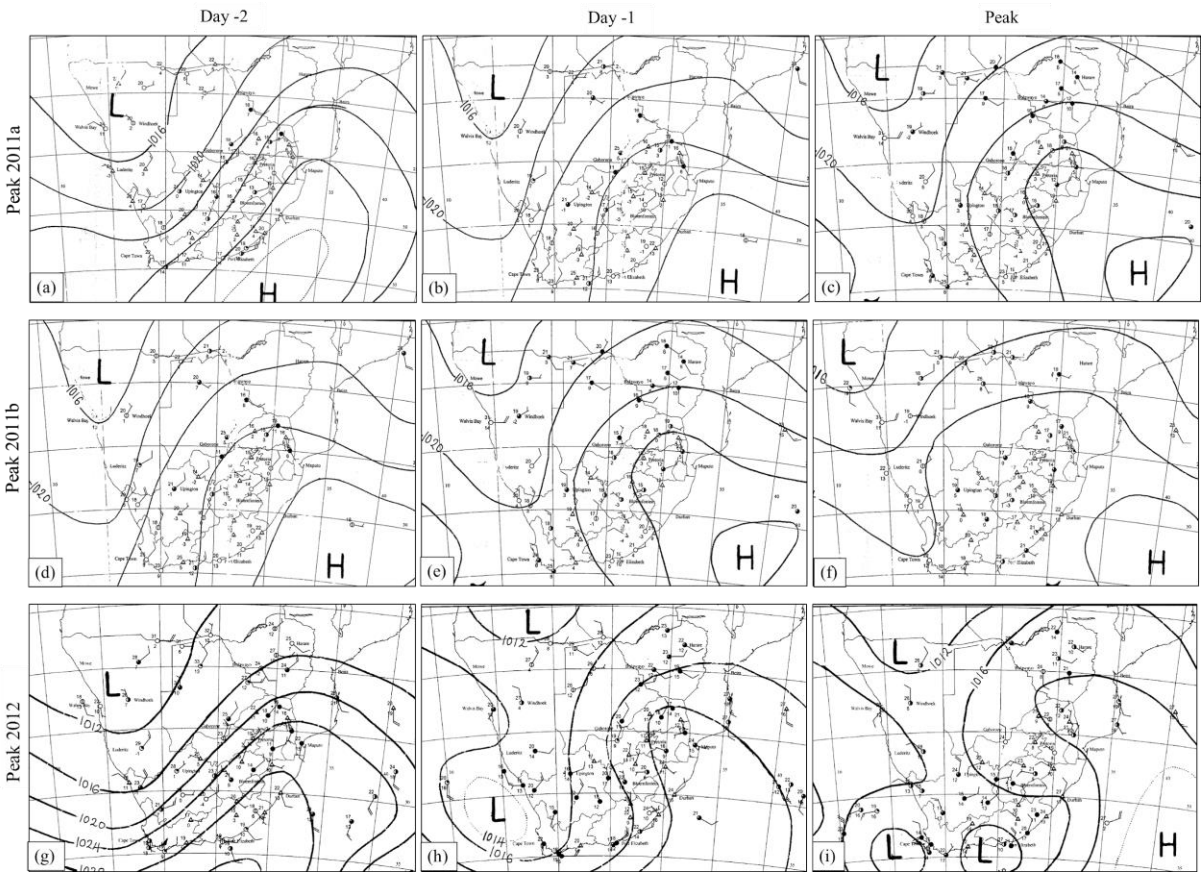

Figure 5.7: Synoptic sea level pressure over the sequence of days linked to RMS peaks 2011a (top row), 2011b (middle row), and 2012 (bottom row). Each row shows the two days before the peak (Day -2; Day -1) and the day of the peak. The observed synoptic charts are only available from 2011 (adapted from South African Weather Service, http://www.weathersa.co.za/climate/publications).

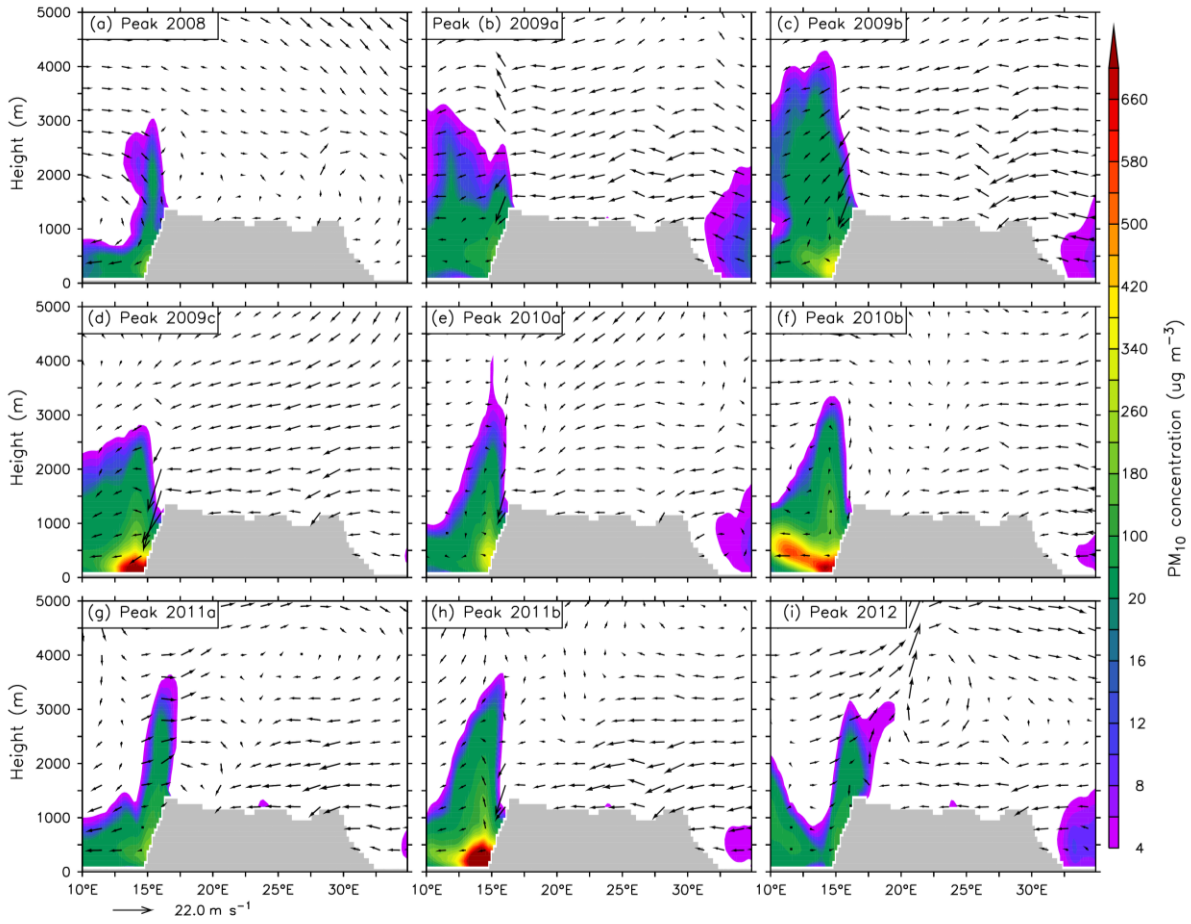

Figure 5.8: Vertical cross-section of the RMS-simulated PM_{10} concentration and wind vector profile (the arrow scale is indicated below the bottom left panel; unit: m s^{-1}) at latitude 24° S (i.e., across the Namibian coast) on Day -2 of each RMS peak. The light grey shading represents topography.

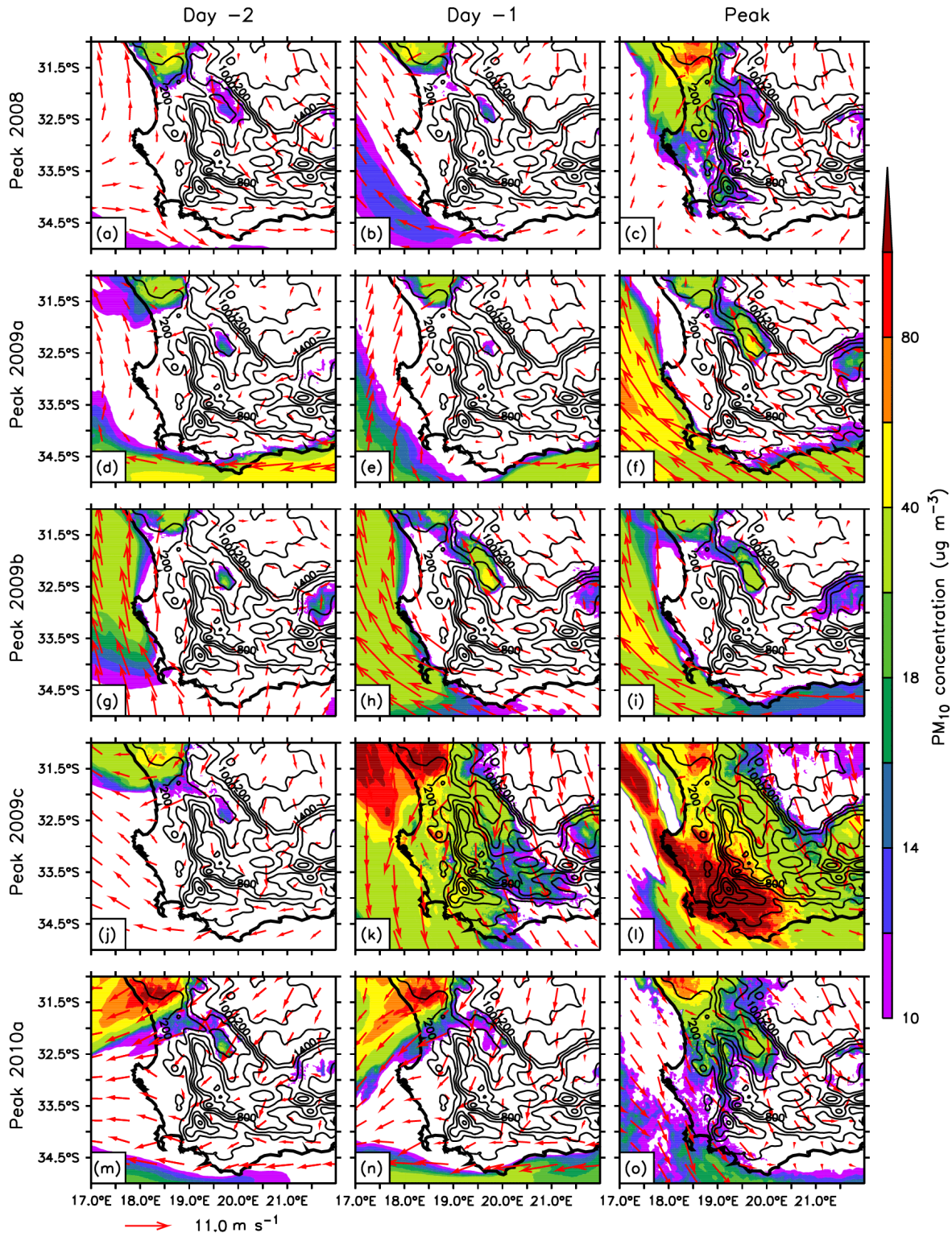

Figure 5.9: Spatial distribution of the RMS-simulated PM_{10} concentration and the associated 10 m wind field (the arrow scale is indicated below the bottom left panel; unit: m s^{-1}) over the Western Cape region, overlain with topography (black contour lines; unit: m), for the sequence of days linked to the RMS PM_{10} peaks in Cape Town. Each row shows the two days before the peak (Day -2; Day -1) as well as the day of peak.

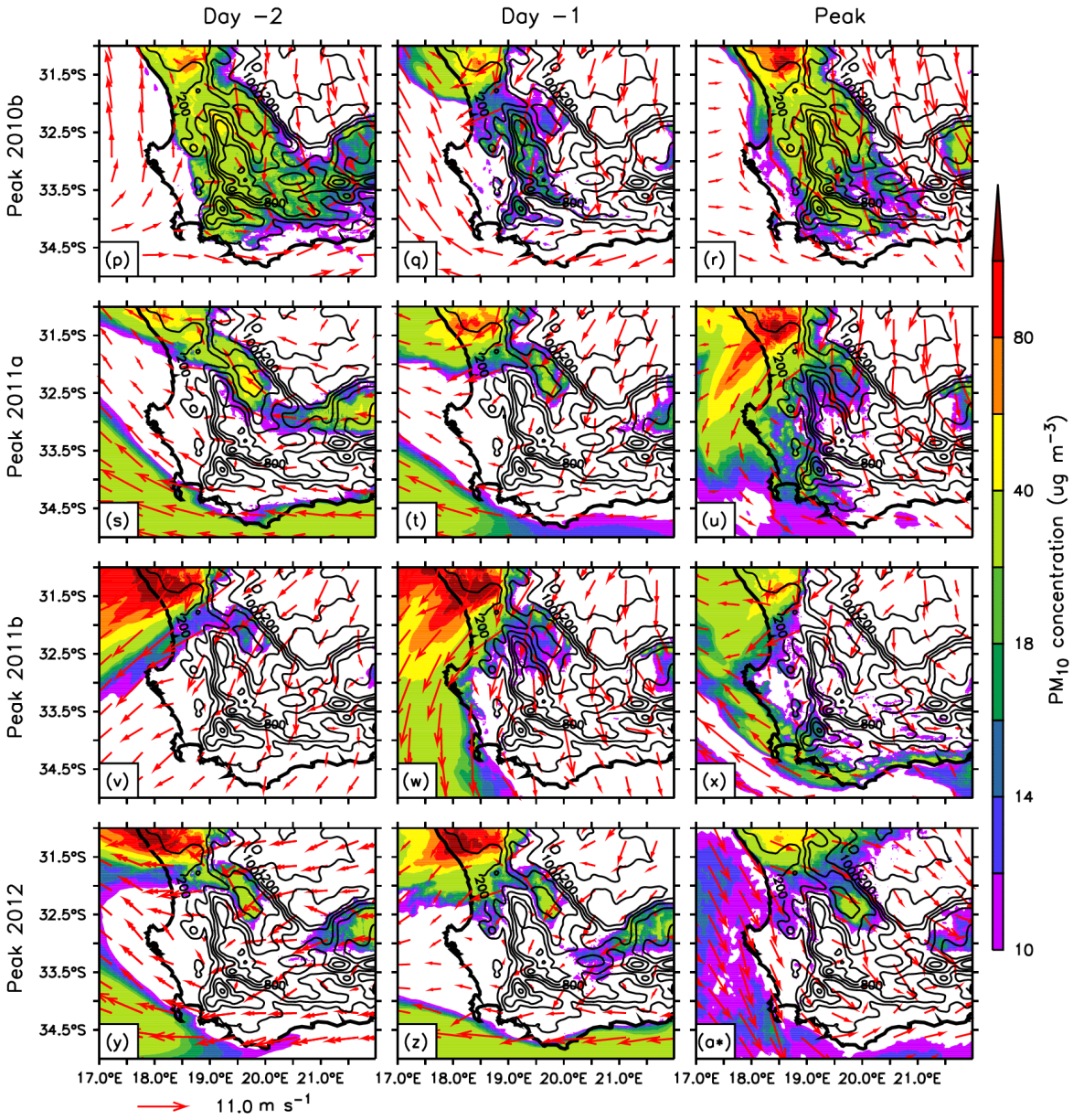

Figure 5.9: (continued).

5.4. Impact of topography

The RMS simulations also show that topography influences the spatial distribution of PM_{10} (Figures 5.9 and 5.10). Over Namibian coast, for instance, the pollutant is mostly channelled along the narrow, steep mountainous area on the coast (Figure 5.10). Along the Namibian-South African border (between about 28° and 29° S), the pollutant spreads eastwards, despite there being no westerly winds (except for the day of peak 2012, and for day -1 as well as the day of peak 2009a), such that its distribution closely follows the shape of the topography. South of the border, the distribution narrows again, following the shape of the topography along the South African west coast. The

influence of topography is also clear at the local scale, over the Western Cape region (Figure 5.9). For instance, on the days of peaks 2008, 2010a, and 2012 (Figures 5.9c, 5.9o, and 5.9a*, respectively), as the PM_{10} travels towards Cape Town, the protruding, ~200 m-tall topographic feature around 32.5° – 33.2° S, 18.5° – 19.0° E blocks some of the pollutant, minimising the amount of remote PM_{10} that reaches the central parts of Cape Town.

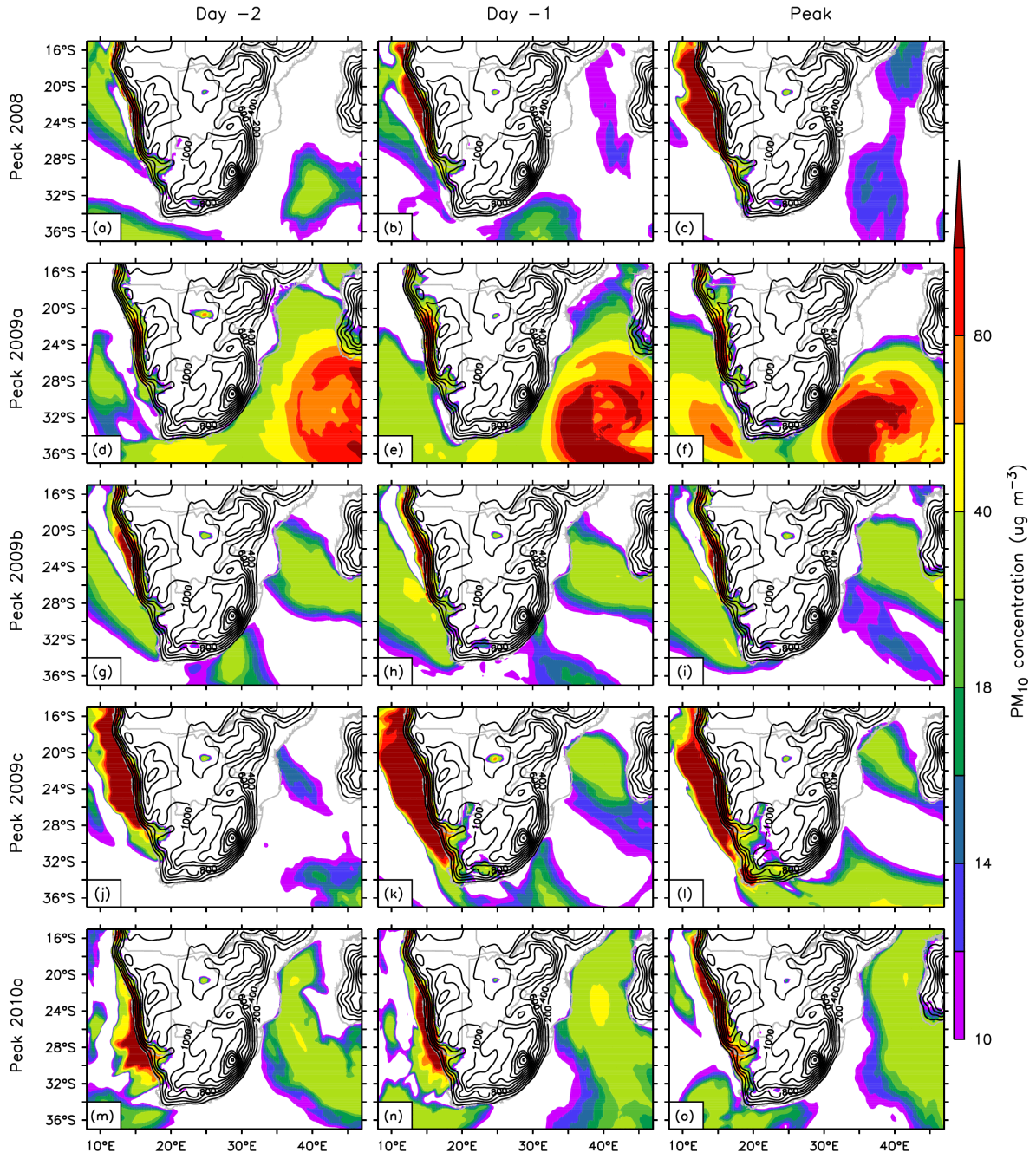

Figure 5.10: Similar to Figure 5.6, but overlain with topography (black contour lines; unit: m).

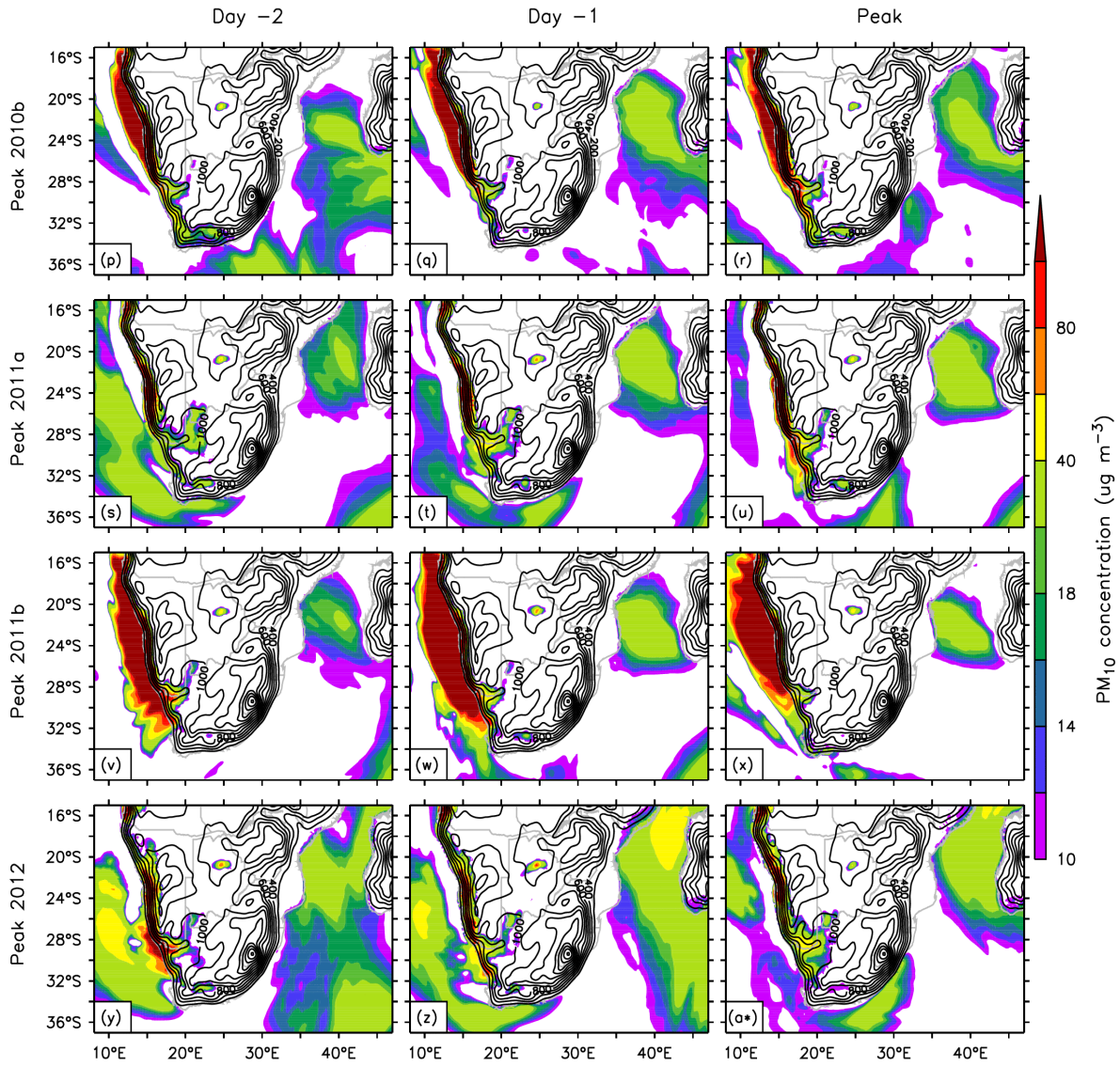

Figure 5.10: (continued).

Chapter 6 – Results and discussion part IV: Sensitivity of the simulated PM_{10} and atmospheric conditions to a change in chemistry parameterisation

Chapter 6 discusses how the WRF-Chem-simulated PM_{10} and atmospheric conditions are sensitive to a change in chemistry parameterisation. It starts by comparing the performance of RGC (in reproducing the observed PM_{10} and wind conditions over Cape Town) with that of RMS (discussed in the previous chapter). The chapter then looks at how the change in chemistry parameterisation alters atmospheric transport and the spatial distribution of PM_{10} during the episodes and simulated peaks. The discussion on the effect of the change in chemistry parameterisation on PM_{10} distribution and transport is based on the RGC peaks, which are days on which RGC simulates the highest PM_{10} concentration in Cape Town over the 11 – 12 windows of the episodes.

6.1. Atmospheric conditions and PM_{10} concentrations over Cape Town

The performance of RGC in reproducing the daily variability of the observed PM_{10} concentration over Cape Town is generally similar to that of RMS but with some differences (Figure 5.1). For instance, while RGC also shows varying performance across the episode windows, in most cases the daily variability of the RGC-simulated PM_{10} is different to that of RMS. In addition, for most of the episode windows, RGC performs better than RMS in capturing the daily variability of the pollutant (Figure 5.1; Table 6.1). For RGC, the correlation between the simulated and observed daily PM_{10} concentration is high for the windows of 2008, 2009b, 2010b, and 2012 ($r = 0.67$, 0.61, 0.71, and 0.77, respectively), poor for episode 2010a ($r = 0.25$), and very poor for episodes 2009a, 2009c, 2011a, and 2011b ($r = 0.10$, -0.04, 0.06, and -0.27, respectively). Generally, RGC also underestimates the concentration of the PM_{10} over Cape Town, however, for each episode window the mean simulated pollutant concentration is higher with RGC than RMS (Figure 5.1; Table 6.1). Moreover, unlike RMS, RGC over-estimates the concentration of the observed PM_{10} over Cape Town in some instances (while RMS only under-estimates the pollutant concentration). The positive bias in the RGC-simulated PM_{10} ranges from 0.18 μg m^{-3} (day +5 2009a) to

93.75 µg m^{-3} (day -3 of 2011b), and the negative bias from 0.8 µg m^{-3} (day +2 of episode 2010b) to 100.30 µg m^{-3} (on the day of episode 2011a). While RGC also captures most of the peaks in PM_{10} concentration over Cape Town earlier or later than in the observations, the peaks occur on a different day to those of RMS in most cases. The local peak in the RGC simulations occurs on the same day as in the RMS simulations for the windows of episodes 2010a and 2011b (i.e., a day later and three days earlier than the observations, respectively), but on the second day of the observed episode for 2008, on the same day as the observations for episodes 2009b and 2012, two days earlier for 2009c, four days earlier and four days later for episodes 2010b and 2011a, respectively, and five days later for episode 2009a (Figure 5.1; Table 6.1).

The capability of RGC to simulate the wind over Cape Town also compares well to that of RMS, though with slight differences (Figures 5.2 and 5.3). RGC also shows varying performance (across the episode windows) in replicating the daily variability of the observed wind speed over Cape Town. The RGC simulations capture the variability very well for episode windows 2009a, 2009b, 2010a, 2010b, and 2012 (r = 0.84, 0.93, 0.84, 0.87, and 0.82, respectively), well for 2009c (r = 0.69), but poorly for 2011a and 2011b (r = 0.40 and 0.33, respectively) (Figure 5.2; Table 6.1). The performance is comparable to that of RMS but shows a slight improvement (a maximum of r = 0.04, episode 2009b) and slight decline (a maximum of r = 0.13, episode 2011b) for some windows (Table 6.1). RGC also underestimates the observed wind speed in some cases and overestimates it in others, with the positive bias ranging from 0.03 m s^{-1} (day +2 of episode 2010b) to 3.50 m s^{-1} (day -1 of 2011a), and the negative bias ranging from 0.04 m s^{-1} (on day +2 of 2010a) to 3.20 m s^{-1} (day -2 of 2009c). As for the wind direction, generally, RGC also captures the south-easterly to south-westerly direction most frequently observed over the episode windows (Figures 5.2 and 5.3).

RGC also shows no direct relationship between its performance in capturing the variability of the PM_{10} and that of the wind over Cape Town. For example, RGC performs very well in capturing the wind speed and direction for the 11-day windows of episodes 2009a and 2010b but performs poorly in capturing the PM_{10} for the same

windows. Therefore, the same explanation for the poor performance of RMS in simulating the PM_{10} despite capturing the wind well can be applied here as well.

Nevertheless, differences in the simulations from the two model set-ups can be explained by a number of factors. The main contributor to the differences is likely the lack of aerosol feedback effects in the RGC simulations (aerosol feedbacks are incorporated in the RMS set-up). Various studies have shown that aerosol effects can have significant impacts on modelled meteorology (Fast et al., 2006; Forkel et al., 2012). For instance, Fast et al (2016) found that WRF-Chem significantly over-estimated simulated shortwave radiation when direct aerosol radiative forcing was neglected. Their modelled solar radiation was much closer to the observations when aerosol feedbacks were considered. The higher PM_{10} concentrations in the RGC simulations (compared to RMS) can be contributed to the lack of wet-scavenging (i.e., removal of particles in the atmosphere by precipitation and clouds) in the RGC configuration. For example, consistent with our results, Wang et al. (2016) found that WRF-Chem simulation without wet-scavenging produced higher pollutant concentrations than with wet-scavenging. They showed that the simulation without wet-scavenging over-estimated the concentration of PM_{10} (as well as other pollutants) when compared with observations. However, in the present study both RMS and RGC under-estimate the observed PM_{10}, which may be due to the lack of exact emission rates of PM_{10} over Cape Town. Nevertheless, the differences in the RMS and RGC simulations could also be due to the different microphysics schemes used in the experiments.

6.2. Air parcel trajectories

The air parcel trajectories computed with the RGC output (Figure 6.1) show some similarities with those of RMS (Figure 5.4), but with some differences. For example, RGC generally agrees with RMS that all air parcels in Cape Town during episodes 2010a, 2011b, and 2012 (Figures 6.1e, 6.1h, and 6.1i, respectively) were from central southern Africa or the Namibian coast, although, for instance, the 10 m air parcel during episode 2012 originated over the coast in RMS but over the interior in RGC. For episode 2011a (Figure 6.1g), RGC generally agrees with RMS that the 10 m air parcel originated south-east over the ocean and the 1000 m air parcel inland from the

north, but disagrees with RMS on the origin of the 100 m air parcel; in the RMS trajectories, the 100 m air parcel originated inland from the north, but originated south-east over the ocean in the RGC trajectories. Overall, compared to RMS, RGC shows less agreement with HYSPLIT on the trajectories of the air parcels in Cape Town during the observed PM_{10} episodes. The comparison of the trajectory analyses of the two parameterisation schemes shows that the lack of aerosol feedbacks can also affect the atmospheric transport in the WRF-Chem simulations. Nonetheless, the discrepancies between the RMS and RGC trajectories could also be a result of the different microphysics options used in the two simulations.

Table 6.1: Summary of the comparison between RMS and RGC in simulating PM_{10} and 10 m wind speed over Cape Town during the 11 – 12-day windows of the PM_{10} episodes. The table shows mean PM_{10} concentration over the episode windows, correlation of the daily mean PM_{10} concentration with observations, day of the peak PM_{10} concentration (relative to the observations), and correlation of the daily mean wind speed with the observations for each parameterisation scheme.

Episode	Mean PM_{10} conc. ($\mu g\ m^{-3}$)		PM_{10} correl. with obs. (r)		PM_{10} peak day rel. to obs.		Wind speed correl. with obs. (r)	
	RMS	RGC	RMS	RGC	RMS	RGC	RMS	RGC
2008	2.90	18.15	0.86	0.67	0	0	-	-
2009a	5.08	23.81	-0.38	0.10	+3	+5	0.86	0.84
2009b	5.33	26.21	-0.16	0.61	-2	0	0.89	0.93
2009c	20.42	43.38	-0.15	-0.04	+5	-2	0.82	0.69
2010a	4.86	33.36	-0.54	0.25	+1	+1	0.87	0.84
2010b	4.21	25.23	0.22	0.71	-3	-4	0.84	0.87
2011a	4.50	32.18	0.14	0.06	+2	+4	0.50	0.40
2011b	4.53	50.71	-0.02	-0.27	-3	-3	0.46	0.33
2012	4.36	13.11	-0.06	0.77	+1	0	0.87	0.82

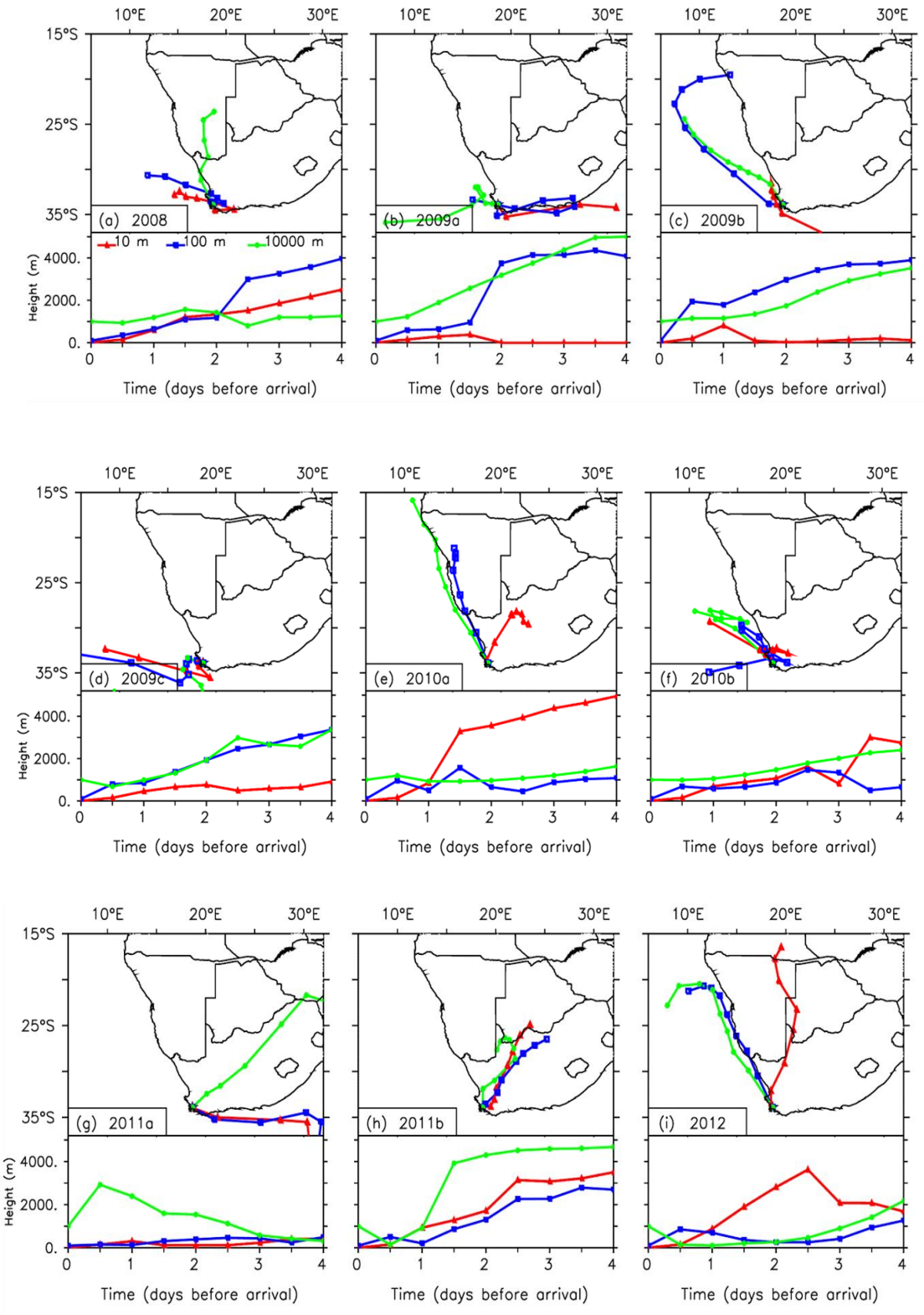

Figure 6.1: Similar to Figure 5.5, but using RGC simulations as input.

6.3. PM_{10} transport and spatial distribution during peak days

The circulation patterns associated with the RGC peaks in Cape Town are generally similar to those of the RMS peaks, also showing a well-established trough along the

west coast prior to (and in some cases, during) the events (Figure 6.2). Similar to the RMS simulations, the trough produces a plume of high PM_{10} concentration along the west coast. Nevertheless, there are some differences between RGC and RMS in the spatial distribution of the PM_{10}. For instance, the RGC simulations generally show lower PM_{10} concentrations along the Namibian coast for the sequence of days linked to peaks 2008 (especially), 2009a, 2009b, and 2010a (Figures 6.2 and 6.3). On the other hand, the RGC simulations generally show much higher PM_{10} concentrations over Cape Town during the peaks compared to RMS (Figure 6.4). In addition, although the RGC simulations show the plume of PM_{10} which extends from the Namibian coast to Cape Town (with the exception of peak 2008), it is difficult to assess how the pollutant concentrations over Cape Town evolve prior to most of the peaks.

In the RGC simulations, the influence of topography on the spatial distribution of the PM_{10} is clear at the continental scale, but not the local scale (Figures 6.4 and 6.5). Channelling of the pollutant along the narrow, steep mountainous area along the Namibian coast is also evident over the sequence of days linked to some of the peaks, for example 2009a, 2011a, and 2012. Similarly, the eastward deviation along the Namibian-South African border (despite the lack of westerly winds) and narrowing south of the border, such that the distribution of the pollutant follows the shape of the topography, is seen in the RGC simulations as well. The effect of topographical features over the Western Cape region on the transport of remote PM_{10} into Cape Town (discussed for the RMS simulations in Chapter 5.4) is not as visible in RGC simulations.

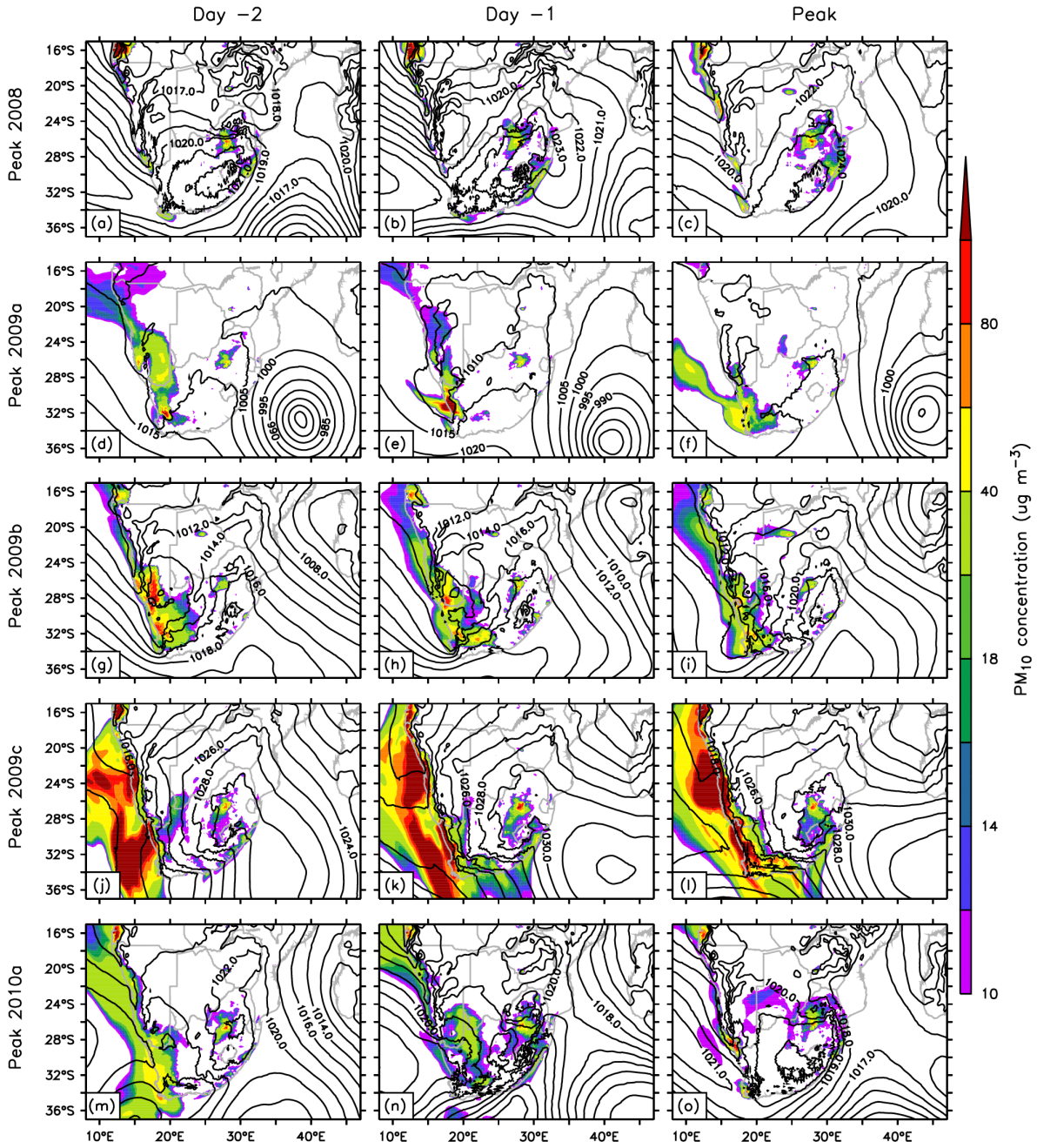

Figure 6.2: Similar to Figure 5.6, but for the RGC simulations and RGC peaks.

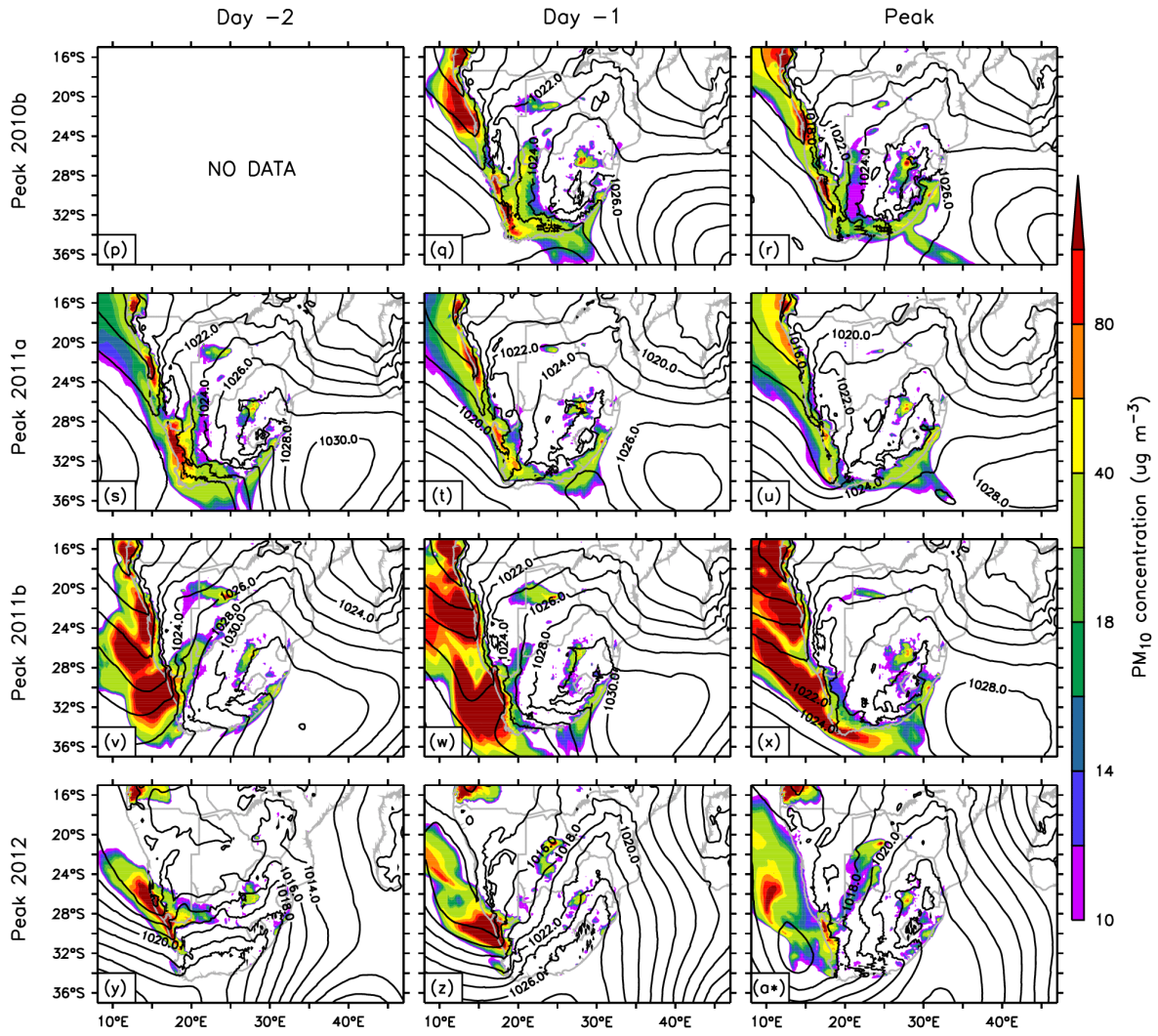

Figure 6.2: (continued).

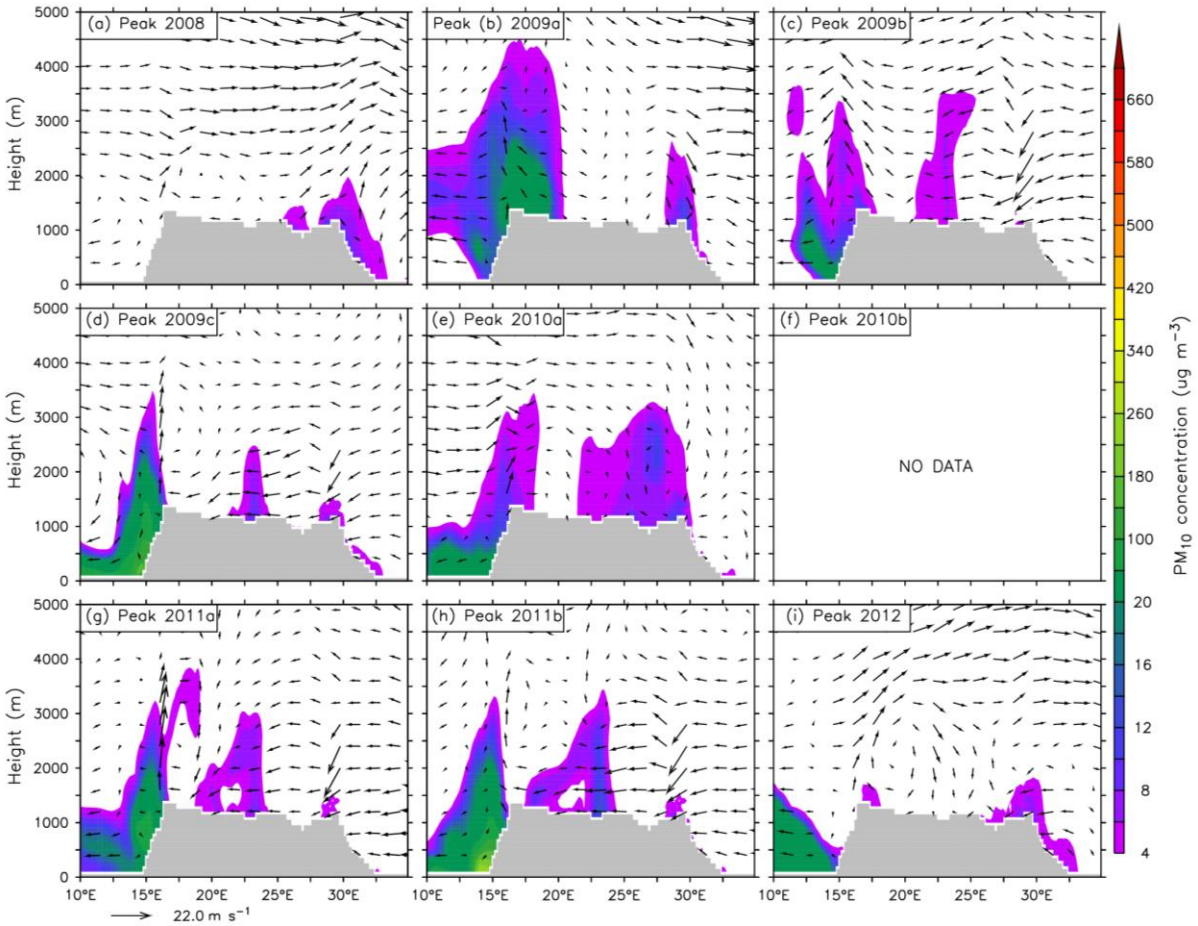

Figure 6.3: Similar to Figure 5.8, but on for the RGC simulations and on Day -2 of the RGC peaks.

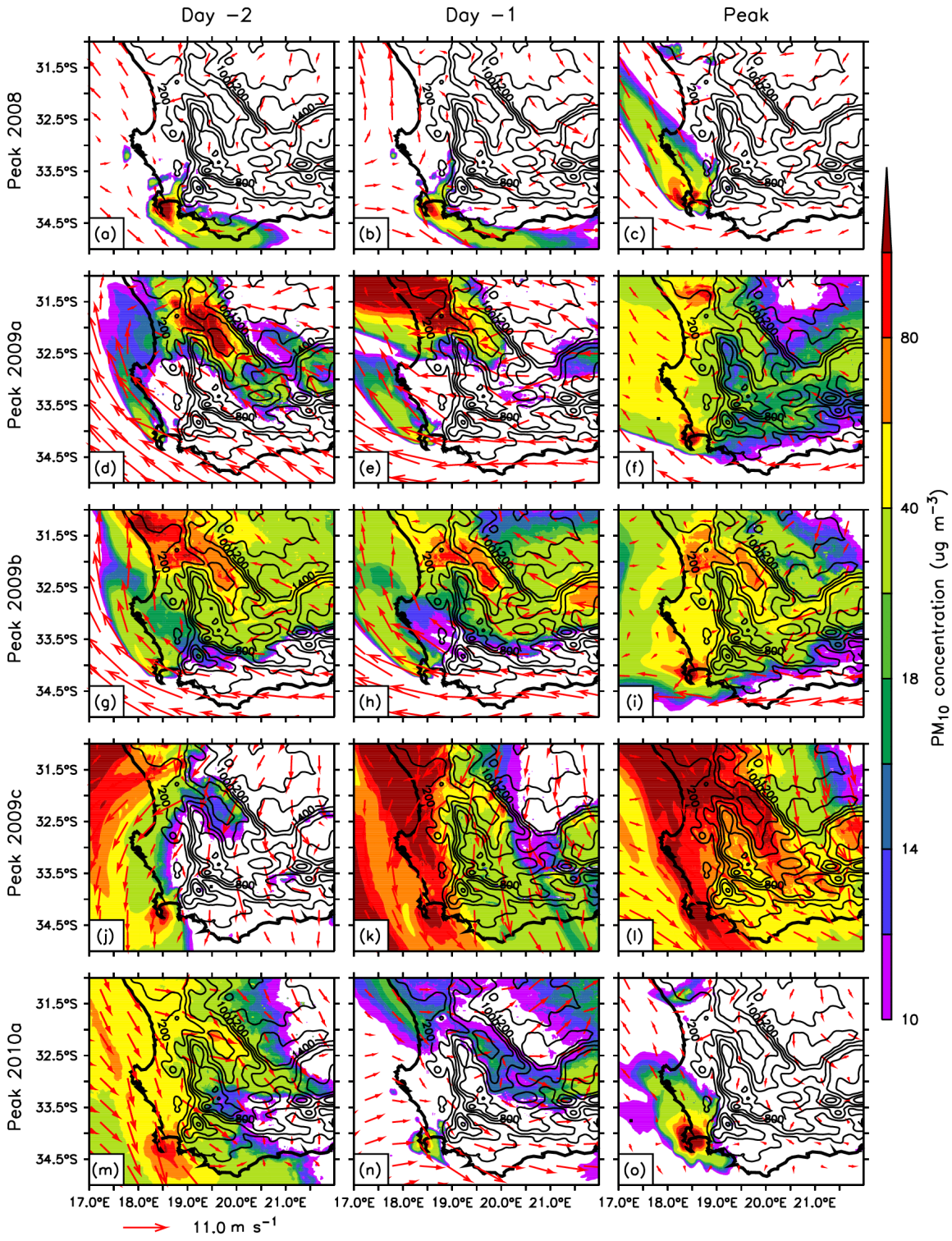

Figure 6.4: Similar to Figure 5.9, but for the RGC simulations and RGC peaks.

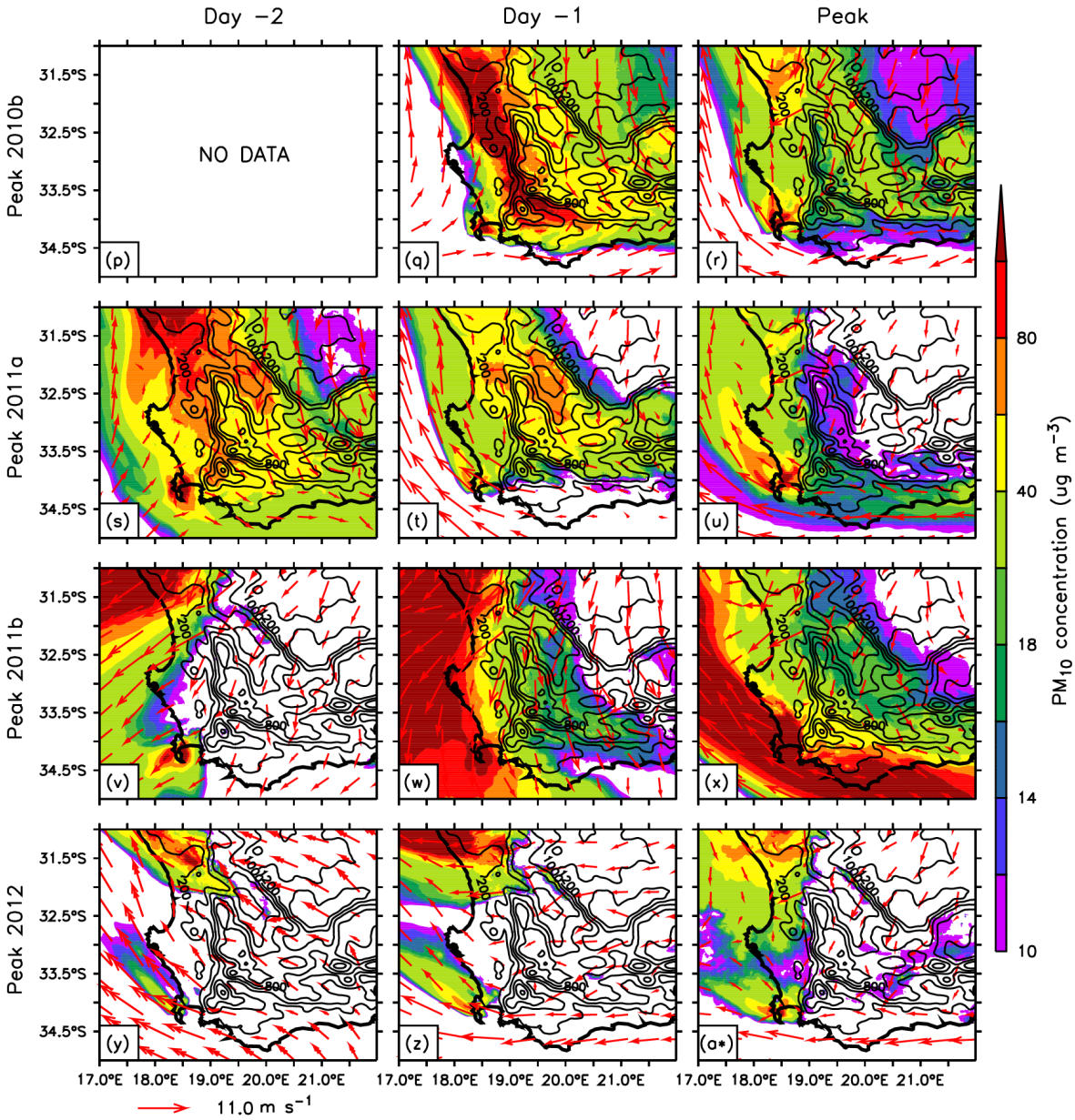

Figure 6.4: (continued).

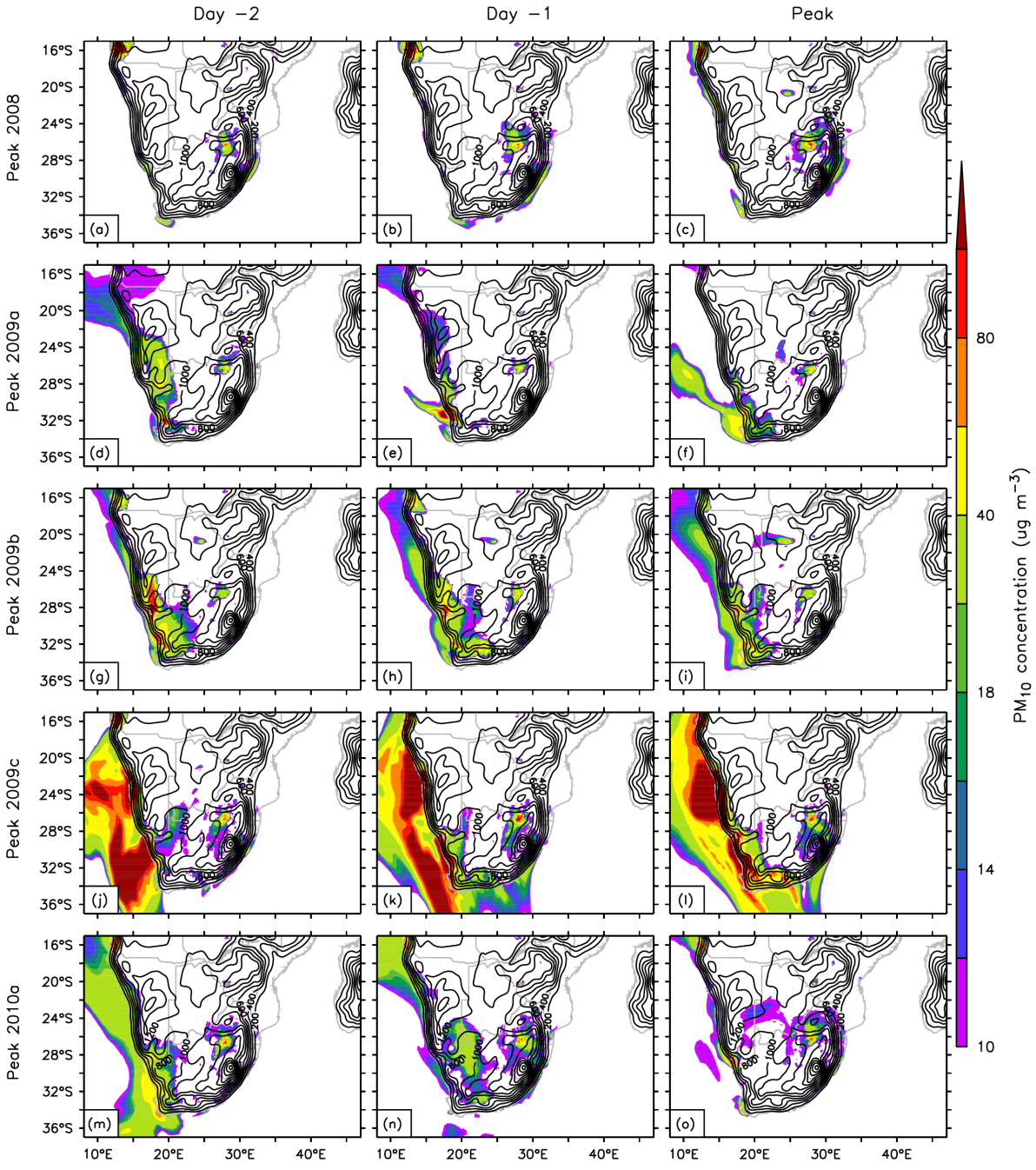

Figure 6.5: Similar to Figure 5.10, but for the RGC simulations and RGC peaks.

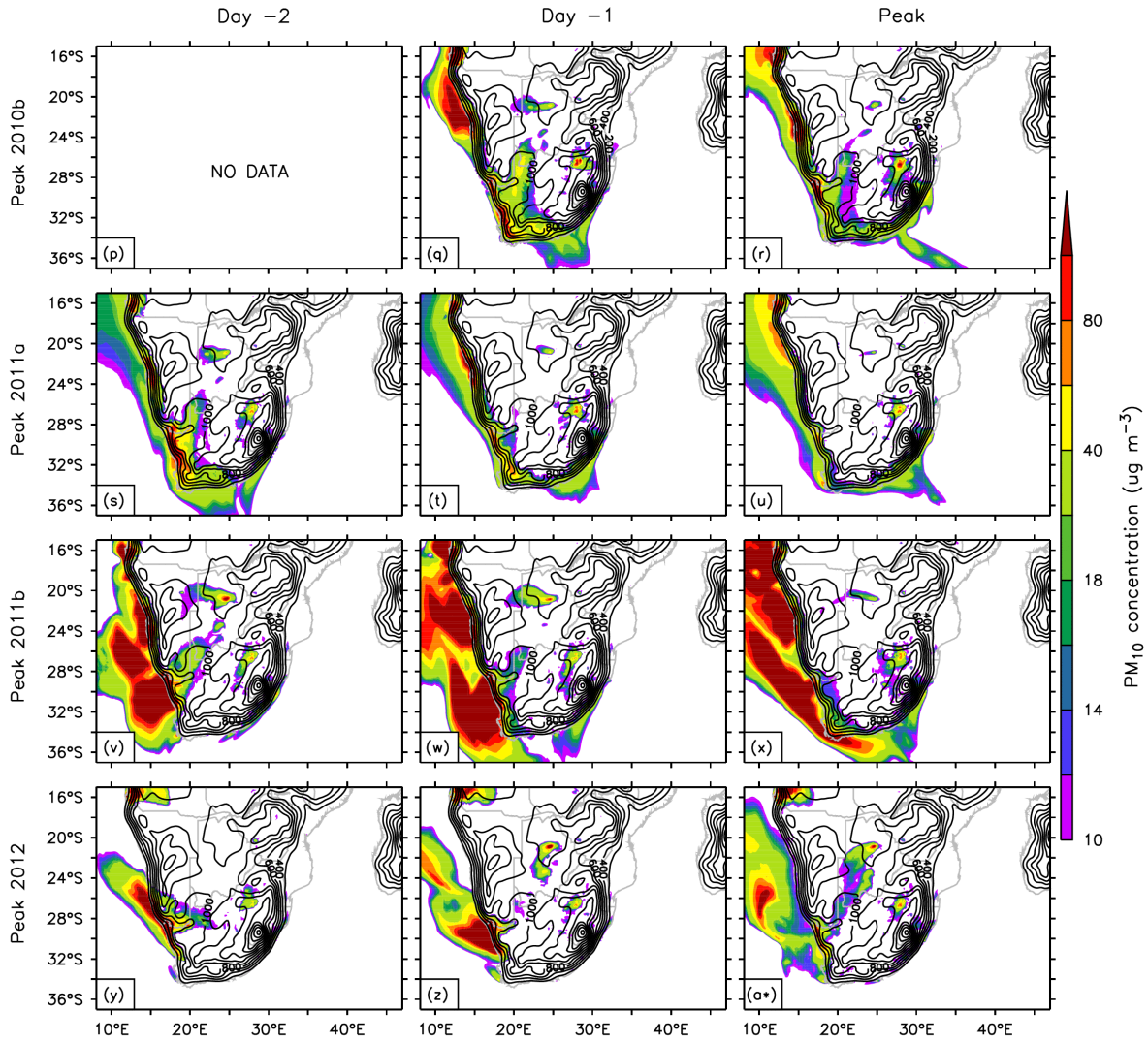

Figure 6.5: (continued).

Chapter 7 – The influence of emissions from Khayelitsha on PM_{10} distribution over Cape Town

This chapter discusses the influence of local PM_{10} emissions from Khayelitsha over the Cape Town metropolitan area by analysing the KAYE simulations. It isolates the influence of the idealised Khayelitsha emissions by subtracting RGC simulations from the KAYE simulations. For this experiment, only the simulations without aerosol feedbacks (i.e., RGC and KAYE) are discussed. The reasoning is that, while the introduction of the local emissions does not alter the wind circulations in the non-aerosol-feedback simulation (i.e., in RGC and KAYE), it does so in the with-aerosol-feedback simulation (i.e., RMS), thereby making it difficult to limit the impact of the local emission to PM_{10} distributions, which is the focus of this chapter.

The simulations show three general patterns in the spatial distribution of Khayelitsha PM_{10} emissions over Cape Town. The first pattern, which is simulated during peak 2009c (Figures 7.1c), is associated with strong north-westerly winds over the city. Under these wind conditions, the Cape Town metropolitan area experiences minimal PM_{10} pollution from Khayelitsha, as most pollution from the township is transported south over False Bay. As can be seen during peak 2009c, only the area over the central to eastern edges of the Bay are affected by the pollution from the township, and the pollution only reaches the two Khayelitsha monitoring sites (North and South Khayelitsha stations). The second pattern is simulated during peaks 2009a, 2009b, and 2012 (Figures 7.1b, 7.1c, and 7.1i, respectively). Although not associated with a single, distinct wind condition over Cape Town, in this distribution pattern, PM_{10} from the township covers most of the southern half of Cape Town (although some pollution is transported south over False Bay). The most intense pollution from the township, seen during peaks 2008, 2010a, 2010b, 2011a, and 2011b (Figures 7.1a, 7.1e, 7.1f, 7.1g, and 7.1h, respectively), is associated with strong southerly winds over Cape Town. For these five peaks, the simulations show that pollution from the township covers almost all of Cape Town, with the pollution being detectable from almost all the monitoring stations in the city.

Figure 7.1 also shows the role of topographical features on the distribution of the pollution from Khayelitsha. For example, under south-westerly wind conditions, the mountainous chain along the eastern parts of Cape Town (centred along ~19.00^{o} E) obstructs the dispersion of the pollution from the township. This is most evident during peaks 2009a, 2010b and 2011b (Figures 7.1b, 7.1f and 7.1h, respectively), where very little pollution is able to disperse beyond mountain chain, thus accumulating the pollution in the low-lying areas west of the obstruction. Topographic influence can also be seen during peaks 2008 and 2011b (Figures 7.1a and 7.1h) for example, where the topographic setting to the north-east of the domain channels and accumulates the pollution along the area between the mountains. The most efficient dispersion of pollution from the township is provided by strong, northerly flows, as seen in the case of peaks 2009c, where most of the PM_{10} is transported south over False Bay.

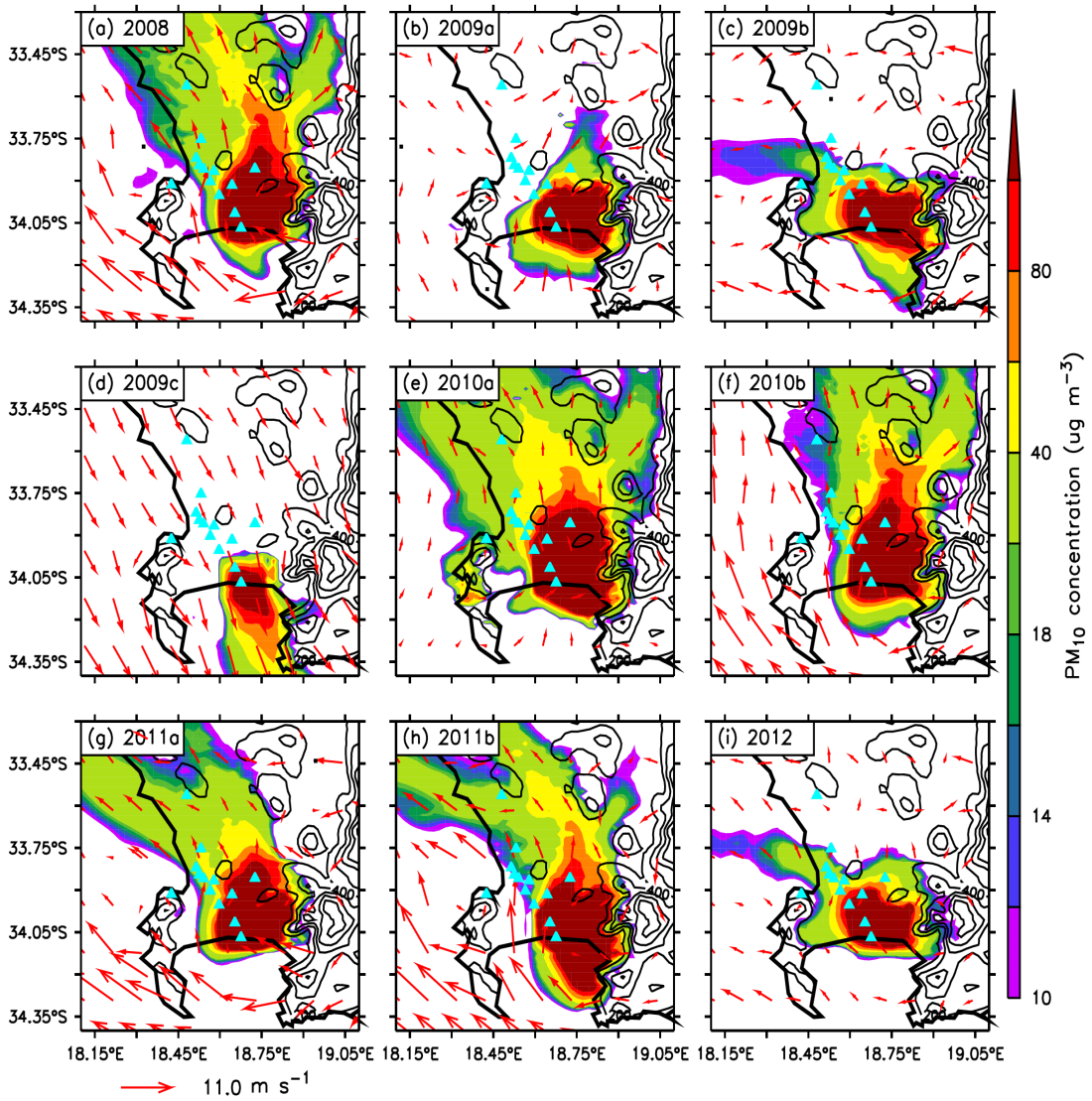

Figure 7.1: The spatial distribution of PM_{10} concentrations in Cape Town resulting solely from emissions in Khayelitsha. The figure shows the spatial distribution of the pollutant for each RGC peak and is overlain with topography (black contours; unit: m) and 10 m wind (the arrow scale is indicated below the lower left panel). The cyan triangles show the locations of the air quality monitoring stations over Cape Town.

Chapter 8 – Conclusions

8.1. Summary

As part of the continuing efforts to understand the causes of poor air quality in Cape Town, the study has investigated how transport of PM_{10} from remote sources can contribute to high PM_{10} episodes over the city. Observations from the Cape Town's quality monitoring stations between 2008 and 2014 and simulations from the WRF-Chem model were analysed for the study. The observations were used to study the temporal variations in PM_{10} concentrations and to identify PM_{10} episodes (which were defined as a day on which the daily average concentration of the pollutant exceeded 75 μg m^{-3} at two or more stations) in the city. WRF-Chem was used to simulate atmospheric conditions and PM_{10} transport over southern Africa during the episodes.

Two chemistry parameterisation schemes were applied in the simulations: RADM2 chemistry parameterisation scheme coupled with the MADE/SORGAM aerosol module (RMS) and RADM2 chemistry parameterisation scheme coupled with the GOCART aerosol module (RGC). The key difference between the two parameterisation schemes is that RMS accounts for aerosol-radiation feedback, indirect aerosol effect, and wet-scavenging, while RGC does not. For both schemes, each simulation was performed for a period comprising the six days before, during, and the five days after the episode. The capability of both WRF-Chem set-ups in simulating the wind and the PM_{10} concentration over Cape Town was evaluated by comparing the simulations with the station observations. To identify the paths of air parcels in Cape Town during each episode, the study also employed four-day back-trajectories from three simulations, one from the HYSPLIT model and one each from the two WRF-Chem model set-ups. A third experiment (KAYE), with the same set-up as RGC, except for an idealized continuous area emission being introduced over Khayelitsha area, was performed to examine the influence of idealized local emissions from the township on the spatial distribution of PM_{10} concentration over Cape Town.

The results of the study can be summarised as follows:

- The diurnal variation of PM_{10} at the stations features two distinct peaks: one in the morning and the other in the afternoon. The peaks are mainly due to traffic emissions, but atmospheric conditions also contribute to the variation.
- Among the stations, North Khayelitsha station shows the highest concentrations, especially in the afternoon and evening. This is attributed to additional PM_{10} emissions from domestic burning of coal, wood, and paraffin for cooking and heating, which are prevalent in the township.
- RMS reproduces the observed wind speed and direction over Cape Town during the episodes reasonably well, but struggles to reproduce the observed PM_{10}. Generally, the RMS simulations underestimate the concentration of the observed PM_{10}, and for most episodes, reproduce the peak PM_{10} concentration some days earlier or later than the observations.
- The back-trajectories from both HYSPLIT and RMS agree that most of the air parcels that arrived in Cape Town during the episodes originated from central southern Africa or the Namibian coast, and travelled over the Kalahari or the Namib Desert (or both) before reaching the city.
- In the RMS simulations, the peaks in PM_{10} concentration over Cape Town are linked with the transport of the pollutant from the north-west coast of southern Africa. The pre-PM_{10} peak days feature a coastal trough, which produces a plume of high PM_{10} concentration along a coast. Northerly flows (in most cases driven by the trough and a continental high-pressure system) channel PM_{10} from the plume into Cape Town to induce the peaks.
- The RMS simulations also show that the topography north of Cape Town can influence the spread of remote PM_{10} into Cape Town by blocking some of the pollutant being transported from the north, minimising the amount reaching some parts of the city.
- The simulations of PM_{10} and air parcel trajectories with WRF-Chem show sensitivity to a change in the chemistry parameterisation.
- Although RGC shows similar general characteristics to RMS in reproducing the wind and PM_{10} concentrations over Cape Town during the episode windows, RGC simulates higher PM_{10} concentrations (although still lower than the observations, on average). Furthermore, in most cases, the RGC simulations capture peak PM_{10} concentrations on a different day to the RMS simulations.

- The trajectories of air parcels arriving in Cape Town during the episodes generated from the RGC simulations are mostly different to those of RMS. In addition, overall, compared to RMS, the RGC trajectories show less agreement with those from HYSPLIT.
- The RGC-simulated peak days show similar circulation patterns to those of RMS, and in some cases, show similar mechanisms of PM_{10} transport from the Namibian coast plume into Cape Town. However, with RGC, higher concentrations of PM_{10} are simulated over Cape Town.

- PM_{10} pollution from Khayelitsha shows three general spatial distribution patterns over the Cape Town metropolitan area, namely, the pollution mostly spreads south over False Bay, covers the southern half of Cape Town, or covers most of Cape Town.
- Local topography along the eastern edges of Cape Town promotes the accumulation of PM_{10} from Khayelitsha, as it can obstruct dispersion of the pollution.
- Strong north-westerly winds provide the most efficient dispersion of the PM_{10}, as they transport the pollution away from the city and over False Bay.

8.2. Recommendations for future research

To provide more robust information for policy-makers, the results of this study can be improved in a number of ways. For instance, while this study indicates that PM_{10} from remote sources can contribute to the PM_{10} concentration over Cape Town, the study could not quantify the percentage of the contribution due to the lack of compressive emission inventories. Future studies should focus on quantifying the contribution of the remotely-transported PM_{10} to local concentrations in Cape Town. This will show whether the poor air quality in the city is locally driven or not. Quantifying the contribution of the remotely transported PM_{10} to local concentrations requires reliable emission inventories for the city, which are currently lacking. Thus, future research should also focus on developing accurate emission inventories for Cape Town (and southern Africa at large). In addition to enabling the contribution of remotely-sourced pollution in Cape Town to be estimated, the emission inventories would also help to improve the modelling of PM_{10} (as well as other pollutants) over the city.

8.3. Publication

Molepo, K.M., Abiodun, B.J., Magoba, R.N., 2019. The transport of PM_{10} over Cape Town during high pollution episodes. Atmospheric Environment 213, 116–132.

References

Aarnio, P., Martikainen, J., Hussein, T., Valkama, I., Vehkamäki, H., Sogacheva, L., Härkönen, J., Karppinen, A., Koskentalo, T., Kukkonen, J., Kulmala, M., 2008. Analysis and evaluation of selected PM_{10} pollution episodes in the Helsinki Metropolitan Area in 2002. Atmospheric Environment 42 (17), 3992–4005.

Abiodun, B.J., Ojumu, A.M., Jenner, S., Ojumu, T.V., 2014. The transport of atmospheric NO_x and HNO_3 over Cape Town. Atmospheric Chemistry and Physics 14, 559–575.

Achilleos, S., Evans, J.S., Yiallouros, P.K., Kleanthous, S., Schwartz, J., Koutrakis, P., 2014. PM_{10} concentration levels at an urban and background site in Cyprus: The impact of urban sources and dust storms 64 (12), 1352–1360.

Ackermann, I.J., Hass, H., Memmesheimer, M., Ebel, A., Binkowski, F.S., Shankar, U., 1998. Modal Aerosol dynamics model for Europe: Development and first applications. Atmospheric Environment 32, 2981–2999.

Ambade, B., 2018. The air pollution during Diwali festival by the burning of fireworks in Jamshedpur city, India. Urban Climate 26, 149–160.

Barman, S.C., Singh, R., Negi, M.P.S., Bhargava, S.K., 2008. Ambient air quality of Lucknow city (India) during use of fireworks on Diwali Festival. Environment Monitoring and Assessment 37, 495–504.

Bell, M.L., Ebisu, K., Belanger, K., 2007. Ambient air pollution and low birth weight in Connecticut and Massachusetts. Environmental Health Perspectives 115 (7), 1118–1124.

Bell, M.L., Levy, J.K., Lin, Z., 2008. The effect of sandstorms and air pollution on cause-specific hospital admissions in Taipei, Taiwan. Occupational & Environmental Medicine 65 (2), 104–111.

Bielawska, M., Wardencki, W., 2014. Influence of meteorological conditions on PM_{10} concentration in Gdańsk. 2014 5th International Conference on Environmental Science and Technology 69, 76–80. doi: https://doi.org/10.7763/IPCBEE.

Charlson, R.J., Schwartz, S.E., Hales, J.M., Cess, R.D., Coakley, J.A., Hansen, J.E., Hofmann, D.J., 1992. Climate forcing by anthropogenic aerosol. Science 255 (5043), 423–430.

Chen, F., Dudhia, J., 2001. Coupling an advanced land-surface/hydrology model with the Penn State/NCAR MM5 modeling system, Part I: Model description and implementation. Monthly Weather Review 129, 569–585.

Chen, L., Yang, W., Jennison, B.L., Goodrich, A., Omaye, S.T., 2002. Air pollution and birth weight in northern Nevada, 1991–1999. Inhalation Toxicology 14, 141–157.

Cheng, S., Wang, F., Li, J., Chen, D., Li, M., Zhou, Y., Ren, Z., 2013. Application of trajectory clustering and source apportionment methods for investigating trans-boundary atmospheric PM_{10} pollution. Aerosol and Air Quality Research 13, 333–342. doi: 10.4209/aaqr.2012.06.0154.

Chin, M., Ginoux, P., Kinne, S., Torres, O., Holben, B.N., Duncan, B.N., Martin, R.V., Logan, J.A., Higurashi, A., Nakajima, T., 2002. Tropospheric aerosol optical thickness from the GOCART model and comparisons with satellite and sunphotometer measurements. Journal of the Atmospheric Sciences 59, 461–483.

Chou, M.-D., Suarez, M.J., 1994. An efficient thermal infrared radiation parameterisation for use in general circulation models. NASA Technical Memorandum, 104606 (3), 85.

Choudhury, A.H., Gordian, M.E., Morris, S.S., 1997. Associations between respiratory illness and PM_{10} air pollution. Archives of Environmental Health 52 (2), 113–117.

City Health Department, 2005. Air Quality Management Plan for the City of Cape Town. City Health Department, Cape Town.

Department of Environmental Affairs, 2009. National Ambient Air Quality Standards Available: https://www.environment.gov.za/sites/default/files/legislations/nemaqa_airquality_g32816gon1210_0.pdf. (accessed January 2017).

Draxler, R.R. and Hess, G. D., 1998. An overview of the HYSPLIT_4 modeling system of trajectories, dispersion, and deposition. Australian Meteorological Magazine 47 (4), 295–308.

Dugandzic, R., Dodds, L., Stieb, D., Smith-Doiron, M., 2006. The association between low level exposures to ambient air pollution and term low birth weight: a retrospective cohort study. Environmental Health 5 (3), 1–8.

Edgerton, S.A., Bian, X., Doran, J C., Fast, J.D., Hubbe, J.M., Malone, E.L., Shaw, W.J., Whiteman, C.D., Zhong, S., Arriaga, J.L., Ortiz, E., Ruiz, M., Sosa, G., Vega, E., Limón, T., Guzman, F., Archuleta, J., Bossert, J.E., Elliot, S.M., Lee, J.T., McNair, L. A., Chow, J.C., Watson, J.G., Coulter, R.L., Doskey, P.V., Gaffney, J.S., Marley, N.A., Neff, W., Petty, R.,1999. Particulate air pollution in Mexico City: A Collaborative Research Project. Journal of the Air and Waste Management Association, 49 (10), 1221–1229. doi: 10.1080/10473289.1999.10463915.

Escobar, G.J., Clark, R.H., Greene, J.D., 2006. Short–term outcomes of infants born at 35 and 36 weeks gestation: We need to ask more questions. Seminars in Perinatology 30, 28–33.

Escudero, M., Stein, A., Draxler, R. R., Querol, X., Alastuey, A., Castillo, S., Avila, A., 2006. Determination of the contribution of northern Africa dust source areas to PM_{10} concentrations over the central Iberian Peninsula using the Hybrid Single-Particle Lagrangian Integrated Trajectory model (HYSPLIT) model. Journal of Geophysical Research Atmospheres 111 (6), 1–15. doi: 10.1029/2005JD006395.

Fast, J.D., Gustafson Jr., W.I., Easter, R.C., Zaveri, R.A., Barnard, J.C., Chapman, E.G., Grell, G.A., Peckham, S.E., 2006. Evolution of ozone, particulates, and aerosol direct radiative forcing in the vicinity of Houston using a fully coupled meteorology-chemistry-aerosol model. Journal of Geophysical Research 111, D21305.

Flentje, H., Briel, B., Beck, C., Collaud Coen, M., Fricke, M., Cyrys, J., Gu, J., Pitz, M., Thomas, W., 2015. Identification and monitoring of Saharan dust: an inventory representative for south Germany since 1997. Atmospheric Environment 109, 87–96. doi: 10.1016/j.atmosenv.2015.02.023.

Folinsbee, L.J., 1992. Human health effects of air pollution. Environmental Health Perspectives 100, 45–56.

Forkel, R., Werhahn, J., Buus, A., Mckeen, S., Peckham, S., Grell, G., Suppan, P., 2012. Effect of aerosol–radiation feedback on regional air quality: A case study with WRF/Chem. Atmospheric Environment 53, 202–211. doi: 10.1016/j.atmosenv.2011.10.009.

Fortelli, A., Scafetta, N., Mazzarella, A., 2016. Influence of synoptic and local atmospheric patterns on PM10 air pollution levels: A model application to Naples (Italy). Atmospheric Environment 143, 218–228.

Freitas, S.R., Longo, K.M., Alonso, M.F., Pirre, M., Marecal, V., Grell, G., Stockler, R., Mello, R. F., Sánchez Gácita, M., 2011. PREP-CHEM-SRC - 1.0: A preprocessor of trace gas and aerosol emission fields for regional and global atmospheric chemistry models. Geoscientific Model Development 4, 419–433.

Gupta, M., Mohan, M., 2013. Assessment of contribution to PM_{10} concentrations from long range transport of pollutants using WRF/Chem over a subtropical urban airshed. Atmospheric Pollution Research 4, 405–410. doi: 10.5094/APR.2013.046.

Grell, G.A., Devenyi, D., 2002. A generalized approach to parameterizing convection combining ensemble and data assimilation techniques. Geophysical Research Letters 29 (14), 1693.

Grell, G.A., Peckham, S.E., Schmitz, R., McKeen, S.A., Frost, G., Skamarock, W.C., Eder, B., 2005. Fully coupled online chemistry within the WRF model. Atmospheric Environment 39, 6957–6975.

Ha, S., Hu, H., Roussos–Ross, D., Haidong, K., Roth, J., Xu, X., 2014. The effects of pollution on adverse birth outcomes. Environmental Research 134, 198–204.

He, H., Tie, X., Zhang, Q., Liu, X., Gao, Q., Li, X., Gao, Y., 2014. Analysis of the causes of heavy aerosol pollution in Beijing, China: A case study with the WRF-Chem model. Particuology 20, 32–40.

Hidy, G.M., Appel, B.R., Charlson, R.J., Clark, W.E., Friedlander, S.K., Hutchison, D.H., Smith, T.B., Suder, J., Wesolowski, J.J., Whitby, K. T., 1975. Summary of the California aerosol characterization experiment. Journal of the Air Pollution Control Association 25 (11), 1106–1114. doi: 10.1080/00022470.1975.10470183.

Hofman, P.L., Regan, F., Cutfield, W.S., 2006. Prematurity – Another example of perinatal metabolic programming? Hormone Research 66, 33–39.

Hong, S.-Y., Dudhia, J., Chen, S.-H., 2004. A revised approach to ice microphysical processes for the bulk parameterization of clouds and precipitation. Monthly Weather Review 132, 103–120.

Hong, S.Y., Noh, Y., Dudhia, J., 2006. A new vertical diffusion package with an explicit treatment of entrainment processes. Monthly Weather Review 134, 2318–2341.

Husar, R.B., Tratt, D.M., Schichtel, B.A., Falke, S.R., Li, F., Jaffe, D., Gasso, S., Gill, T., Laulainen, N.S., Lu, F., Reheis, M.C., Chun, Y., Westphal, D., Holben, B.N., Gueymard, C., McKendry, I., Kuring, N., Feldman, G.C., McClain, C., Frouin, R.J., Merrill, J., DuBois, D., Vignola, F., Murayama, T., Nickovic, S., Wilson,W.E., Sassen, K., Sugimoto, N., Malm, W.C., 2001. Asian dust events of April 1998. Journal of Geophysical Research 106 (D16), 18317–18330.

Jenner, S.L., Abiodun, B.J., 2013. The transport of atmospheric sulfur over Cape Town. Atmospheric Environment 79, 248–260.

Jeong, U., Kim, J., Lee, H., Jung, J., Kim, Y.J., Song, C.H, Koo, J-H., 2011. Estimation of the contributions of long range transported aerosol in East Asia to carbonaceous aerosol and PM concentrations in Seoul, Korea using highly time resolved measurements: A PSCF model approach. Journal of Environmental Monitoring 13 (7), 1905-1918. doi: 10.1039/C0EM00659A.

Jury, M., Tegen, A., Ngeleza, E., Du Toit, M., 1990. Winter air pollution episodes over Cape Town. Boundary-Layer Meteorology 53, 1–20.

Kabatas, B., Pierce, R.B., Unal, A., Rogal, M.J., Lenzen, A., 2018. April 2008 Saharan dust event: Its contribution to PM_{10} concentrations over the Anatolian Peninsula and relation with synoptic conditions. Science of the Total Environment 633, 317–328. doi: 10.1016/j.scitotenv.2018.03.150.

Kelly, K.E., Jaramillo, I.C., Quintero-Núñez, M., Wagner, D.A., Collins, K., Meuzelaar, H.L.C., Lighty, J.A.S., 2010. Low-wind/high particulate matter episodes in the calexico/mexicali region. Journal of the Air and Waste Management Association 60 (12), 1476–1486.

Krivacsy, Z., Blazso, M., Shooter, D., 2005. Primary organic pollutants in New Zealand urban aerosol in winter during high PM_{10} episodes. Environmental Pollution 139, 195–205. doi: 10.1016/j.envpol.2005.05.018.

Kuik, F., Lauer, A., Beukes, J.P., Van Zyl, P.G., Josipovic, M., Vakkari, V., Laakso, L., Feig, G.T., 2015. The anthropogenic contribution to atmospheric black carbon concentrations in southern Africa: A WRF-Chem modeling study. Atmospheric Chemistry and Physics 15 (15), 8809–8830. doi: 10.5194/acp-15-8809-2015.

Kumar, A., Jiménez, R., Belalcázar, L.C., Rojas, N.Y., 2016. Application of WRF-Chem model to simulate PM_{10} concentration over Bogota. Aerosol and Air Quality Research 16, 1206–1221. doi: 10.4209/aaqr.2015.05.0318.

Lee, H.N., Tanaka, T., Chiba, M., Igarashi, Y., 2003. Long range transport of Asian dust from dust storms and its impact on Japan. Water, Air and Soil Pollution: Focus 3 (2), 231–243.

Lee, Y.C., Yang, X., Wenig, M., 2010. Transport of dusts from East Asian and non-East Asian sources to Hong Kong during dust storm related events 1996–2007. Atmospheric Environment 44 (30), 3728–3738.

Lenschow, P., Abraham, H., Kutzner, K., Lutz, M., Preub, J., Reichenbficher, W., 2001. Some ideas about the sources of PM_{10}. Atmospheric Environment 35 Supplement No. 1, S23–S33.

Leys, J.F., Heindenrich, S.K., Strong, C.L., McTainsh, G.H., Quigley, S., 2011. PM10 concentrations and mass transport during “Red Dawn” – Sydney 23 September 2009. Aeolian Research 3 (3), 327–342.

Lin, Y.L., Farley, R.D., Orville, H.D., 1983. Bulk parameterisation of the snow field in a cloud model. Journal of Applied Meteorology and Climatology 22, 1065–1092.

Matthaios, V.N., Triantafyllou, A.G., Koutrakis, P., 2017. PM_{10} episodes in Greece: Local sources versus long-range transport — observations and model simulations. Journal of the Air & Waste Management Association 67, 105–126.

Menéndez, I., Derbyshire, E., Engelbrecht, J.P., Suchodoletz, H., von Zöller, L., Dorta, P.,Carrillo, T., Rodríguez de Castro, F., 2009. Saharan dust and the aerosols on the Canary Islands: past and present. In: M., Cheng, W., Liu (Eds.), Airborne Particulates, Nova Science Publishers, Inc., New York, pp. 39–80.

Middleton, N., Yiallouros, P., Kleanthous, S., Kolokotroni, O., Schwartz, J., Dockery, D., Demokritou, P., Koutrakis, P., 2008. A 10-year time-series analysis of respiratory and cardiovascular morbidity in Nicosia, Cyprus: the effect of short-term changes in air pollution and dust storms. Environmental Health 7, 1–16.

Mira-Salama, D., Grüning, C., Jensen, N.R., Cavalli, P., 2008. Source attribution of urban smog episodes caused by coal combustion. Atmospheric Research 88, 294–304. doi: 10.1016/j.atmosres.2007.11.025.

Mlawer, E.J., Taubman, S.J., Brown, P.D., Iacono, M.J., Clough, S.A., 1997. Radiative transfer for inhomogeneous atmospheres: RRTM, a validated correlated-k model for the longwave. Journal of Geophysical Research 102, 16663–16682.

National Environmental Management: Air Quality Amendment Act, No. 39 of 2004, 2004.

Nava, S., Becagli, S., Calzolai, G., Chiari, M., Lucarelli, F., Prati, P., Traversi, R., Udisti, R., Valli G., Vecchi, R., 2012. Saharan dust impact in central Italy: An overview on three years elemental data records. Atmospheric Environment 60, 444–452.

Neophytou, A.M., Yiallouros, P., Coull, B.A., Kleanthous, S., Pavlou, P., Pashiardis, S., Dockery, D.W., Koutrakis, P., Laden, F., 2013. Particulate matter concentrations during desert dust outbreaks and daily mortality in Nicosia, Cyprus. Journal of Exposure Science and Environmental Epidemiology 23, 275–280.

Nzotungicimpaye, C.M., Abiodun, B.J., Steyn, D.G., 2014. Tropospheric ozone and its regional transport over Cape Town. Atmospheric Environment 87, 228–238.

Olivier, J.G.J., Bouwman, A.F., Van der Maas, C.W.M., Berdowski, J.J.M., Veldt, C., Bloos, J.P.J., Visschedijk, A.J.H., Zandveld, P.Y.J., Haverslag, J.L., 1996. Description of EDGAR Version 2.0: A set of global emission inventories of greenhouse gases and ozone depleting substances for all anthropogenic and most natural sources on a per country basis and on 1^{o} x 1^{o} grid. RIVM Techn, Report No. 771060002, TNO-MEP report No. R96/119, National Institute of Public Health and the Environment/Netherlands Organisation for Applied Scientific Research, Bilthoven, Netherlands.

Parent, M.-É., Rousseau, M.-C., Boffetta, P., Cohen, A., Siemiatycki, J., 2007. Exposure to diesel and gasoline engine emissions and the risk of lung cancer. American Journal of Epidemiology 165 (1), 53–62

Perrino, C., 2010. Atmospheric particulate matter. Proceedings of a C.I.S.B minisymposium – March, 35–43.

Pohjola, M.A., Rantamäki, M., Kukkonen, J., Karppinen, A., Berge, E., 2004. Meteorological evaluation of a severe air pollution episode in Helsinki on 27–29 December 1995. Boreal Environment Research 9, 75–87.

Pope, C.A., III, 1991. Respiratory hospital admission associated with PM_{10} pollution in Utah, Salt Lake, and Cache Valleys. Archives of Environmental Health 46, 90–97.

Pope, C.A., III, Dockery, D.W., Spengler, J.D., Raizenne, M.E., 1991. Respiratory health and PM_{10} pollution. A daily time series analysis. American Review of Respiratory Disease 144, 668–674.

Pope, C.A., III, Burnett, R.T., Thun, M.J., Calle, E.E., Krewski, D., Ito, K., Thurston, G.D., 2002. Lung cancer, cardiopulmonary mortality, and long-term exposure to fine particulate air pollution. The Journal of the American Medical Association 287, 1132–1141.

Pope, C.A., III, Dockery, D.W., 2006. Health effects of fine particulate air pollution: Lines that connect. Journal of the Air & Waste Management Association 56 (6), 709-742. doi: 10.1080/10473289.2006.10464485.

Pope, R.J., Marshall, A.M., O'Kane, B.O., 2016. Observing UK Bonfire Night pollution from space: analysis of atmospheric aerosol. Weather 71 (11), 288–291.

Rodriguez, S., Querol, X., Alastuey, A., Kallos, G., Kakaliagou, O., 2001. Saharan dust contributions to PM_{10} and TSP levels in southern and E. Spain. Atmospheric Environment 35, 2433–2447.

Rolph, G., Stein, A., Stunder, B., 2017. Real-time Environmental Applications and Display sYstem: READY. Environmental Modelling and Software 95, 210–228.

Ryall, D.B., Derwent, R.G., Manning, A.J., Redington, A.L., Corden, J., Millington, W., Simmonds, P.G., O'Doherty, Carslaw, N., Fuller, G.W., 2002. The origin of high particulate concentrations over the United Kingdom, March 2002. Atmospheric Environment 36 (8), 1363–1378.

Saha, S., Moorthi, S., Pan, H., Wu, X., Wang, J., Nadiga, S., Tripp, P., Kistler, R., Woollen, J., Behringer, D., Liu, H., Stokes, D., Grumbine, R., Gayno, G., Wang, J., Hou, Y., Chuang, H., Juang, H. H., Sela, J., Iredell, M., Treadon, R., Kleist, D., Van Delst, P., Keyser, D., Derber, J., Ek, M., Meng, J., Wei, H.,

Yang, R., Lord, S., van den Dool, H., Kumar, A., Wang, W., Long, C., Chelliah, M., Xue, Y., Huang, B., Schemm, J., Ebisuzaki, W., Lin, R., Xie, P., Chen, M., Zhou, S., Higgins, W., Zou, C., Liu, Q., Chen, Y., Han, Y., Cucurull, L., Reynolds, R. W., Rutledge, G., Goldberg, M., 2010. NCEP Climate Forecast System Reanalysis (CFSR) 6-hourly Products, January 1979 to December 2010. Research Data Archive at the National Center for Atmospheric Research, Computational and Information Systems Laboratory. Available at: https://doi.org/10.5065/D69K487J (accessed 20 November 2017).

Saha, S., Moorthi, S., Wu, X., Wang, J., Nadiga, S., Tripp, P., Behringer, D., Hou, Y., Chuang, H., Iredell, M., Ek, M., Meng, J., Yang, R., Mendez, M. P., van den Dool, H., Zhang, Q., Wang, W., Chen, M., Becker, E., 2011. NCEP Climate Forecast System Version 2 (CFSv2) 6-hourly Products. Research Data Archive at the National Center for Atmospheric Research, Computational and Information Systems Laboratory. Dataset. Available at: https://doi.org/10.5065/D61C1TXF (accessed 20 November 2017).

Sati, A.P., Mohan, M., 2014. Analysis of air pollution during a severe smog episode of November 2012 and the Diwali Festival over Delhi, India. International Journal of Remote Sensing 35 (19), 6940–6954. doi: 10.1080/01431161.2014.960618.

Schell, B., Ackermann, I.J., Hass, H., Binkowski, F.S., Ebel, A., 2001. Modeling the formation of secondary organic aerosol within a comprehensive air quality model system. Journal of Geophysical Research 106, 28275–28293.

Schultz, M. G., Rast, S., van het Bolscher, M., Pulles, T., Brand, R., Pereira, J., Mota, B., Spessa, A., Dalsøren, S., van Nojie, T., Szopa, S., 2007. REanalysis of the TROpospheric chemical composition over the past 40 years (RETRO) - A long-term global modeling study of tropospheric chemistry. Final Report, Jülich/Hamburg, Germany.

Seo, J., Leem, J., Ha, E., Kim, O., Kim, B., Lee, J., Park, H., Kim, H., Hong, Y., Kim, Y., 2010. Population-attributable risk of low birthweight related to PM_{10} pollution in seven Korean cities. Paediatric and Perinatal Epidemiology 24, 140–148.

Skamarock, W.C., Klemp, J.B., Dudhia, J., Gill, D.O., Barker, D.M., Duda, M.G., Huang, X.-Y., Wang, W., Powers, J.G., 2008. A Description of the Advanced Research WRF Version 3. Technical note NCAR/TN475+STR. Mesoscale and Microscale Meteorology Division, National Center for Atmospheric Research, Boulder, Colorado, USA.

Sonnenschein–van der Voort, A.M. et al., 2014. Pre–term birth, infant weight gain, and childhood asthma risk: A meta–analysis of 147,000 European children. Journal of Allergy and Clinical Immunology 133 (5), 1317–1329.

Stein, A.F., Draxler, R.R., Rolph, G.D., Stunder, B.J.B., Cohen, M. D., Ngan, F., 2015. NOOA's HYSPLIT atmospheric transport and dispersion modeling system. Bulletin of the American Meteorological Society 96, 2059–2077.

Stockwell, W.R., Middleton, P., Chang, J.S., Tang, X., 1990. The second generation regional acid deposition model chemical mechanism for regional air quality modeling. Journal of Geophysical Research 95 (D10), 16343–16367.

Su, L., Yuan, Z., Fung, J.C.H., Lau, A.K.H., 2015. A comparison of HYSPLIT backward trajectories generated from two GDAS datasets. Science of the Total Environment 506–507, 527–537.

Sun, J., Liu, T., Lei, Z., 2000. Sources of heavy dust fall in Beijing, China on April 16, 1998. Geophysical Research Letters 27, 2105–2108.

Tesfaye, M., Mengitsu Tsidu, G., Botai, J., Sivakumar, V., Rautenbach, C. J. D., 2015. Mineral dust aerosol distributions, its direct and semi-direct effects over South Africa based on regional climate model simulation. Journal of Arid Environments 114, 22–40. doi: 10.1016/j.jaridenv.2014.11.002.

Tessema, M.A., 2011. Particulate matter (PM_{10}) pollution in Khayelitsha, Cape Town (unpublished M.Sc. thesis). African Institute for Mathematical Sciences, South Africa.

Tie, X., Cao, J., 2009. Aerosol pollution in China: Present and future impact on environment. Particuology 7, 426–431.

Tie, X., Wu, D., Brasseur, G., 2009. Lung cancer mortality and exposure to atmospheric aerosol particles in Guangzhou, China. Atmospheric Environment 43, 2375–2377.

Triantafyllou, A.G., 2001. PM_{10} pollution episodes as a function of synoptic climatology in a mountainous industrial area. Environmental Pollution 112 (3), 491–500. doi: 10.1016/S0269-7491(00)00131-7.

Viana, M., Querol, X., Alastuey, A., Cuevas, E., Rodriguez, S., 2002. Influence of African dust on the levels of atmospheric particulates in the Canary Islands air quality network. Atmospheric Environment 36, 5861–5875.

Vieno, M., Heal, M.R., Twigg, M.M., Mackenzie, I.A., Braban, C.F., Lingard, J.J.N., Ritchie, S., Beck, R.C., Móring, A., Ots, R., Marco, C.F. Di, Nemitz, E., Sutton, M.A., Reis, S., 2016. The UK particulate matter air pollution episode of March–April 2014: More than Saharan dust. Environmental Research Letters 11 (2016) 059501.

Walton, N.M., 2005. Characterisation of Cape Town brown haze (unpublished M.Sc. thesis). University of Witwatersrand.

Wang, Y.Q., Zhang, X.Y., Arimoto, R., Cao, J.J., Shen, Z.X., 2004. The transport pathways and sources of PM_{10} pollution in Beijing during spring 2001, 2002 and 2003. Geophysical Research Letters 31 (14), L14110. doi: 10.1029/2004GL019732.

Weber, S.J., 2004. An investigation of the primary sources of the Cape Town Brown Haze (unpublished M.Sc. thesis). University of Cape Town.

Whittemore, A.S., Korn, E.L., 1980. Asthma and air pollution in the Los Angeles area. American Journal of Public Health 70 (7), 687–696.

WHO (World Health Organization), 2005. Air quality guidelines for particulate matter, ozone, nitrogen dioxide and sulphur dioxide: Global update 2005. WHO, Geneva, Switzerland.

WHO (World Health Organization), 2006. Health risks of particulate matter from long-range transboundary air pollution. Joint WHO/Convention Task Force on the Health Aspects of Air Pollution. WHO regional office for Europe, Copenhagen, Denmark.

Wicking-Baird, M.C., De Villiers, M.G., Dutkiewicz, R., 1997. Cape Town Brown Haze Study. Report No. Gen 182, Energy Research Institute, University of Cape Town, Cape Town.

Wild, O., Zhu, X., Prather, M.J., 2000. Fast-J: Accurate simulation of in- and below-cloud photolysis in tropospheric chemical models. Journal of Atmospheric Chemistry 37 (3), 245–282.

Yitshak-Sade, M., Novack, V., Ifergane, G., 2015. Air pollution and ischemic stroke among young adults. Stroke 46: 3348–3353.

Zhao, T.L., Gong, S.L., Zhang, X.Y., Jaffe., D.A., 2008. Asian dust storm influence on North American ambient PM levels: observational evidence and controlling factors. Atmospheric Chemistry and Physics 8, 2717–2728.